Impacts of anthropogenic aerosols on regional climate: extreme events, stagnation, and the United States warming hole

Nora R. Mascioli

Submitted in partial fulfillment of the
requirements for the degree of
Doctor of Philosophy
in the Graduate School of Arts and Sciences

COLUMBIA UNIVERSITY

2018

Abstract

Impacts of anthropogenic aerosols on regional climate: extreme events, stagnation, and the United States warming hole

Nora Mascioli

Extreme temperatures, heat waves, heavy rainfall events, drought, and extreme air pollution events have adverse effects on human health, infrastructure, agriculture and economies. The frequency, magnitude and duration of these events are expected to change in the future in response to increasing greenhouse gases and decreasing aerosols, but future climate projections are uncertain. A significant portion of this uncertainty arises from uncertainty in the effects of aerosol forcing: to what extent were the effects from greenhouse gases masked by aerosol forcing over the historical observational period, and how much will decreases in aerosol forcing influence regional and global climate over the remainder of the 21st century?

The observed frequency and intensity of extreme heat and precipitation events have increased in the U.S. over the latter half of the 20th century. Using aerosol only (AER) and greenhouse gas only (GHG) simulations from 1860 to 2005 in the GFDL CM3 chemistry-climate model, I parse apart the competing influences of aerosols and greenhouse gases on these extreme events. I find that small changes in extremes in the "all forcing" simulations reflect cancellations between the effects of increasing anthropogenic aerosols and greenhouse gases. In AER, extreme high temperatures and the number of days with temperatures above the 90th percentile decline over most of the U.S., while in GHG high temperature extremes increase over most of the U.S. The

spatial response patterns in AER and GHG are significantly anti-correlated, suggesting a preferred regional mode of response that is largely independent of the type of forcing. Extreme precipitation over the eastern U.S. decreases in AER, particularly in winter, and increases over the eastern and central U.S. in GHG, particularly in spring. Over the 21st century under the RCP8.5 emissions scenario, the patterns of extreme temperature and precipitation change associated with greenhouse gas forcing dominate.

The temperature response pattern in AER and GHG is characterized by strong responses over the western U.S. and weak or opposite signed responses over the southeast U.S., raising the question of whether the observed U.S. "warming hole" could have a forced component. To address this question, I systematically examine observed seasonal temperature trends over all time periods of at least 10 years during 1901-2015. In the northeast and southern U.S., significant summertime cooling occurs from the early 1950s to the mid 1970s, which I partially attribute to increasing anthropogenic aerosol emissions (median fraction of the observed temperature trends explained is 0.69 and 0.17, respectively). In winter, the northeast and southern U.S. cool significantly from the early 1950s to the early 1990s, which I attribute to long-term phase changes in the North Atlantic Oscillation and the Pacific Decadal Oscillation. Rather than being a single phenomenon stemming from a single cause, both the warming hole and its dominant drivers vary by season, region, and time period.

Finally, I examine historical and projected future changes in atmospheric stagnation. Stagnation, which is characterized by weak winds and an absence of precipitation, is a meteorological contributor to heat waves, extreme pollution, and drought. Using CM3, I show that regional stagnation trends over the historical period

(1860-2005) are driven by changes in anthropogenic aerosol emissions, rather than rising greenhouse gases. In the northeastern and central United States, aerosol-induced changes in surface and upper level winds produce significant decreases in the number of stagnant summer days, while decreasing precipitation in the southeast US increases the number of stagnant summer days. Outside of the U.S., significant drying over eastern China in response to rising aerosol emissions contributed to increased stagnation during 1860-2005. Additionally, this region was found to be particularly sensitive to changes in local aerosol emissions, indicating that decreasing Chinese emissions in efforts to improve air quality will also decrease stagnation. In Europe, I find a dipole response pattern during the historical period wherein stagnation decreases over southern Europe and increases over northern Europe in response to global increases in aerosol emissions. In the future, declining aerosol emissions will likely lead to a reversal of the historical stagnation trends, with increasing greenhouse gases again playing a secondary role.

Aerosols have a significant effect on a number of societally important extreme events, including heat waves, intense rainfall events, drought, and stagnation. Further, uncertainty in the strength of aerosol masking of historical greenhouse gas forcing is a significant source of spread in future climate projections. Quantifying these aerosol effects is therefore critical for our ability to accurately project and prepare for future changes in extreme events.

Table of Contents

List of Figures

List of Tables

Acknowledgements

First and foremost, thank you to my advisors Arlene Fiore and Michael Previdi. Thank you for your support and guidance over the years. You have inspired me and challenged me, and helped me develop as a scientist. Thank you also to Mingfang Ting, for your advice and for your questions. Thank you to Gus Correa and Larry Rosen, without your expertise this research would never have gotten off the ground.

Thank you to all of my colleagues at Lamont who have provided wisdom and guidance during my time here, especially Dan Westervelt, Alex Karembelas, George Milly, Antara Banarjee, and Deepti Singh. A special thanks go out to my fellow students, especially Etienne Dunn-Siguin, Nandini Ramesh, Catherine Pomposi, Sophia Brumer, Sage Li, Olivia Clifton, Jean Guo, Xiaomeng Jin, and Colleen Baublitz

I would also like to thank Ross Salawitch and Tim Canty for encouraging me to pursue atmospheric science in the first place.

Finally, thanks of course to my family and friends. Thank you for all of your love and support. And especially thank you for your patience whenever I get carried away talking about atmospheric aerosols.

In memory of Eileen Manuel, who showed me the importance of always questioning

Chapter 1 Introduction

1.1 Past climate changes and future implications

Annual mean global surface temperature increased 0.85K from 1880-2012, which is attributed primarily to human activity (Bindoff et al. 2013; Hartmann et al. 2013). Annual global mean precipitation increased as well, on the order of 1-3mm/day from 1901-2008, and the scientific community has attributed some of the observed trend, particularly over Northern Hemisphere land areas, to anthropogenic climate change (Bindoff et al. 2013; Hartmann et al. 2013). These changes over the historical period were driven principally by rising concentrations of greenhouse gases, particularly CO_2, CH_4, N_2O, and tropospheric O_3. Anthropogenic aerosol emissions have also increased over the same period. Because aerosols have a net cooling effect on the climate, we expect that they have masked some of the greenhouse gas-induced warming. This presents a serious challenge to our understanding of past climate change because the radiative forcing due to aerosols is highly uncertain, and as a result the uncertainty in the total historical radiative forcing is also large (Figure 1.1). In the future, anthropogenic aerosol emissions are projected to decrease globally while greenhouse gas emissions continue to rise, reducing this aerosol-masking effect. Understanding how much aerosols have masked greenhouse gases during the instrumental era is therefore critical for our ability to accurately project future climate.

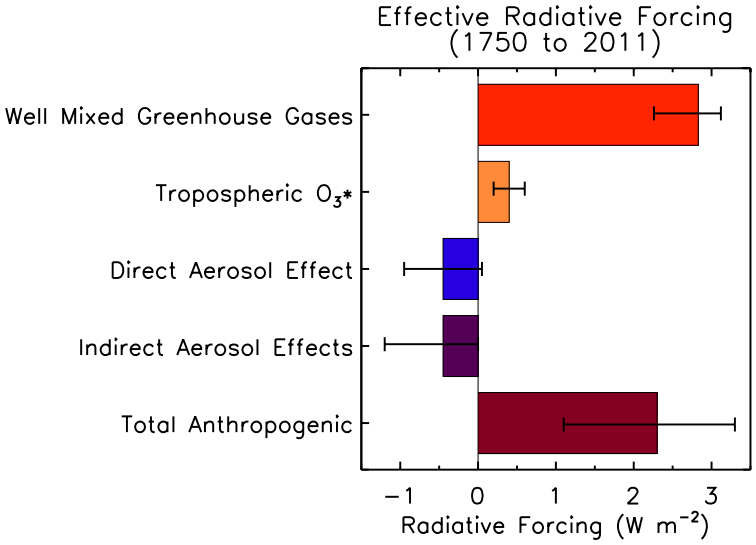

Figure 1.1 The best estimates of the globally averaged effective radiative forcing (ERF; top-of-atmosphere radiative forcing after allowing for atmospheric temperature, water vapor, and clouds to adjust) from 1750-2011 due to the primary drivers of anthropogenic climate change: well-mixed greenhouse gases (CO_2, CH_4, N_2O, halogen gases), tropospheric O_3*, and the direct and indirect aerosol effects as assessed by IPCC AR5 WGI and reported in Table 8.6 of Myhre et al. 2013. Error bars denote the 5 to 95% confidence range.

***Radiative Forcing (after stratospheric temperature adjustment but without allowing for tropospheric adjustment) is presented for tropospheric O_3 rather than ERF due to insufficient information (Myhre et al. 2013).**

While changes in annual global mean temperature and precipitation provide a useful metric, patterns of regional and seasonal change are more informative for evaluating the societal impacts of climate change. Further, changes in the extreme tails of the temperature and precipitation distribution (e.g. heat waves, flooding, drought), can be especially costly relative to changes occurring near the mean (Handmer et al. 2012). In this research, I use global climate models to evaluate the effect of aerosols on the frequency and magnitude of extreme temperature and precipitation events in the U.S., and to project the future impacts of declining aerosol emissions (Chapter 2). This joint analysis of extreme temperature and precipitation highlights a robust temperature-precipitation relationship in the southeast U.S. wherein changes in the hydrological cycle buffer the region against changes in temperature. This buffering effect leads me to pose

the question of whether or not aerosols may be driving the observed regional temperature trends in the southeast U.S. over the historical period (known as the "warming hole"), which I explore in Chapter 3.

In order to better understand the possible implications of aerosol effects on extreme temperature and precipitation, Chapter 4 examines aerosol-induced changes in atmospheric stagnation. Stagnation events are associated with high-pressure systems and are characterized by weak winds and an absence of precipitation. They can persist for days to weeks, increasing the likelihood of heat waves, drought, and severe air pollution. Finally, in Chapter 5, I summarize the results and conclusions of Chapters 2-4 and discuss the implications and future research directions for my work. The remainder of this chapter provides background material and context for the ensuing chapters.

1.2 Atmospheric Aerosols

Aerosols, small bits of particulate matter suspended in the atmosphere, remain a significant source of uncertainty in our understanding of past and future climate. They vary considerably in size, with diameters ranging from nanometers to microns, and chemical composition, typically composed of sulfate, nitrate, black and organic carbon, ammonium, sea salt, and mineral dust. Aerosol particles are commonly mixed with each other, either in an external mixture (i.e. air sample contains different aerosol species), or in an internal mixture, in which individual aerosol particles contain a mixture of different aerosol components (e.g. a particle containing black carbon coated with sulfate).

Some aerosols are emitted directly (e.g. black carbon and mineral dust), while other aerosols (e.g. sulfate) form in the atmosphere from the emissions of precursor species. Aerosols and their precursors have a number of anthropogenic and natural

sources. Anthropogenic aerosols are produced primarily from fossil fuel combustion (e.g. coal-fired power plants and vehicle emissions, particularly from diesel engines), and biomass burning. Natural sources of aerosols include biogenic emissions, dust, sea spray, wildfires, and volcanic eruptions.

Unlike greenhouse gases such as CO_2, CH_4, and N_2O, aerosols in the troposphere typically only remain there for days to weeks before being removed by wet or dry deposition. Despite their short atmospheric lifetime, aerosols have a profound impact on climate: 1) by scattering or absorbing incoming solar radiation, and 2) by altering cloud properties by serving as cloud condensation nuclei and ice nuclei and by changing atmospheric stability. Sulfate, nitrate, organic carbon, and sea salt predominantly scatter incoming solar radiation, cooling the climate. Black carbon and brown carbon (a subset of organic carbon) primarily absorb solar radiation, warming the climate overall, although they may cause local surface cooling. Mineral dust aerosols can both scatter and absorb depending on their size and chemical composition. Mineral dust is currently believed to be a net scatterer, but the sign of its overall radiative effect is uncertain (Boucher et al. 2013). The optical properties of aerosols also depend on their mixing state adding an additional layer of complexity. Figure 1.2 shows the modeled aerosol optical depth (AOD) at 550nm, a measure of aerosol scattering and absorption (i.e. aerosol extinction), for the present (year 2000) and the change from 1860 to 2000 in the GFDL-CM3. AOD is elevated in regions with high anthropogenic emissions (e.g. eastern China, India, Europe, and the eastern U.S.), as well as in regions with large natural emissions (e.g. western Africa). AOD has increased in almost all regions of the globe between 1860 and 2000. Taken together, the radiative forcing of climate due to aerosol

interactions with incoming solar radiation is known as the direct effect. The global mean net direct effect of aerosols in 2011 relative to 1750 is estimated to be -0.45 ± 0.5 Wm^{-2} (Figure 1.1, see also Myhre et al. 2013).

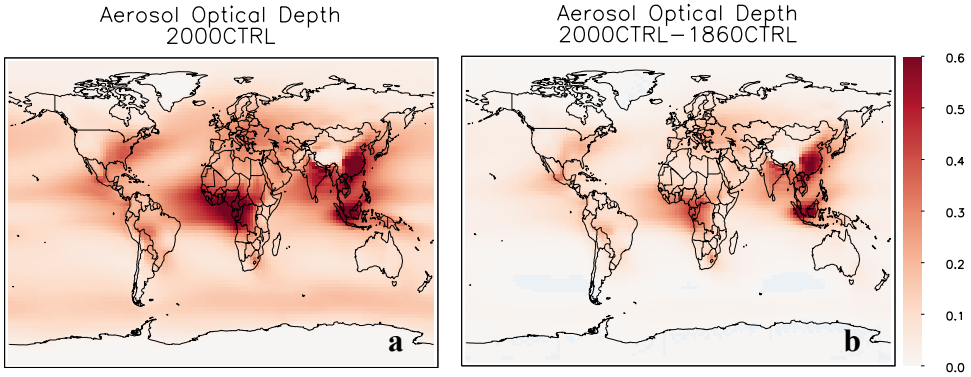

Figure 1.2 (a) Modeled aerosol optical depth at 550nm in the present (year 2000 control simulation) and (b) the difference in aerosol optical depth between the present (2000) and pre-Industrial (1860) control simulations from GFDL-CM3

A more uncertain and potentially more significant pathway for aerosols to affect climate is through their effects on clouds and cloud microphysics. Increasing aerosol number concentrations provide more particles to act as cloud condensation and ice nuclei. This will tend to decrease the average droplet size within the cloud, as more small droplets form (and fewer large droplets). Because the droplets are smaller, they are less likely to rain out, increasing the lifetime of the cloud (cloud-lifetime effect, Albrecht 1989). In addition, clouds made up of many small droplets reflect more sunlight than clouds made up of fewer large droplets for the same amount of cloud water (cloud-albedo effect, Twomey 1977). Absorbing aerosols such as black carbon can cause cloud burn-off by altering the vertical temperature profile around the cloud (semi-direct effect). The current best estimate of the global mean indirect radiative effect of aerosols in 2011 relative to 1750 is -0.45 Wm^{-2} with an uncertainty range of -1.2 – 0 Wm^{-2} (Myhre et al. 2013, Figure 1.1).

1.3 Extreme weather

Extreme weather events such as heat waves, extreme rainfall, and drought have serious societal impacts including on human health, infrastructure, and economies. Since the 1980s, extreme events have led to global economic losses and damages ranging from a few billion US dollars to over 200 billion US dollars per year (Handmer et al. 2012). The frequency and duration of heat waves has increased over the 20th century, particularly over Europe, Asia, and Australia (Hartmann et al. 2013). The signal-to-noise ratio is smaller for extreme precipitation, but overall the frequency and intensity of extreme precipitation events has increased since the 1950s, particularly over central North America (Donat et al. 2013; Hartmann et al. 2013; Kunkel et al. 2008). Similarly, there is considerable spatial heterogeneity in changes in drought, but studies have found increasing drought trends over the last 60 years over a number of regions of the world such as southern Europe, and West Africa, as well as decreasing trends over regions such as central North America (Seneviratne et al. 2012).

Over the U.S., significant changes have been observed in both temperature and precipitation extremes (Kunkel et al. 2008). The frequency and spatial extent of heat waves has increased significantly over the second half of the 20th century, as has the temperature on the hottest days (Kunkel et al. 2008; Peterson et al. 2008; Portmann et al. 2009). Although they are not generally significant outside of the central U.S., observations show increasing trends in the frequency and intensity of extreme rainfall in the U.S. over the latter half of the 20th century (e.g. Karl and Knight 1998; Groisman et al. 2005, Kunkel et al. 2008, Powell and Keim 2015). However, despite the overall increase in extreme precipitation frequency, there have been positive trends in drought in

the western and southern U.S. in recent decades (Cook et al. 2004; Ficklin et al. 2015; Weiss et al. 2009).

A number of studies have attributed changes in heat extremes to anthropogenic activities, principally the rapid rise in greenhouse gas concentrations (Christidis et al. 2011; Meehl et al. 2007; Morak et al. 2013; Zwiers et al. 2011). Detection and attribution of changes in precipitation extremes is more difficult than for temperature due to greater internal variability of precipitation (Bindoff et al. 2013), but it is likely that anthropogenic activities have influenced extreme precipitation trends, through impacts on atmospheric moisture content (Allen and Ingram 2002; Stott et al. 2010; Trenberth et al. 2003). However, the extent to which changes in U.S. and global temperature and precipitation extremes during the historical period have been masked by increasing emissions of atmospheric aerosols remains uncertain. This has implications for our ability to make future projections of extremes as aerosol emissions are projected to decline over the course of the 21st century while greenhouse gas concentrations continue to rise. Chapter 2 addresses this topic by separating out the effects of greenhouse gases and aerosols on extreme temperature and precipitation in the United States in a modeling framework.

1.4 The southeastern U.S. warming hole

In my analysis in Chapter 2, I find that changes in precipitation buffer the southeastern U.S. against expected changes in temperature over century-long time scales. Observational analysis shows that near surface temperatures in the southeast and central U.S. have cooled slightly over the 20th century, commonly referred to as the U.S. "warming hole", in contrast with the overall positive temperature trend in the U.S. and

globally (Hartmann et al. 2013). It is well established that temperatures in this region are highly sensitive to changes in the hydrological cycle including changes in precipitation, soil moisture, and cloud cover (Leibensperger et al. 2012; Meehl et al. 2012; Misra et al. 2012; Pan et al. 2004; Portmann et al. 2009; Robinson 2002; Weaver 2013; Yu et al. 2014), but attribution of the warming hole to internal variability or anthropogenic forcing remains a topic of debate within the scientific community.

It has been theorized that the warming hole is caused by internal variability tied to changes in sea surface temperature (SST; Robinson et al. 2002; Kunkel et al. 2006; Meehl et al. 2012; Weaver 2012), or that it is a forced response either to changes in anthropogenic aerosols (Leibensperger et al. 2012; Yu et al. 2014) or changes in land use (Misra et al. 2012). However, there are inconsistencies in the literature in the definition of the timing, season, and location of the warming hole, which, as I will show, are important for understanding the mechanisms driving the observed temperature changes in the southeast and central U.S.

1.5 Atmospheric stagnation

In Chapter 4, I broaden the scope of my investigation to consider aerosol impacts on a more global scale. Specifically, I examine aerosol impacts on one of the meteorological conditions that is often associated with extreme temperature and pollution events: atmospheric stagnation. Stagnant days are defined as days when surface winds are less than 3.2 ms^{-1}, 500hPa winds are less than 13 ms^{-1}, and there is an absence of precipitation (Wang and Angell 1999), conditions often associated with a high-pressure system. These conditions can persist over a region for days to weeks allowing for a build up of pollutants (Jacob and Winner 2009; Tai et al. 2010) and the clear skies, weak

winds, and prolonged dry conditions can trigger heat waves (Kunkel et al. 1996; Meehl and Tebaldi 2004; Palecki et al. 2001).

Several studies have projected future changes in atmospheric stagnation and found that it will generally increase globally, although with significant regional variations (Horton et al. 2012; Horton et al. 2014), but as of yet there has been no research into the role of atmospheric aerosols in influencing stagnation. I expect aerosols to affect stagnation in a number of ways, including: through their effects on the earth's radiation budget, which can alter circulation patterns and affect precipitation; through their indirect effects on cloud microphysics and tendency to suppress drizzle; and through their impacts on local atmospheric stability. In Chapter 4, I quantify the impact of changes in the global aerosol burden on regional stagnation, and I also identify stagnation changes due to changes in regional aerosol emissions.

1.6 Scientific Questions

My dissertation objectives are to address the following questions:

- How do aerosols affect the frequency and magnitude of extreme temperature and precipitation in the U.S.? How do aerosol effects compare with the effects of greenhouse gases? How will extreme events change as aerosol emissions decrease in the future? (Chapter 2)
- What are the relative contributions of aerosol forcing and internal variability in explaining the U.S. "warming hole"? Do they vary with season and time period? (Chapter 3)

- How do aerosols influence the occurrence of atmospheric stagnation events in different regions? What is the role of local vs. remote aerosol emissions? (Chapter 4)

My principal tool in Chapters 2 and 4 is GFDL-CM3, a global climate model. CM3 (described in detail in Chapter 2) is a state of the art model that includes cloud-aerosol interactions (indirect effects) and interactive tropospheric and stratospheric chemistry (Donner et al. 2011). In Chapter 3, I use a subset of models, including CM3, that participated in the 5th Coupled Model Inter-comparison Project (CMIP5; Taylor et al., 2012) combined with an in depth analysis of regional temperature trends using GISTEMP observations (Hansen et al. 2010).

In Chapter 2, I use daily temperature and precipitation data from single-forcing experiments performed with CM3 to isolate and quantify the respective roles of aerosols and greenhouse gases on extreme temperature and precipitation events in the U.S. In Chapter 3, I examine observed and modeled temperature trends over the U.S. over a variety of time periods. By considering trends over different periods and seasons, I can identify times over which different influences, such as aerosols and internal variability in the ocean and atmosphere, are important. In Chapter 4, I analyze stagnation changes in a set of single forcing experiments performed with CM3 to quantify the role of aerosols in driving the modeled historical stagnation trends. Further, using a set of sensitivity simulations I am able to identify the impact of aerosols from specific source regions and separate these responses from the overall response to changes in the global aerosol burden. Finally, Chapter 5 discusses the conclusions of this thesis and outlines future research directions.

Chapter 2 Temperature and precipitation extremes in the United States: Quantifying the responses to anthropogenic aerosols and greenhouse gases

[Mascioli, N. R., A. M. Fiore, M. Previdi, and G. Correa (2016), Temperature and precipitation extremes in the United States: Quantifying the response to anthropogenic aerosols and greenhouse gases, *J. Climate*, 29, 7, 2689-2701, doi:10.1175/JCLI-D-15-0478.1]

2.1 Introduction

U.S. observations indicate increases over recent decades in extreme high temperatures, heat waves, and heavy rainfall events, with far reaching implications for human health, agriculture, air quality, water management, and economic growth. The number of unusually hot days per year has risen 2-3% over the U.S. since 1950, with the most significant increases occurring in the western U.S. (Kunkel et al. 2008; Peterson et al. 2008; Portmann et al. 2009). The number of heat waves has also increased significantly since 1960, as has the area of the U.S. experiencing unusually hot daily high temperatures (Kunkel et al. 2008). Over the 20th century, U.S. extreme precipitation events have increased in frequency and intensity, particularly over the central U.S. (e.g. Karl and Knight 1998; Groisman et al. 2005, Kunkel et al. 2008). The amount of precipitation occurring on the heaviest precipitation days has increased more rapidly than the total precipitation (Groisman et al. 2004). Additionally, the area of the U.S.

influenced annually by extreme precipitation events (>50mm) increased significantly from 9% to 11% over the 20th century (Karl and Knight 1998).

These observed changes in climate extremes have adverse impacts on human health and the economy. Summer heat waves have been shown to increase mortality by 2-5%; approximately 1000 deaths per year can be attributed to these events in the U.S. (Anderson and Bell 2011; Changnon et al. 1996). Furthermore, extreme temperatures and heat waves have also been shown to correlate with extreme air pollution events (Logan et al. 1989; Tai et al. 2010; Tai et al. 2012; Leung et al. 2005; and others). Heavy storms can incur property damage and threaten human life (Lott and Ross 2006), including through major flood events and flash floods (Kunkel et al. 2013). Studies have shown that extreme precipitation contributes to the spread of disease in the U.S. (Curreiro et al. 2001; Engelthaler et al. 1999; Glass et al. 2000). Taken together, extreme heat and precipitation events cost the U.S. billions of dollars in damages each year (Lott and Ross 2006).

Natural and manmade systems are generally adapted to the current range of extreme events. Therefore, changes in the frequency, magnitude, and duration of these events pose significant challenges and risks (Kunkel et al. 2008). CMIP5 models show increases at the end of the 21st century relative to 1901-60 in U.S. monthly mean summer temperatures of 5-7°C (Maloney et al. 2014). Similarly, U.S. maximum summer temperatures are projected to increase by 5-7°C relative to 1981-2000 (Sillmann et al. 2013a). Under the A1B future scenario, heat waves in the U.S. continue to increase in both duration and frequency over the 21st century over the Great Plains region, the Pacific Northwest, the Northeast U.S., and the Southeastern U.S. (Lau and Nath 2012).

Following RCP8.5, CMIP5 models project increases by the end of the 21st century, relative to 1901-1960, in mean winter precipitation over most of the U.S., with the largest increases (0.5 – 1.0 mm day^{-1}) occurring in the northeast and northwest U.S. (Maloney et al. 2014). Annually, CMIP5 models project significant increases of 5-15% relative to 1981-2000 in total precipitation in the northern U.S. (Sillmann et al. 2013a). The contribution to the total annual precipitation coming from days with extremely high rainfall is projected to increase by 20-40% over the central U.S. and 40-70% over the eastern and western U.S. (Sillmann et al. 2013a).

There remains a considerable amount of uncertainty in our understanding of past climate and projections for the future, which derives partly from uncertainty in the effects of atmospheric aerosols, which typically cool the climate, both directly and via interactions with clouds (Boucher et al. 2013). Aerosols are short-lived in the atmosphere and their emissions from anthropogenic sources are projected to decline over the next century. It is important therefore to understand how they are affecting the present climate in order to project accurately the effects of their removal. Here, we use a set of "single forcing" experiments performed by a state-of-the-art general circulation model (GCM) to investigate the historical changes in extreme temperature and precipitation in the United States in response to anthropogenic forcing. These single-forcing simulations allow us to assess individually the effects of anthropogenic aerosols and greenhouse gases, revealing patterns of change not visible in the full historical simulations due to cross-cancellations.

Section 2.2 describes the model simulations and defines the extreme indices that we examine. In section 2.3, we discuss the modeled changes in U.S. extreme heat and

precipitation as a result of increasing aerosols and greenhouse gases over the historical period (1860-2005). Section 2.4 projects future 21st century changes in extremes under the RCP8.5 scenario, in which greenhouse gas concentrations increase while aerosol emissions decrease. Finally, conclusions are presented in Section 2.5.

2.2 Methods

2.2.1 Model description, simulations, and significance testing

We use the GFDL CM3 chemistry-climate model to evaluate changes in extreme temperature and precipitation over the United States induced by changes in aerosol and greenhouse gas burdens. CM3 simulations use a cubed sphere grid with 48 vertical levels; archived fields are regridded to a 2°× 2.5° latitude/longitude grid. In addition to its atmospheric component (AM3), CM3 includes the modular ocean model (MOM), a land component with dynamic vegetation (LM3), and a sea ice model, described in Donner et al. (2011). Of key importance for our study is the inclusion in AM3 of a more complex aerosol scheme, relative to earlier versions of the model, in which prognostic aerosols interact with clouds, as well as interactive tropospheric and stratospheric chemistry (Horowitz 2006; Ming et al. 2005; Ming et al. 2007; Naik et al. 2013). Aerosol concentrations are calculated from the ACCMIP historical (Lamarque et al. 2010) and RCP8.5 future (van Vuuren et al. 2011) emissions inventories, and undergo atmospheric transport, chemical transformations, and wet and dry deposition. AM3 accounts for anthropogenic and biomass burning emissions of aerosols and aerosol precursors, including sulfur dioxide, black carbon, and organic carbon (Lamarque et al. 2010), and volcanic emissions of sulfur dioxide (Dentener et al. 2006). The model includes a simple

representation of secondary organic aerosol production, including natural sources from plants (Dentener et al. 2006) and anthropogenic sources from the oxidation of butane (Tie et al. 2005). Dimethyl sulfide (DMS; a sulfate precursor) emissions from seawater (Chin et al. 2002), dust (Ginoux et al. 2001), sea salt (Monahan et al. 1986), and secondary organic aerosol production from sea spray (O'Dowd et al. 2008) respond to meteorology and thus changes in climate.

In AM3, prognostic aerosols alter cloud properties by acting as cloud condensation nuclei. This affects the size distribution of droplets in the cloud, producing clouds with smaller droplets, which reflect more incoming solar radiation (cloud albedo effect; Twomey 1977). In addition, smaller droplets are lighter and so less likely to precipitate out of the cloud, increasing its lifetime (cloud lifetime effect; Albrecht 1989). Both of these indirect effects of aerosols on clouds will tend to reduce incoming solar radiation, cooling the climate (Boucher et al. 2013). In the model, aerosol indirect effects occur only in liquid clouds; cloud droplet activation depends on the type of aerosol (sulfate, organic carbon and sea salt), its size distribution (assumed separately for each aerosol species), and updraft velocities within shallow cumulus and stratiform clouds (Donner et al. 2011; Golaz et al. 2013). Monthly mean cloud droplet sizes in AM3 have been compared with satellite retrievals (MODIS) and found to match many of the observed features such as enhancement in cloud droplet sizes off the east coasts of continents (Donner et al. 2011). Model-simulated droplet sizes are, however, generally biased low (Donner et al. 2011), although the MODIS retrievals of cloud droplet sizes are uncertain and generally larger than other satellite based estimates (Han et al. 1994).

As part of the fifth Coupled Model Intercomparison Project (CMIP5), a number of simulations were designed to explore key regions of uncertainty in the climate system, for example forcing due to anthropogenic aerosols (Taylor et al. 2012). We use daily surface air temperature and precipitation data from five of the simulations designed for CMIP5: the "aerosol only" simulations, with anthropogenic aerosols as the only time-varying forcing and all other forcings held at pre-Industrial levels (AER); "greenhouse gas only" simulations, with anthropogenic greenhouse gases as the only time-varying forcing (GHG); the full historical simulations (HIST), with all natural and anthropogenic forcings (including land-use changes) varying in time; a future emissions scenario, RCP8.5, in which greenhouse gases increase from 2006 through 2100, while anthropogenic aerosols decrease (Riahi et al. 2011); and an 800-year pre-Industrial control run. Additionally, we analyze a modified future scenario in which greenhouse gases follow their trajectory from RCP8.5, while aerosol concentrations are held constant at 2005 levels (RCP8.5_2005Aer; Westervelt et al. 2015). The AER, GHG, RCP8.5, and RCP8.5_2005Aer simulations each consist of three ensemble members, differing only in their initial conditions; the historical simulation has five ensemble members; and the pre-Industrial control run consists of a single ensemble member. The AER, GHG, and historical simulations are run from 1860 through 2005.

We consider the ensemble mean changes in each CM3 simulation. The statistical significance of these changes is assessed using two methods. In the first method, we use a z-test to determine where the difference between 30-year means is statistically different from zero (95% confidence). In the second method, the 800-year control run is split into distinct 30-year segments. We then construct a probability density function for the

difference between the means of two randomly selected 30-year segments. Differences in the forced simulations that fall outside the 95% confidence interval of this distribution are considered to be outside the range of modeled internal variability.

2.2.2 Extreme indices

The extreme climate indices defined by the Expert Team on Climate Change Detection and Indices (ETCCDI; Sillmann et al. 2013a,b) serve as the basis for our analysis, with a focus on two temperature indices (TXx, TX90p) and two precipitation indices (PRCPTOT, R99p). TXx is the maximum of the maximum daily temperature over a given time period. TX90p represents the number of days with a maximum temperature above the 90^{th} percentile. The 90^{th} percentile threshold in a given grid cell on calendar day *i* is defined by constructing the probability distribution of daily maximum temperature during days *i-2* through *i+2* over a 30 year base period. PRCPTOT is the total precipitation over a given time period. R99p, representing extreme precipitation, is the total amount of precipitation occurring on days with precipitation values above the 99^{th} percentile of the climatology. For the two threshold based indices, TX90p and R99p, we use 1961-1990 as the climatological base period in each simulation. We focus primarily on summertime TXx and TX90p and winter and spring PRCPTOT and R99p. Further details on these indices are provided in Sillmann et al. (2013a,b).

2.2.3 Model evaluation

CM3 captures the observed global climatology from 1981-2000 in the two metrics for extreme temperature as determined from the ERA40, ERA-Interim, NCEP1 and NCEP2 reanalyses (Sillmann et al. 2013b). CM3 summertime mean temperatures are

biased cold (−2.24°C), distributed evenly over the continental U.S., with respect to CRU observations from 1979-2005 (Donner et al. 2011; Sheffield et al. 2013). The summer cold bias is likely due to a "cloud lifetime effect" (aerosol second indirect effect) that is too strong in the model (Ackermann et al. 2004; Golaz et al. 2013; Guo et al. 2011; Levy et al. 2013; Quaas et al. 2011). Despite the bias, the model roughly captures the spatial distribution of observed summertime temperatures: both the monthly mean (Sheffield et al. 2013) and TXx (Figure 2.1).

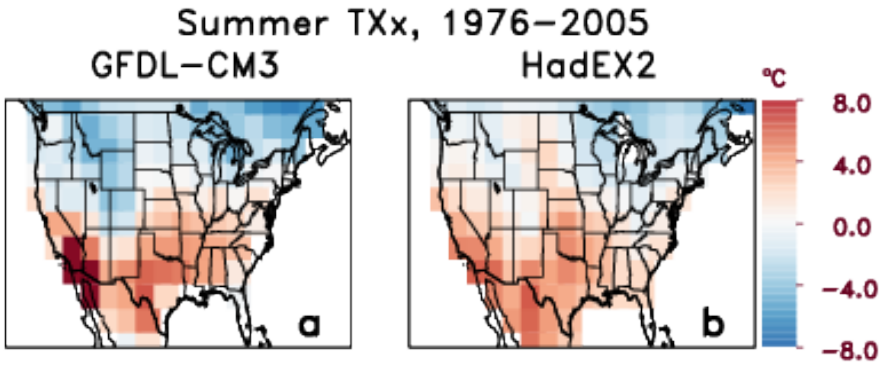

Figure 2.1 Spatial anomalies of 1976-2005 summer TXx relative to the U.S. mean of 31.6°C and 35.4°C in CM3 and HadEX2, respectively in (a) the CM3 historical simulation and (b) observations (HadEX2). The pattern correlation coefficient (r) is 0.51.

Comparing the simulated number of days per season with at least 20mm precipitation (R20mm) with observations from GPCP and TRMM shows that the model is able to capture both the magnitude and spatial distribution of this index in winter and spring (Figure 2.2). CM3 exceeds observed seasonal mean precipitation over much of North America in winter in comparison to the 1979-2005 climatology from GPCP (Sheffield et al. 2013), most pronounced over western North America (+52.7% of the observed mean), and much smaller over eastern North America (+4.46% of observed mean). Sheffield et al. (2013) also find a small low bias in mean precipitation over

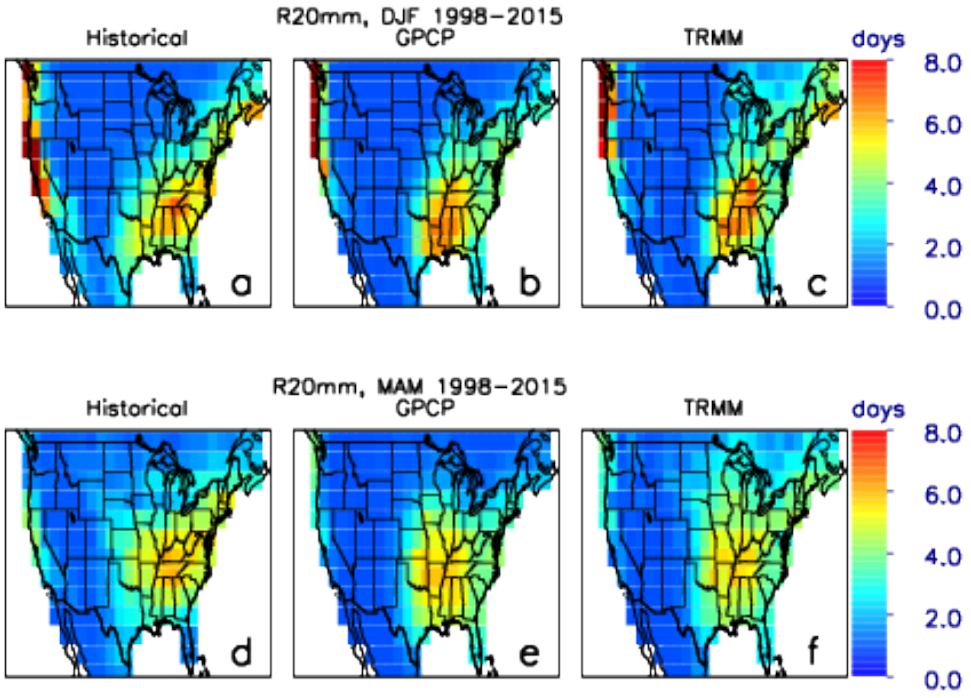

Figure 2.2 Average number of days per season (1998-2015) with at least 20mm of precipitation (R20mm) in (a,d) the CM3 historical simulation and observations from (b,e) GPCP and (c,f) TRMM in winter (top) and spring (bottom). The pattern correlation coefficients between CM3 and GPCP are 0.83 (winter) and 0.85 (spring). The pattern correlation coefficients between CM3 and TRMM are 0.78 (winter) and 0.85 (spring). The historical simulation has been extended to 2015 using RCP8.5

central North America in winter (−2.6% of the observed mean). Despite these biases, CM3 generally captures the observed spatial distribution of wintertime precipitation (Sheffield et al. 2013). In summer, CM3 captures observed mean precipitation over eastern (bias of -4.38%) and central North America (bias of +7.45%), but is biased high over western North America (+54.74% of the observed mean; Sheffield et al. 2013). The model does not capture the observed spatial distribution of U.S. summertime precipitation, a common weakness amongst CMIP5 models, most likely due to a failure to represent the dynamical conditions that produce summertime precipitation (Sheffield et al. 2013; G. Vecchi, personal communication, April 10, 2015).

2.3 Historical changes over the U.S.: greenhouse gases vs. aerosols

2.3.1 Temperature extremes

In this section we examine summertime changes in TX90p and TXx, which provide information on changes in the magnitude and frequency of extreme high temperatures, using the AER, GHG, and HIST simulations (Section 2.1). Significant changes in summertime TX90p occur in AER and GHG between 1860-1889 and 1976-2005 (Figure 2.3a,b). Increases in atmospheric aerosols generally lead to decreases in TX90p while rising greenhouse gases generally lead to increases. Increasing greenhouse gases produce warming outside of the range of modeled internal variability everywhere in the U.S., while increasing aerosols produce cooling outside of this range over most of the U.S., with the exception of the southeast U.S. Changes in the historical simulations, from 1860-2005, are generally not statistically significantly outside the range of internal variability as determined from the pre-Industrial control simulation (Figure 2.3c). As discussed in Section 2.3, the forcing in AER is most likely too strong, resulting in the absence of a significant temperature response in HIST. However, the CM3 representation of observed spatial distributions of mean and extreme temperatures provides confidence that the model is useful for analysis of the spatial patterns of

response to aerosol and greenhouse gas forcing.

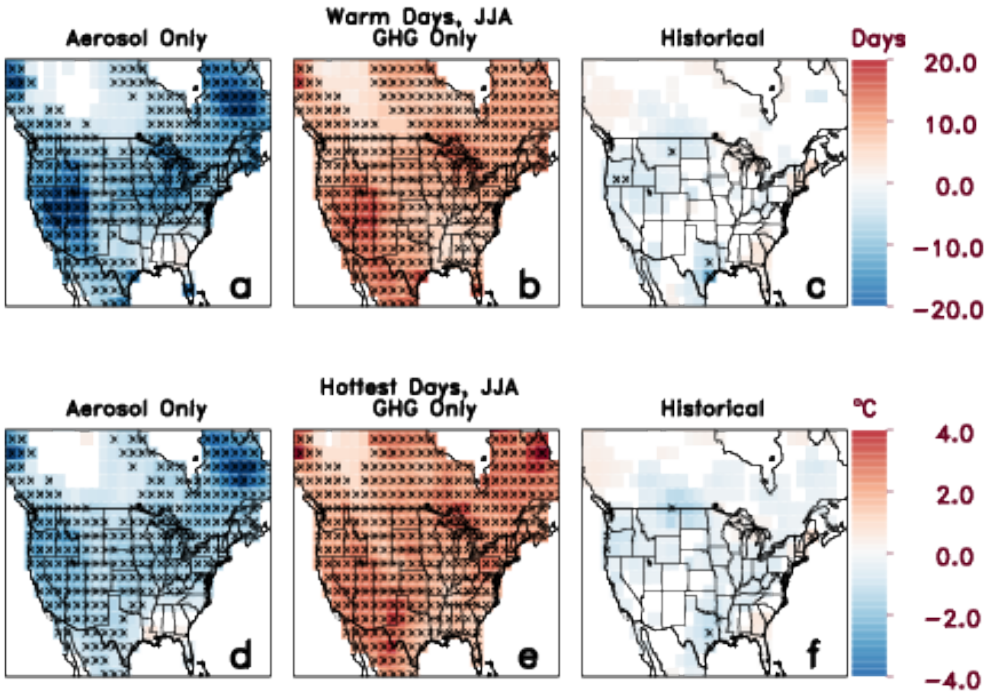

Figure 2.3 Changes in the 30-year ensemble mean values of summer (JJA) TX90p (top) and TXx (bottom) between the beginning (1860-1889) and end (1976-2005) of the aerosol-only (a,d), greenhouse gas only (b,e), and historical simulations (c,f). Ocean regions and grid cells where the change is not significantly different from zero (95% confidence) are whited out. Xs denote that the changes are outside of the range of natural variability (95% confidence), as determined from the model's pre-Industrial control simulation and described in Section 2.2

Anthropogenic greenhouse gases are generally long-lived and thus well mixed in the atmosphere, while aerosols have a heterogeneous spatial distribution. However, Figure 2.3a,b shows a statistically significant spatial anti-correlation between the response patterns associated with greenhouse gases and aerosols over the U.S., ($r = -0.72$). In both AER and GHG the largest temperature changes occur in the western U.S. (−14.0 and +11.5 days respectively), with relatively weaker changes in the northeast U.S. (−9.6 and +10.9 days), and little to no statistically significant change in the southeast U.S. (−4.8 and +7.2 days). This response pattern is consistent with observations showing a

relative intensification of warming in the western U.S. in comparison with the eastern U.S. over the 20th century (Donat et al. 2013; Meehl et al. 2012). Due to the similarity in spatial response pattern and magnitude between GHG and AER, there is a cancellation between these two competing effects in the "all forcing" simulation, resulting in little to no change in TX90p in Figure 2.3c, though we note that the aerosol forcing is likely too strong.

TXx similarly shows a significant anti-correlation between the effects of greenhouse gases and aerosols, with a pattern correlation coefficient of −0.64 (Figure 2.3d,e). The largest responses to anthropogenic forcing occur in the western U.S., where aerosols reduce TXx by −2.0°C and greenhouse gases increase TXx by 2.3°C. The response in the southeast U.S. is relatively weak, with aerosols reducing TXx by −0.6°C (not statistically significant at the 95% confidence level) and greenhouse gases increasing TXx by 1.6°C. As for TX90p, cancellations between the effects of aerosols and greenhouse gases on TXx result in relatively small changes in the historical simulation (Figure 2.3f).

The lack of statistically significant cooling in the southeast U.S. in the aerosol only simulations and collocated warming minimum in the greenhouse gas only simulations are of particular interest because observations of both mean and extreme temperature in this region show a cooling trend from 1901-2012, referred to as the "warming hole" (e.g. Hartmann et al. 2013; Meehl et al. 2012; Leibensperger et al. 2012; Donat et al. 2013). Previous studies focusing on the warming hole have identified several potential natural and anthropogenic causes of this feature, such as changes in local hydroclimate (Portmann et al. 2009; Weaver 2013), changes in sea surface temperature

forcing from the Pacific and Atlantic (Meehl et al. 2012; Weaver 2013), and cooling induced by aerosol forcing (Leibensperger et al. 2012; Yu et al. 2014). In the GFDL CM3 model, which is one of the few CMIP5 models that captures the warming hole (Kumar et al. 2013; Pan et al. 2013), the persistence of a muted temperature response in the southeast U.S. over multiple decades, and across multiple ensemble members and different forcing scenarios, suggests a characteristic response to radiative forcing in this model, rather than internal variability or cooling due to anthropogenic aerosols. Further analysis of this feature is presented in Chapter 3.

2.3.2 Precipitation extremes

Overall, aerosols tend to reduce precipitation in the U.S. while greenhouse gases tend to increase it (Figure 2.4). However, the spatial distribution of changes in precipitation varies by season and type of forcing. This finding is consistent with previous modeling studies that found that the precipitation response pattern is dependent on the type of forcing agent and its spatial distribution (e.g. Kloster et al. 2009; Shindell et al. 2012). Wintertime extreme precipitation in the eastern U.S. increases significantly in GHG (18 mm in the southeast and 7.2 mm in the northeast) and decreases significantly in AER (−14 mm in the southeast and −4.5 mm in the northeast), with a spatial anti-correlation ($r = -0.62$; Figure 2.4a,b). Changes elsewhere in the U.S. are not significant in winter. In the spring, extreme precipitation in AER decreases slightly in the eastern U.S., but it is not significant (Figure 2.4d). However, in GHG, springtime extreme precipitation increases over most of the central and eastern U.S.A (Figure 2.4e). In this season, the anti-correlation between AER and GHG is weak ($r = -0.24$), suggesting that different mechanisms determine the springtime impacts of aerosols and greenhouse gases

on extreme precipitation. Changes in HIST are shown for both seasons for completeness, but are not significant due to cancellations between the effects of aerosols and greenhouse gases (Figure 2.4c,f). Changes in extreme precipitation in summer and fall are less significant than those in winter and spring (not shown).

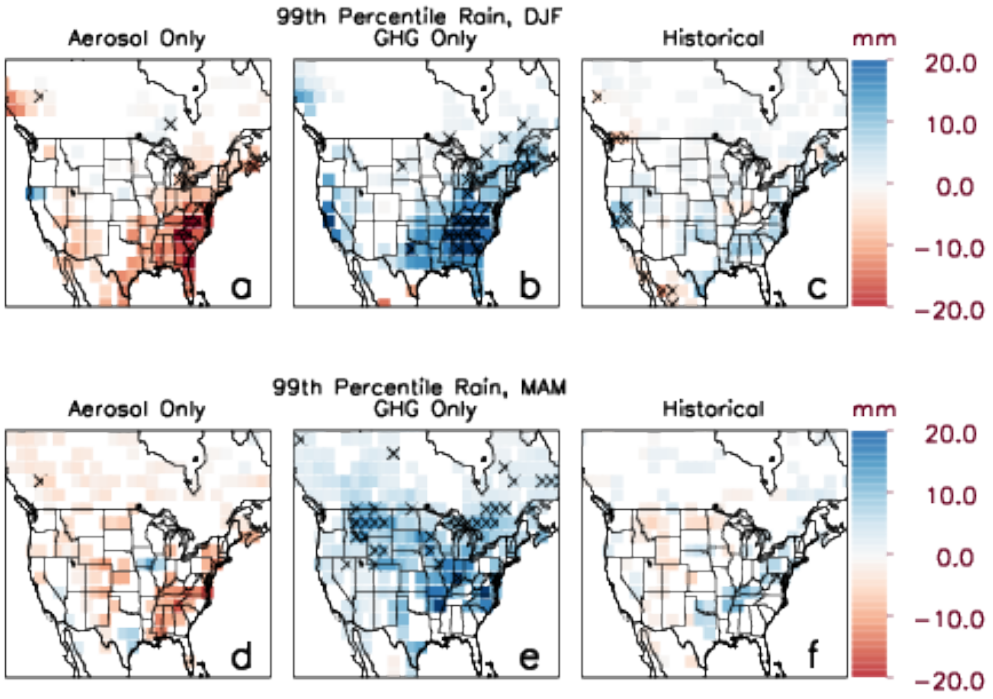

Figure 2.4 Changes in the 30-year ensemble mean values of R99p between the beginning (1860-1889) and end (1976-2005) of the aerosol only (left), greenhouse gas only (middle) and historical (right) scenarios in winter (top) and spring (bottom). Statistical significance testing is as in Figure 2.3

2.4 Future changes in U.S. temperature and precipitation extremes

2.4.1 Extreme temperatures become the new normal

Under the RCP8.5 scenario, in which anthropogenic radiative forcing reaches approximately 8.5 W m^{-2} by 2100 (relative to the pre-Industrial), the well-mixed greenhouse gases increase steadily throughout the 21st century, while emissions of short-lived pollutants (aerosols, and aerosol and tropospheric ozone precursors) decrease

dramatically due to air quality regulations (Riahi et al. 2011). By mid-century, the warming signal associated with the combined effects of increasing greenhouse gas concentrations and decreasing aerosol concentrations is apparent over the U.S., with increases in TX90p on the order of 40 to 50 days per summer (Figure 2.5a,b), and increases in TXx between 2.5 to 6.0°C (Figure 2.5c,d). The combined effects of increasing greenhouse gases and removing the masking by anthropogenic aerosols produce much larger changes than in either HIST or in the observed changes over the historical period (Donat et al. 2013; Sillmann et al. 2013b). The large increase in TX90p in the southeast U.S. at the start of the 21st century is a consequence of the shape of the temperature distribution in the region and does not indicate rapid warming. By the end of the 21st century, TX90p saturates with respect to the 1961-1990 climatology and almost all summer days lie above the 90th percentile thresholds. TXx also increases substantially by 5 to 10°C across the U.S. These results are consistent with projected increases in monthly mean temperature over the U.S. of 6±3°C in the CMIP5 multi-model mean (Maloney et al. 2014). For both TX90p and TXx, the spatial pattern of the temperature response in the 21st century is similar to the GHG simulation (not shown). Significant warming occurs everywhere by mid-century, although the southeast U.S. warms more

slowly than the rest of the country.

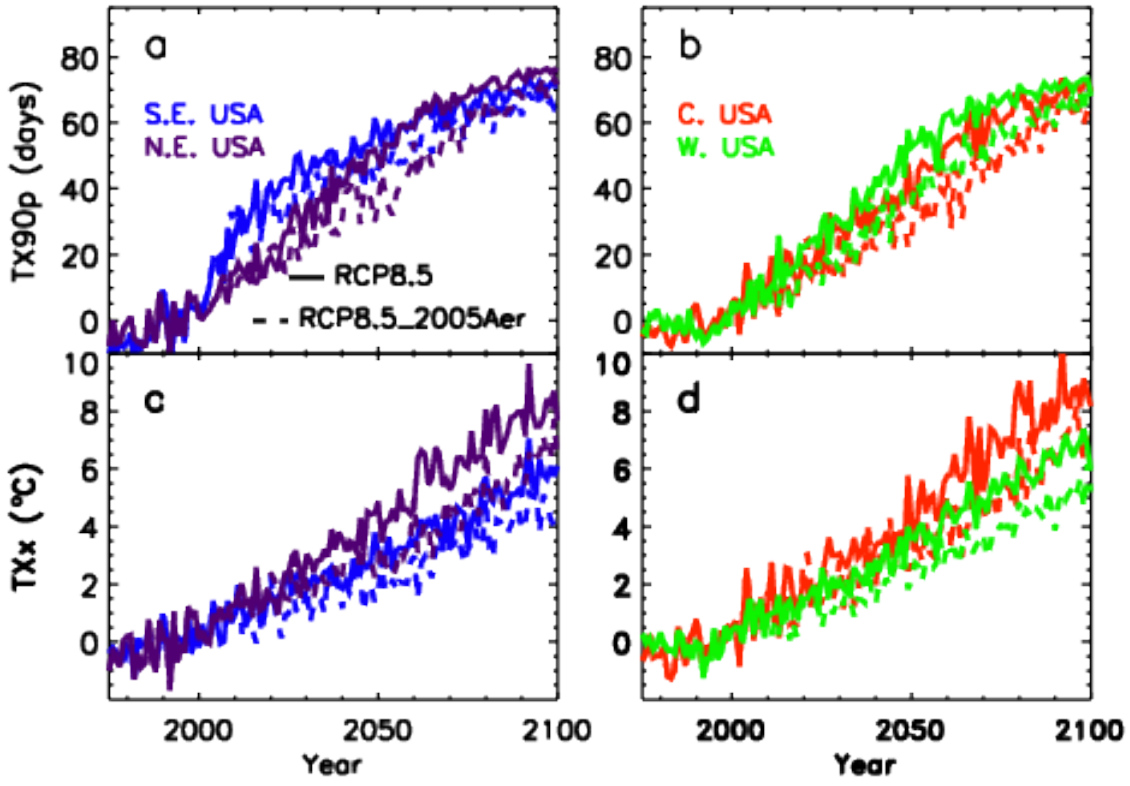

Figure 2.5 Summertime TX90p (top) and TXx (bottom) for RCP8.5 (solid) and RCP8.5_2005Aer (dashed) for different regions in the U.S., expressed as anomalies with respect to 1976-2005. The tapering off in TX90p at the end of the 21st century is an artifact of the index becoming saturated with respect to the 1961-1990 thresholds.

We investigate next how long it will take before future anthropogenic climate change can be expected to exceed the range of modeled internal variability (which does not occur in HIST due to cancellation between aerosols and greenhouse gases). We define the time of emergence as the first year when the difference between the 30-year mean centered on that year and the end of the twentieth century (1976-2005) is outside of the range of variability in the pre-Industrial control simulation at the 95% confidence level (following the approach described previously). For both TX90p and TXx, the climate change signal becomes detectable within the first few decades of the 21st century over most of the U.S (Figure 2.6a,b). In some regions, such as the western U.S. and the

northeast U.S., the signal has emerged within 15 years of the reference period (1976-2005), consistent with the rapid increases shown in Figure 2.5.

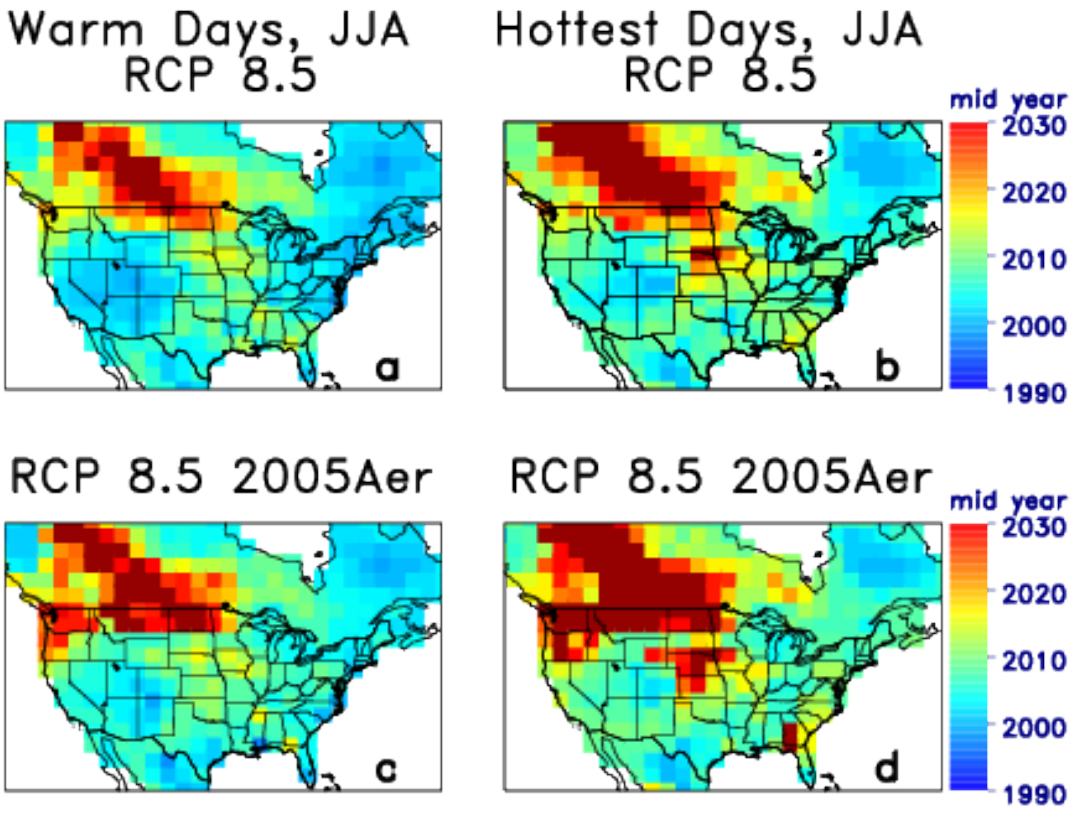

Figure 2.6 Time of emergence for changes in 30-yr mean TX90p (a)(c) and TXx (b)(d) relative to the present day (1976-2005) for the RCP8.5 (top) and RCP8.5_2005AER (bottom) scenarios. Colors indicate the midpoint of the earliest 30-yr period for which the difference is outside the range of natural variability between 30-year periods within the pre-Industrial control run (see Section 2.2).

In order to separate the effects of decreasing aerosol concentrations and increasing greenhouse gas concentrations, we examine a second future scenario, RCP8.5_2005Aer, in which greenhouse gas concentrations follow the RCP8.5 trajectory while aerosols are held constant at 2005 levels. The dashed lines in Figure 2.5 show that holding aerosols constant reduces future increases in TX90p and TXx relative to RCP8.5. By mid-century, TX90p is reduced by an average of 15 days per summer in the eastern U.S., and by an average of 10 days per summer in the central and western U.S. (RCP8.5

– RCP8.5_2005AER). By the end of the 21st century, TX90p is reduced by an average of 10 days per summer over the continental U.S., although even with aerosols held constant at 2005 levels, the index is approaching saturation. Similarly, the continued presence of aerosols at 2005 levels reduces mid-century increases in TXx by 1.5°C over the eastern U.S., and 1.0°C over the central and western U.S. By the end of the century increases in TXx are reduced by 1.5°C (RCP8.5 – RCP8.5_2005AER) in the southeast U.S., and 1.75°C in the rest of the U.S. on average.

Even with aerosols held constant at 2005 levels, statistically significant increases in extreme temperatures still occur over the continental U.S. due to rising greenhouse gases. By mid-century, TX90p increases by 25 to 35 days per summer across most of the U.S., and by 55 to 65 days per summer by the end of the century (RCP8.5_2005AER), when more than two thirds of the summer days are above the 1961-1990 90th percentile threshold. TXx increases by 2.5 to 3.5°C by mid-century, and by 5 to 6°C by the end of century, reflecting the dominant influence of greenhouse gases. For both indices, the time of emergence (Figure 2.6c,d) is delayed by at most 5 years over most of the U.S. when aerosols are maintained at 2005 levels.

2.4.2 Extreme precipitation: shifting towards a wetter future

Future changes in extreme precipitation also show patterns associated with the greenhouse gas signal evident from the 1860-2005 GHG simulation. By the end of the 21st century, wintertime R99p has increased significantly over the eastern and northwest U.S. (Figure 2.7). In the southeast and northeast U.S., R99p increases by 32 mm and 42 mm respectively (Figure 2.7a), while it increases in the western U.S. by 18 mm (Figure 2.7b). In spring, R99p increases significantly over the eastern and north-central U.S.

(Figure 2.7c,d). By the end of the 21st century, springtime R99p has increased by 30 mm in the southeast U.S., and by 40 mm in the northeast U.S. (Figure 2.7c). On average, comparing 2070-2099 to 1976-2005, springtime R99p increases by 9.5 mm in the central U.S. (Figure 2.7d), but with a region in the north-central U.S. that increases by 30 mm (not shown). Summertime changes in extreme precipitation are generally not significant (not shown). Finally, in fall, there are statistically significant increases in R99p in the northeast and northwest, averaging 25 and 15 mm by end of century respectively (Figure 2.7e,f). In contrast with winter and spring, there are generally no statistically significant changes in total precipitation in this season (not shown) indicating a change in the shape of the overall distribution of precipitation, with a tendency towards more extreme precipitation.

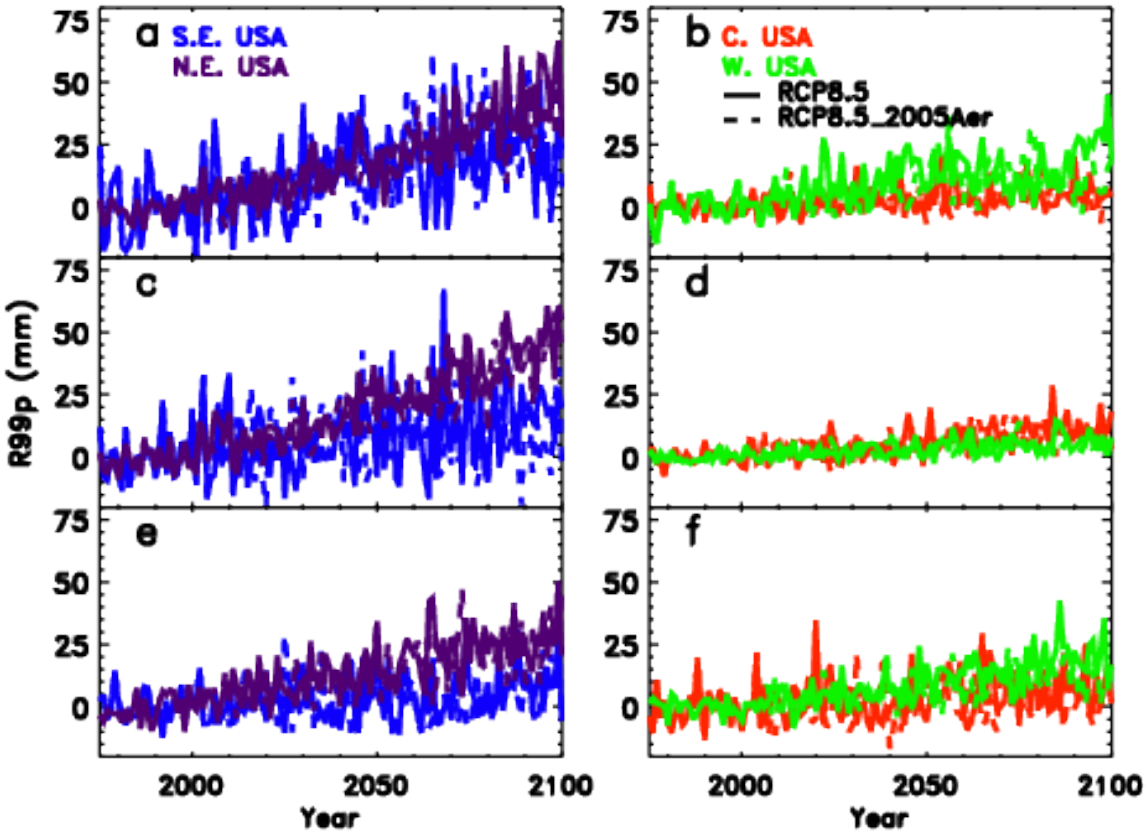

Figure 2.7 Winter (top), spring (middle), and fall (bottom) R99p for RCP8.5 (solid) and RCP8.5_2005Aer(dashed) for different regions in the U.S., expressed as anomalies with respect to 1976-2005.

The climate change signal is slower to emerge for precipitation than for temperature. The changes emerge as significant early in the 21st century in the eastern U.S. in winter and spring (Figure 2.8a,b); in the western U.S. in winter, the signal emerges by 2050; and in autumn, the signal emerges late in the 21st century in the Midwest and Pacific Northwest (not shown). The impacts of reductions in aerosol concentrations on extreme precipitation are minimal over the 21st century (Figure 2.7),

and changes in the time of emergence are small (Figure 2.8c,d).

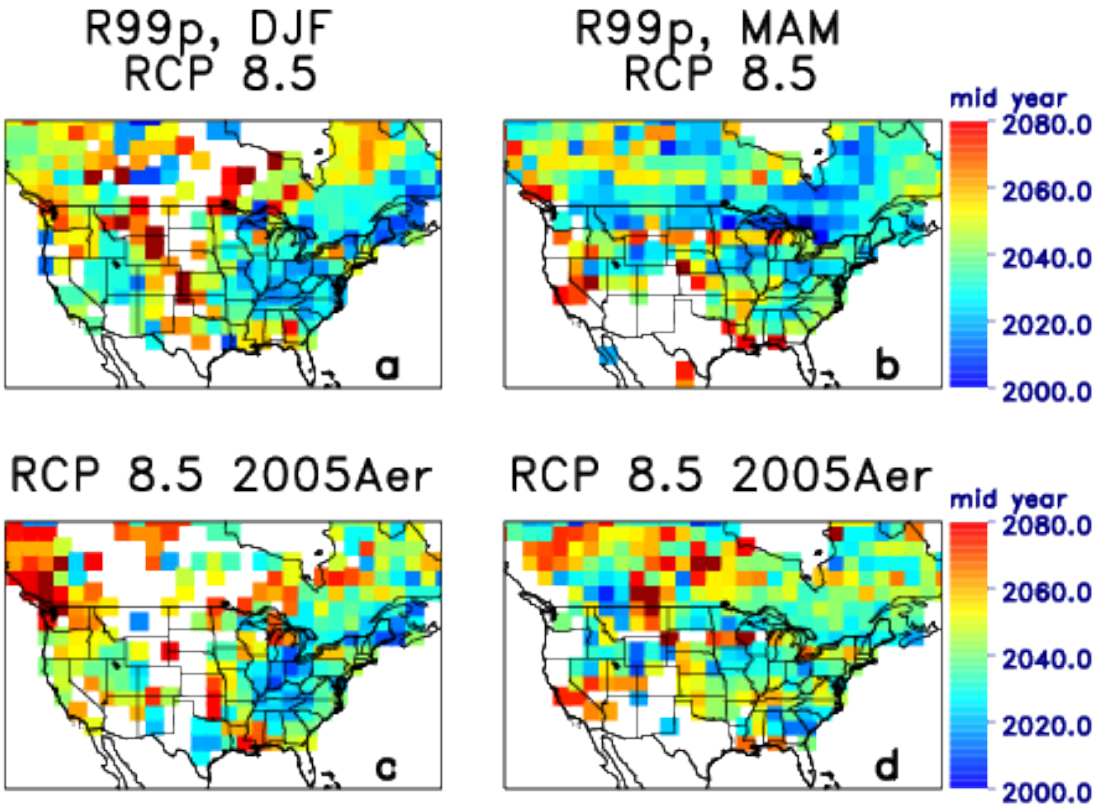

Figure 2.8 Time of emergence for changes in 30-yr mean R99p for winter (left) and spring (right) relative to the present day (1976-2005) for the RCP8.5 (top) and RCP8.5_2005Aer (bottom) scenarios. White areas over the continent denote regions where the signal does not emerge over the 21st century.

2.5 Conclusions

We use the ETCCDI extreme climate indices as a metric for investigating changes in extreme temperature and precipitation in the U.S. High temperature extremes in the U.S. generally decrease in response to aerosols and increase in response to greenhouse gases. We identify clear regional patterns of response to forcing: the western U.S. has the strongest response to both aerosols and greenhouse gases, while the weakest response occurs in the southeast U.S. (Figure 2.3). This compares well with observations of temperature trends in the U.S., and lends confidence to the model representation of

spatial patterns of temperature extremes, despite the excessively strong aerosol indirect effects (Golaz et al. 2013; Meehl et al. 2012; Sheffield et al. 2013).

Overall, simulated precipitation changes during the historical period concentrate in the eastern and central U.S., the regions where the model best captures the observed patterns of the present day precipitation climatology (Sheffield et al. 2013). In the CM3 model, aerosols tend to reduce extreme precipitation, while greenhouse gases tend to increase it, particularly in the spring (Figure 2.4). Although changes in the historical simulation are not significantly different from zero, we note that in the GHG simulation there are large increases in R99p in the Midwest, particularly in spring. This coincides with observed statistically significant increases in extreme precipitation in the Midwest in spring, suggesting that the observed trend may be attributable to greenhouse gases (Kunkel et al. 2008).

The signal associated with greenhouse gases emerges clearly by the end of the 21st century for all indices in the extreme warming scenario, RCP8.5, although due to the strength of the aerosol effects in CM3 it is likely that extreme temperature (over the U.S.) and precipitation (over the eastern U.S.), increase too rapidly in the first half of the 21st century. As a result of the combined effects of increasing greenhouse gas concentrations and decreasing aerosol emissions (but primarily the former), by the end of the century, the entire summer lies above the 90th percentile of daily maximum temperature from 1961-1990. Seasonal extreme precipitation in winter and spring in the northeast and central U.S. increases by up to 40 mm. In fall, extreme precipitation increases in the northeast and northwest U.S. despite a lack of significant changes in total precipitation, indicating a change in the shape of the precipitation distribution. Total summertime

precipitation increases in the southeast U.S., although there are no significant changes in extreme precipitation in that region.

Extreme events have major impacts on human health and economics. In order to predict future changes in these damaging events, we need to improve our understanding of how extreme temperature and precipitation respond to different types of anthropogenic forcing. In the GFDL CM3 model, there are no statistically significant changes in these extremes in the full historical simulation during 1860-2005. However, using single-forcing simulations for the same time period, we find that anthropogenic aerosols and greenhouse gases individually have significant impacts on extremes. The cancellation between the effects of aerosols and greenhouse gases results in the absence of statistically significant changes in the historical simulations, although it is likely that this masking by aerosols is too strong in the model. In the future, as aerosol emissions decrease and greenhouse gas concentrations continue to increase, the impacts of anthropogenic climate change on extreme weather in the U.S. will emerge.

Chapter 3 Timing and seasonality of the United States "warming hole"

[Mascioli, N. R., A. M. Fiore, M. Previdi, and M. Ting (2017), Timing and seasonality of the United States "warming hole", *Env. Res. Lett.*, 12, 3, 034008, doi:10.1088/1748-9326/aa5ef4]

3.1 Introduction

Global surface temperatures have increased by 0.85°C over the past century while temperatures in the southeast and central United States have cooled slightly (Hartmann et al. 2013). This long-term U.S. cooling, referred to as the "warming hole", has been investigated in a number of observational and model-based studies (Appendix **Error! Reference source not found.**). These studies examine different time periods, seasons, and metrics, and therefore yield conflicting results as to whether the warming hole is primarily a response to natural variability or anthropogenic forcing. Here we begin to reconcile these disparate studies by providing a systematic approach to characterizing U.S. temperature trends. We demonstrate that anthropogenic aerosols have a significant impact on the warming hole in summer, particularly during the 1950-1970 period, while negative temperature trends during the winter in the second half of the 20th century contain signals of internal climate variability in the ocean and atmosphere.

Past studies have shown that the warming hole is likely influenced by changes in rainfall, soil moisture, and cloud cover over the southeast and central U.S. (Leibensperger et al. 2012; Meehl et al. 2012; Misra et al. 2012; Pan et al. 2004; Portmann et al. 2009;

Robinson 2002; Weaver 2013; Yu et al. 2014). These hydrological processes, in turn, may be affected by remote changes in Pacific and Atlantic sea surface temperatures (SSTs), either due to internal variability or anthropogenic forcing (Kunkel et al. 2006; Leibensperger et al. 2012; Meehl et al. 2012; Robinson 2002; Weaver 2013), and/or by the regional effects of anthropogenic aerosols (Leibensperger et al. 2012; Yu et al. 2014) and land use changes (Misra et al. 2012) over the U.S. Changes in biogenic aerosol abundances may also contribute to the warming hole in summer (Goldstein et al. 2009), but currently available observations and models are insufficient to test this hypothesis.

An important element of this discussion is the lack of a single consistent definition of the warming hole across these various studies. Depending on the time period, season, and temperature index considered, the warming hole is found in the central (Kunkel et al. 2006; Pan et al. 2004; Robinson 2002; Wang et al. 2009; Weaver 2013), the north central (Pan et al. 2013; Portmann et al. 2009), the southeast (Portmann et al. 2009; Meehl et al. 2012; Misra et al. 2012; Hartmann et al. 2013), or the eastern (Meehl et al. 2012; Donat et al. 2013) United States (Appendix Table 3.3). The region of focus matters because surface temperatures in different regions of the U.S. respond to different physical mechanisms; for example, central U.S. surface temperatures are strongly influenced by changes in local hydroclimate driven by shifts in the Great Plains low-level jet (Leibensperger et al. 2012; Pan et al. 2004; Weaver 2013) in response to changes in Pacific and Atlantic SSTs (Weaver 2013; Weaver and Nigam 2008), whereas the northeast U.S. is sensitive to changes in the summer storm tracks (Folland et al. 2009). Similarly, variability in winter and summer surface temperatures in the U.S. is driven by different mechanisms: we expect North Atlantic Oscillation (NAO) variability

to be more pronounced in winter (Hurrell et al. 2003), while anthropogenic aerosol forcing is stronger in summer due to greater insolation. Finally, as shown in Figures 3.1 and 3.2, spatial patterns of observed temperature trends over the U.S. vary significantly over different time periods. Over the long-term period 1901-2005, the western and northern regions of the U.S. have warmed more rapidly than the eastern and southern regions of the U.S. in both seasons, a feature which global climate models typically do not capture (Kumar et al. 2013; Kunkel et al. 2006). However, as shown in the center and right panels of Figures 3.1 and 3.2, regions of cooling shift to the central, southern, and eastern U.S. over different time periods. The variability in the spatial distribution of temperature trends in Figures 3.1 and 3.2 serves to highlight the need for a comprehensive exploration of the warming hole over different regions, seasons and time periods.

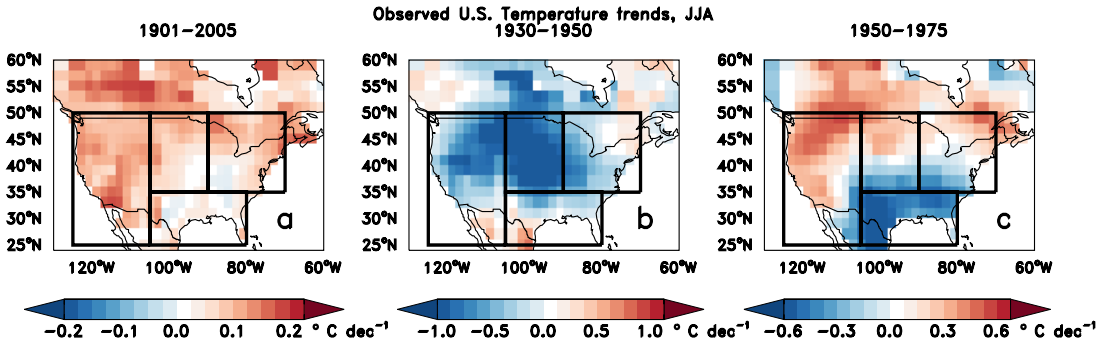

Figure 3.1 Trends in observed (GISTEMP) surface air temperature (°C/decade) in summer from 1901-2005 (left), 1930-1950 (center), and 1950-1975 (right). The boxes denote the four regions discussed in the paper: the northeast U.S. (35 – 50°N, 70 – 90°W), the southern U.S. (25 – 35°N, 80 – 105°W), the north central U.S. (35 – 50°N, 90 – 105°W), and the western U.S. (25 – 50°N, 105 – 125°W).

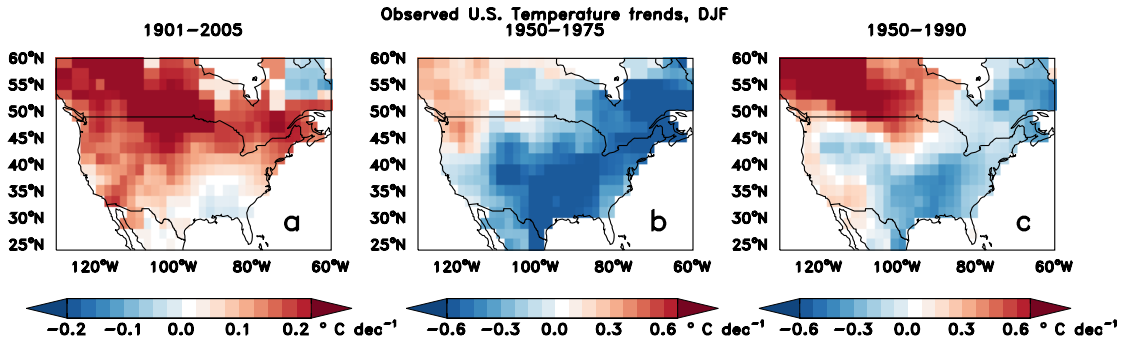

Figure 3.2 As in Figure 3.1, but for winter

Kumar et al. (2013) use a moving 30-year window to investigate the dependence of the warming hole on the time period over which temperature trends are computed. We build upon this analysis by systematically examining temperature trends of different lengths for different regions and seasons, assessing the dependence of the trends on the selected start and end years, and identifying physical driving mechanisms. In order to fully characterize the variability in U.S. temperature trends, we analyze winter and summer temperature trends over all possible periods of at least 10 years during 1901-2015 in the four regions shown in Figure 3.1: the northeast U.S. (35 – 50°N, 70 – 90°W), the southern U.S. (25 – 35°N, 80 – 105°W), the north central U.S. (35 – 50°N, 90 – 105°W), and the western U.S. (25 – 50°N, 105 – 125°W). These regions are chosen to highlight the areas of maximum cooling in summer in the 1930-1950 and 1950-1975 periods. We show that temperature trends in the U.S. depend on different factors in different seasons and time periods: anthropogenic aerosols play a role in the observed summer warming hole, while the winter warming hole is driven by the Pacific Decadal Oscillation (PDO) and the NAO.

3.2 Data and methods

We examine observed U.S. monthly mean surface temperature trends from the GISTEMP dataset (Hansen et al. 2010), on a 2°×2° latitude/longitude grid, available from 1880-2015. Linear temperature trends (ten years or longer) are computed using the ordinary least squares method. We assess the statistical significance of trends using a standard t-test, adjusting the sample size to account for autocorrelation as in Santer et al. (2000). Additionally, we analyze observed temperature trends using the HadCRUT4 (Morice et al. 2012) and NCEP GHCN (Fan and van den Dool 2008) datasets. Our conclusions are robust and independent of the dataset used (not shown).

We compare observed surface temperature trends with simulations from 11 global climate models (CanESM2, CCSM4.0, CESM1 CAM5, CSIRO Mk3.6.0, FGOALS-g2, GFDL-CM3, GFDL-ESM2M, GISS-E2-H, GISS-E2-R, IPSL-CM5A-LR, NorESM1-M; see Table 3.1 for details and references) that represent a subset of models from the Coupled Model Intercomparison Project Phase 5 (CMIP5; Taylor *et al* 2012). The 11 models were selected because they each performed a full historical simulation (HIST), with all natural and anthropogenic forcings varying from 1850-2005; an "aerosol only" simulation (AER), with anthropogenic aerosols as the only time-varying forcing and all other forcings held at pre-Industrial levels; and a "greenhouse gas only" simulation (GHG), with anthropogenic greenhouse gases as the only time-varying forcing. There is large uncertainty in the forcing due to anthropogenic aerosols, but the models considered here cover the range from weak/moderate aerosol forcing (FGOALS-g2, IPSL-CM5A-LR, GISS-E2-R) to strong aerosol forcing (GFDL-CM3, CESM1 CAM5; Boucher *et al* 2013). We compute the multi-model mean by using the first ensemble member from each

of the 11 models so as not to skew the results to favor the forced response from models with larger ensembles. Trends are computed as trends in the multi-model mean.

Table 3.1 ***List of CMIP5 models used in this study. Each model performed a historical, aerosol only, and greenhouse gas only simulation.***

Model name	Reference	Resolution (lat × lon)
Second Generation Canadian Earth System Model (CanESM2)	Environment Canada (2010)	64 × 128
Community Climate System Model, version 4.0 (CCSM4.0)	Gent et al. (2011)	192 × 288
Community Atmosphere Model, version 5.0 [CESM1(CAM5)]	Neale et al. (2012)	192 × 288
Commonwealth Scientific and Industrial Research Organisation Mark, version 3.6.0 (CSIRO Mk3.6.0)	Rotstayn et al. (2009)	96 × 192
The Flexible Global Ocean Atmosphere Land System model (FGOALS-g2)	Li et al. (2013)	60 × 128
Geophysical Fluid Dynamics Labrotary Climate Model, version 3 (GFDL-CM3)	Donner et al. (2011)	90 × 144
GFDL Earth System Model with MOM4 ocean component (GFDL-ESM2M)	Dunne et al. (2012)	90 × 144
Goddard Institute for Space Studies model E coupled with the HYCOM ocean model (GISS-E2-H)	Schmidt et al. (2014)	90 × 144
GISS model E coupled with the Russell ocean model (GISS-E2-R)	Schmidt et al. (2014)	90 × 144
L'Institut Pierre-Simon Laplace Coupled Model, version 5 coupled with NEMO (low resolution) (IPSL-CM5A-LR)	Dufresne et al. (2013)	96 × 96
Norwegian Earth System Model, version 1 (NorESM1-M)	Bentsen et al. (2013)	96 × 144

We additionally examine the effect of SST forcing on U.S. temperature trends using a 16-member ensemble of Global Ocean Global Atmosphere (GOGA) simulations (Guo et al. 2017). The GOGA simulations were performed with the National Center for Atmospheric Research Community Atmosphere Model version 5 (NCAR CAM5), with an Eulerian spectral dy-core in T42 horizontal resolution and 30 vertical levels. The NCAR CAM5-GOGA experiment is coupled to the interactive Community Land Model version 4 (CLM4) and the Los Alamos Sea Ice Model version 4 (CICE4) with prescribed sea ice concentrations. The observed Hadley center SST and sea ice (Rayner et al. 2003) for the period 1870 to 2014 are prescribed over the global oceans. These simulations are designed to test the atmospheric response to observed changes in SSTs and evaluate the contribution of SSTs to the warming hole.

3.3 Location and timing of the summer warming hole: A role for aerosols and internal variability

We begin by examining U.S. surface temperature trends during summer. The panels on the left of Figure 3.3 show the observed trends in mean summer temperatures in each U.S. region (see Figure 3.1) as a function of the start (horizontal axis) and end years (vertical axis). In the north central U.S., the sign of the long-term trends (50 or more years) depends on the time period considered. Trends starting in the 1930s are negative (see also Figure 3.1b), while those starting before or after the 1930s are generally positive (Figure 3.3a). The 1930s were an exceptionally hot and dry decade in the U.S., commonly known as the “Dust Bowl”. For example, the summers of 1934 and

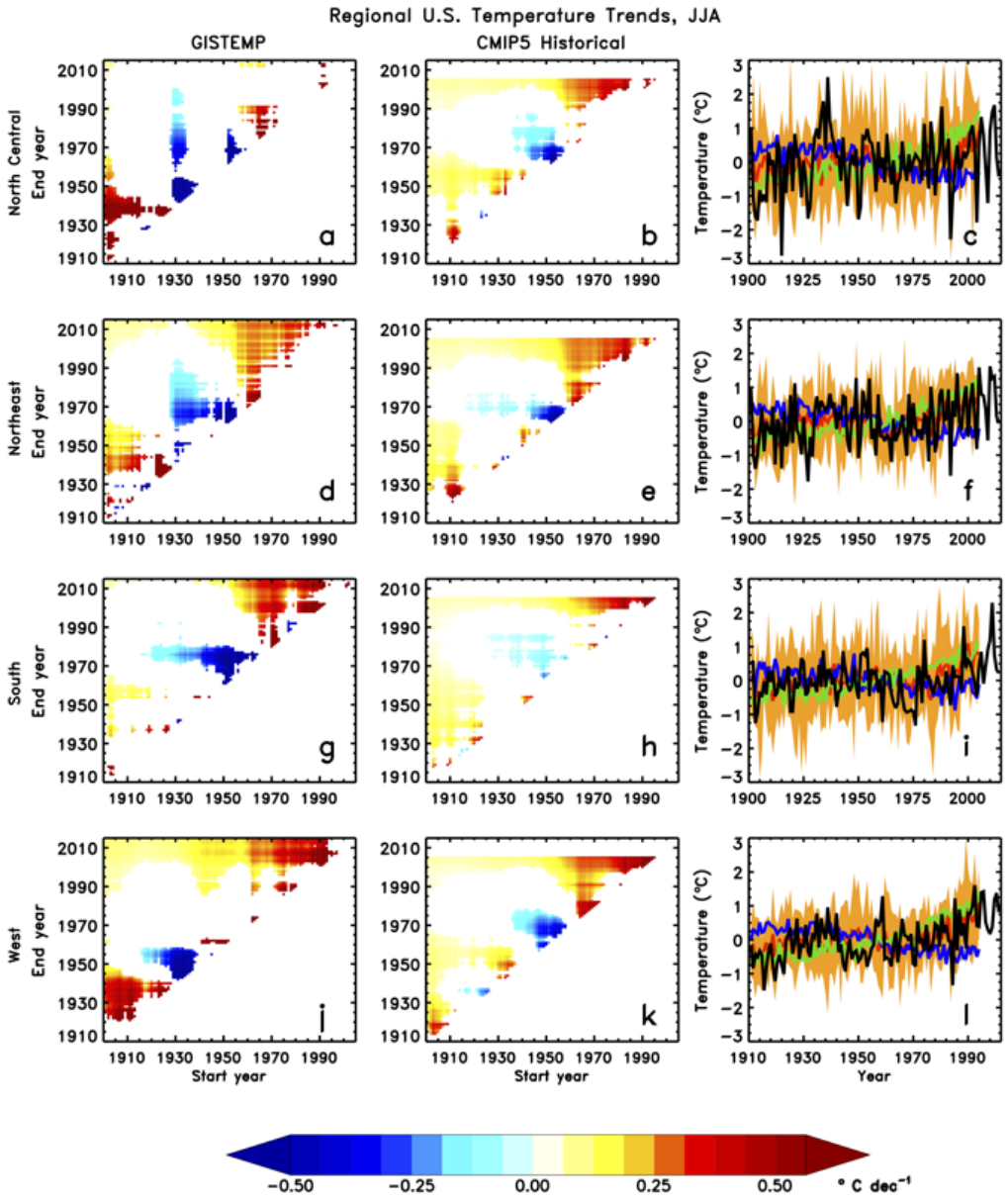

Figure 3.3 Trends in summertime mean surface temperatures (°C /decade) from GISTEMP (left) and the multi-model mean historical forcing scenario from CMIP5 (middle) in the north central U.S. (a,b), northeast U.S. (d,e), southern U.S. (g,h), and western U.S. (j,k). The colours show the value of the trend as a function of the start and end years of the time period considered. Trends that are not significantly different from zero at the 95% confidence level are whited out. The right panels show the regional time series of summertime mean temperature anomalies from GISTEMP (black), the historical all forcing scenario (red), the aerosol only scenario (blue), and the greenhouse gas only scenario (green). Orange shading shows the range of the individual models in the historical scenario. All temperatures are anomalies with respect to 1901-2005.

1936 remain two of the hottest on record, particularly in the north central U.S. (Donat et al. 2013; Peterson et al. 2013). The Dust Bowl was most likely the result of internal variability in Pacific SSTs (Donat et al. 2015; Schubert et al. 2004; Seager et al. 2008), potentially amplified by dust aerosol and land use changes (Cook et al. 2009), and/or by internal atmospheric variability (Hoerling et al. 2009). Negative summertime temperature trends in the north central U.S. starting in the 1930s reflect their start date occurring during the Dust Bowl, and can be interpreted as a recovery from this anomalously warm decade. Trends in the northeast are also influenced by a period of high temperatures in the 1930s associated with the Dust Bowl (Figure 3.3d). This should be borne in mind when considering studies (Kunkel et al. 2006; Leibensperger et al. 2012) that analyze temperature trends starting in this time period. Long-term summertime temperature trends in the southern U.S. starting prior to 1955 are generally not significant (Figure 3.3g). Temperatures decrease from the 1950s to the mid 1970s in all three regions, most strongly in the southern U.S. Long-term temperature trends ending in the 2000s in the western U.S. are uniformly positive (Figure 3.3j).

Table 3.2 ***Correlation coefficients (r) between the observed and CMIP5 multi-model mean regional surface temperature time series from 1901-2005. Bolded values are significant at the 95% confidence level. The significance of correlations is evaluated with a t-test.***

	Summer (JJA)	Winter (DJF)
North Central U.S.	0.10	0.13[a]
Northeast U.S.	**0.26**	0.13[a]
South U.S.	**0.29**	-0.12
Western U.S.	**0.40**	0.13[a]

[a]*significant at 90% confidence level*

The CMIP5 HIST multi-model mean captures the timing of transitions between positive and negative trends in observed summertime temperatures in the northeast and southern U.S. over the latter half of the 20th century (compare Figure 3.3e,h with Figure 3.3d,g). Outside of the north central U.S., where the observed summer temperature trends are strongly influenced by the 1930s Dust Bowl, the multi-model mean temperature time series is significantly correlated with the observed temperature (Table 3.2). This correlation suggests a role for external forcing in driving temperature trends in the U.S., as by averaging over the CMIP5 ensemble, we are increasing the signal (anthropogenic climate change) to noise (internal variability) ratio. We note, however, that the magnitude of the modeled trends is generally less than observed, implying that internal variability (reduced by averaging) also contributed to the observed trends, and/or that the forced response is too weak in the CMIP5 models. The multi-model mean, which tends to average out internal variability, does not produce a Dust Bowl, and therefore does not reproduce the observed cooling in the north central U.S. beginning in the 1930s. CMIP5 models capture the positive hundred-year temperature trends in the western U.S., implying a forced response to rising greenhouse gases (Figure 3.3k,l). Outside of the north central U.S., temperature trends from 1970 onwards are significantly positive in both the observations and the CMIP5 multi-model mean. This is most likely due to increased positive forcing from greenhouse gases combined with reductions in the

negative forcing due to aerosols (Figure 3.3, Figure 3.4).

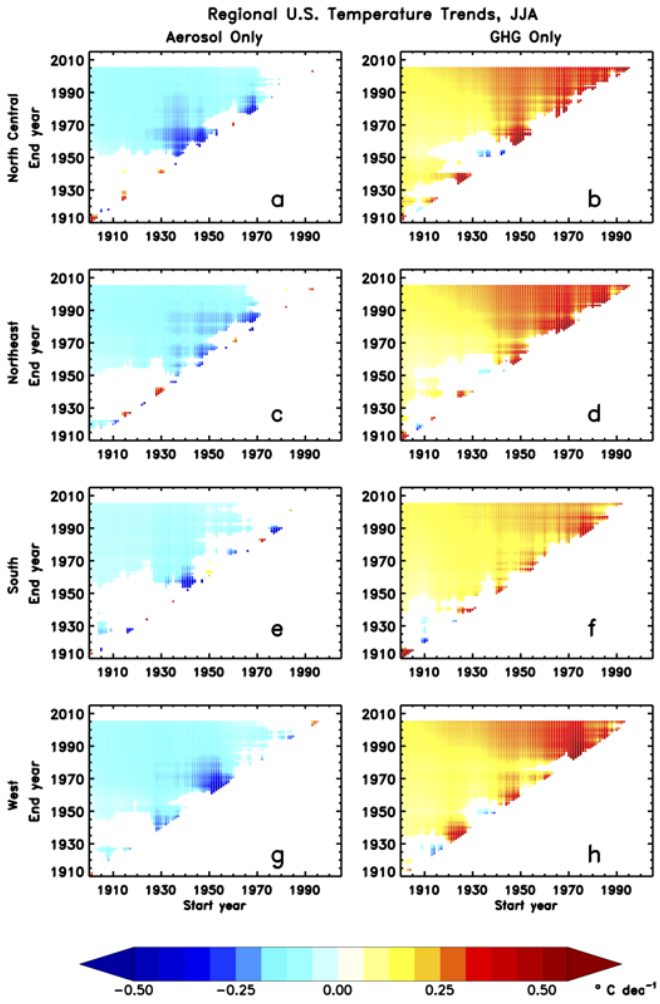

Figure 3.4 Modeled summertime mean surface temperature trends (°C /decade) in AER (left), and GHG (right) in the north central U.S. (a,b), northeast U.S. (c,d), southern U.S. (e,f), and western U.S. (g,h). The colors show the value of the trend as a function of the start and end years of the time period considered. Trends that are not significantly different from zero at the 95% confidence level are whited out.

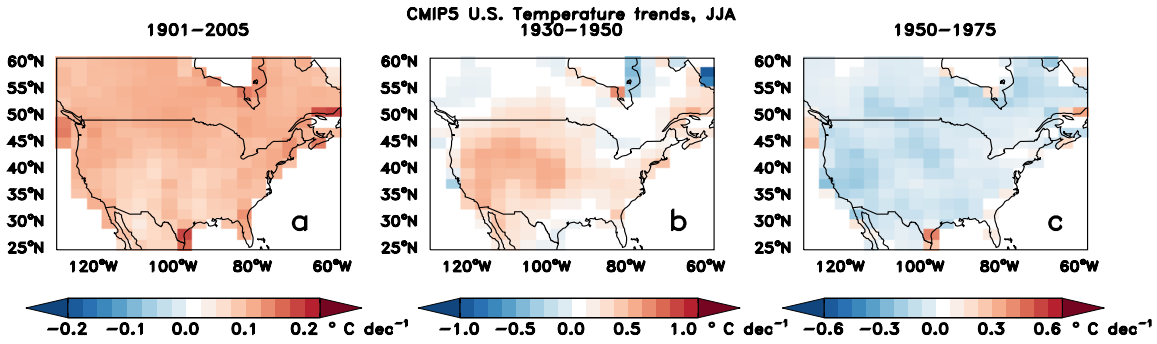

Figure 3.5 As in Figure 3.1, but for the CMIP5 multi-model mean (HIST)

As the second half of the twentieth century has been a focus in the warming hole literature, we examine this period more closely. Several studies have attributed the U.S. warming hole to forcing by U.S. anthropogenic aerosols (Leibensperger et al. 2012; Yu et al. 2014). Figure 3.3 shows significant observed cooling from the 1950s to the mid-1970s in the southern and northeast U.S. and to a lesser extent in the north central U.S. (see also Figure 3.1c). These trends are qualitatively captured by the CMIP5 models. In the northeast U.S., the HIST scenario captures most of the magnitude of the observed trends from the 1950s (start dates between 1950 and 1954) to the mid 1970s (end dates between 1973 and 1976), with a median ratio of modeled to observed trends of 0.69. In the southern U.S., HIST captures the timing of the negative trends, but does not produce the full magnitude of the observed trends with a median ratio of 0.17. The HIST, AER, and GHG scenarios in Figure 3.3c,f,i, and Figure 3.4 indicate that the mid-century cooling trends in the CMIP5 models are at least in part a forced response to rising anthropogenic aerosols.

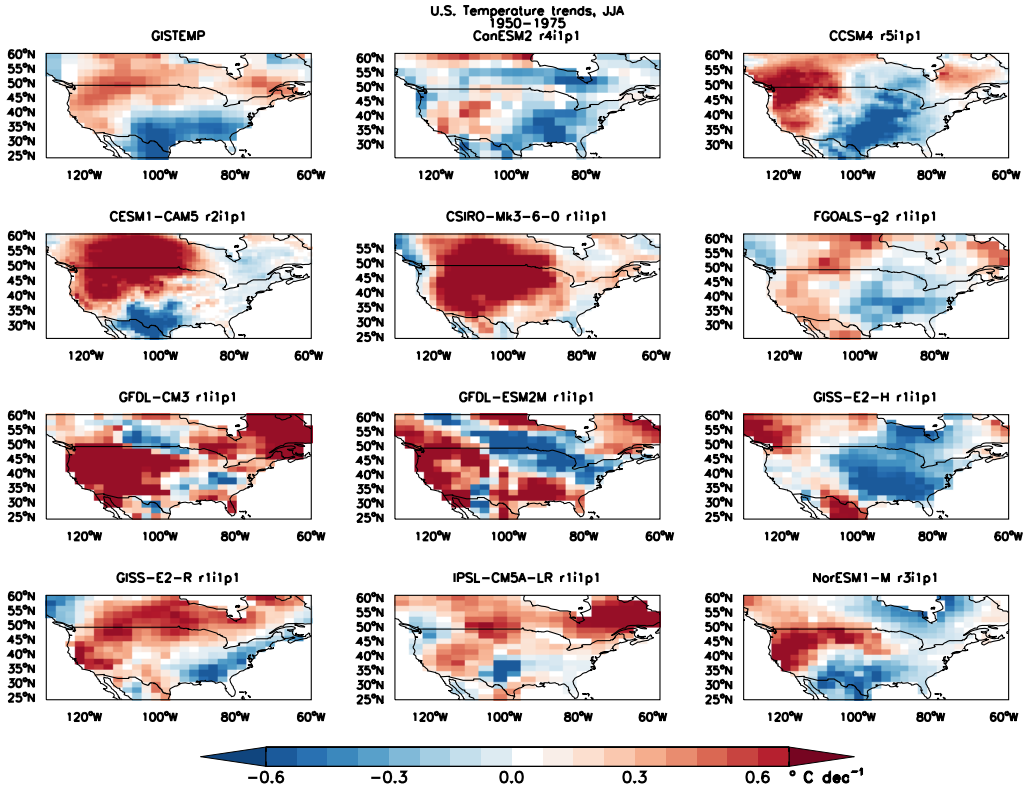

Figure 3.6 Comparisons between observed and modeled summertime mean surface temperature trends (°C /decade) from 1950-1975. For each model considered, we show the ensemble member with the highest spatial correlation with respect to the observations. Note that this does not represent the subset of ensemble members used to compute the CMIP5 multi-model mean.

Although the CMIP5 multi-model mean qualitatively captures the observed cooling in the southern and northeast U.S. during 1950-1975, it does not reproduce the observed spatial pattern of temperature trends during this period (Figure 3.5c vs. Figure 3.1c). However, the observations represent a single realization of the climate system, while the multi-model mean is a composite of 11 models that averages over internal variability with the goal of identifying the forced response. When we compare the observations to individual ensemble members from each model, we can find in many of the models at least one ensemble member that captures features of the observed warming hole, with cooling in the eastern and/or southern U.S. (Figure 3.6). We also find in many

of the models at least one ensemble member that produces a pattern that is spatially anti-correlated with the observations, with warming in the eastern and/or southern U.S. (Figure 3.7). We conclude that cooling in the U.S. during this period is influenced by anthropogenic aerosols, but that the specific spatial pattern of observed temperature change, with cooling in the south central and eastern U.S. and warming in the western U.S., is likely to be strongly influenced by internal variability.

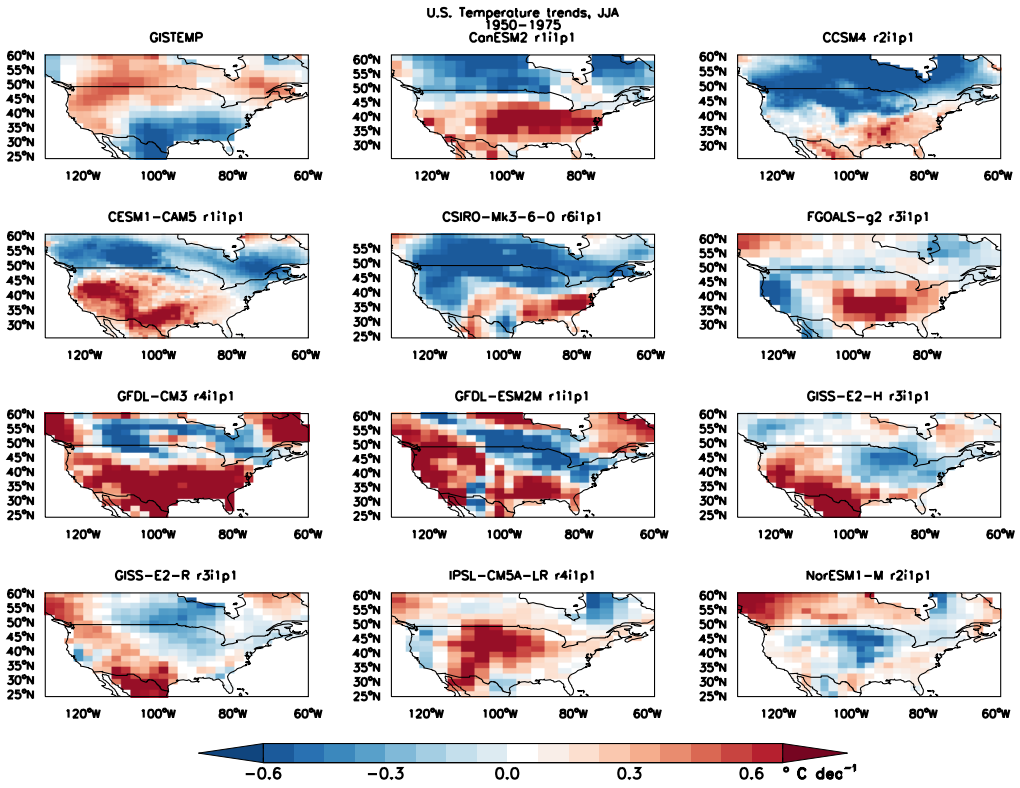

Figure 3.7 As in Figure 3.6, but showing the ensemble members with the smallest correlation with the observations

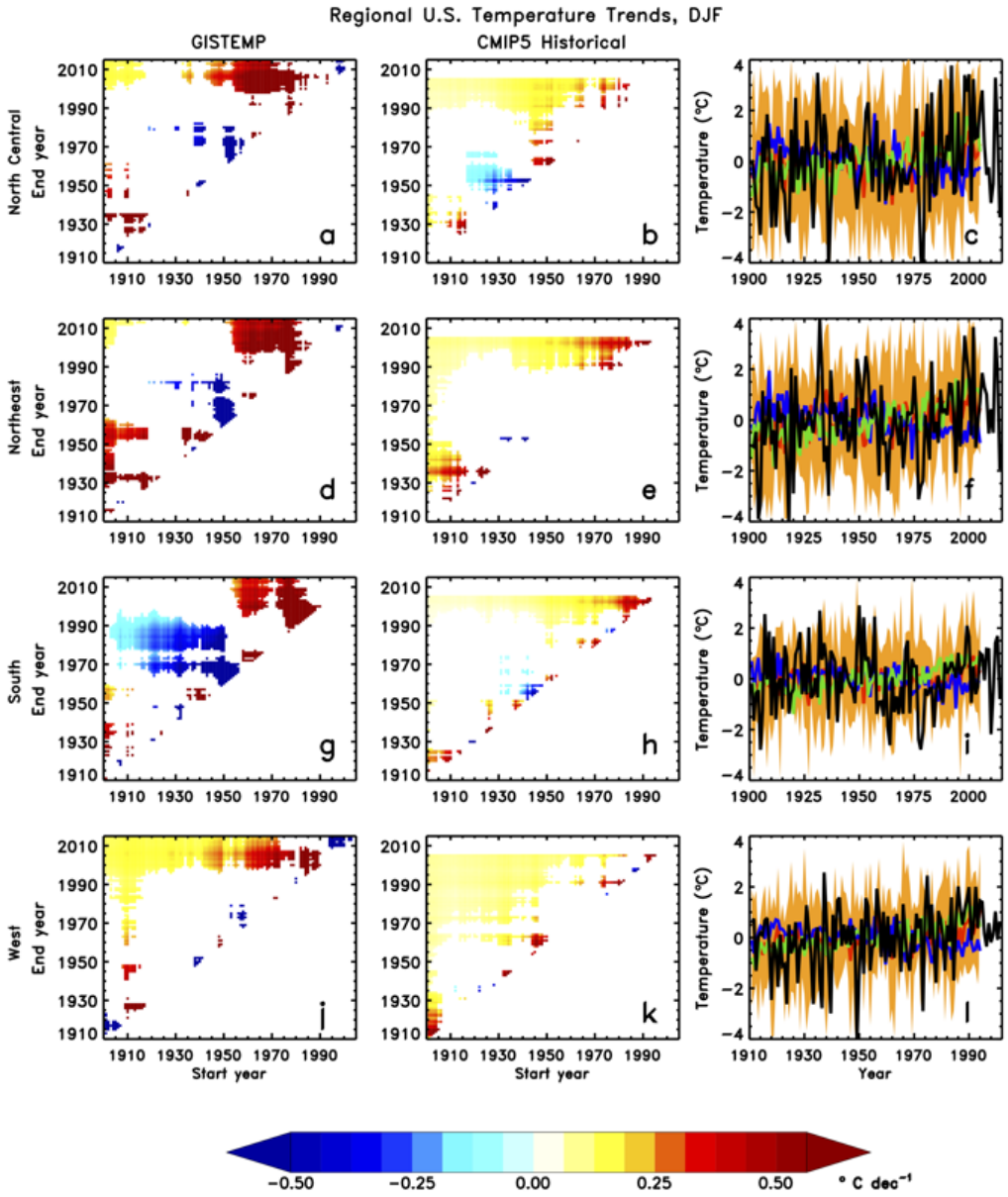

Figure 3.8 As in Figure 3.3, but for winter

3.4 Winter cooling trends linked to the PDO and NAO

Interannual variability of surface temperature is significantly enhanced in winter as compared with summer (Figure 3.8), confounding detection of significant temperature trends on decadal-to-multidecadal time scales. Observed long-term wintertime temperature trends in the north central U.S. depend somewhat on the start and end year,

but are generally positive (Figure 3.8a). In the northeast and southern U.S., long-term trends beginning prior to 1950 are generally small or negative, while significant warming occurs between 1950 and the present. As was the case in summer, the observed long-term wintertime temperature trends in the western U.S. are generally positive. Notably, there is significant mid-century cooling over most of the U.S., most pronounced in the southern U.S., which we examine further below.

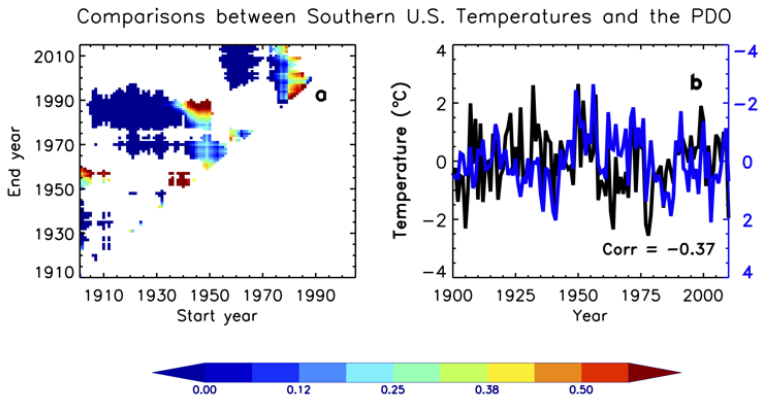

Figure 3.9 Comparisons between observed wintertime surface temperature in the southern U.S. and the PDO index (Zhang et al 1997). (a) The ratio of the temperature trends in the regressed PDO index (see text) to the observed trends. Time periods where the observed trend is insignificant are whited out. (b) The time series of the observed temperature anomalies (black) and the PDO Index (blue). All time series are anomalies with respect to 1901-2005.

The left and middle columns of Figure 3.8, as well as the correlation values in Table 3.2, indicate that the CMIP5 multi-model mean does not capture the observed mid-century negative temperature trends in the northeast and southern U.S., suggesting that these trends may be the result of internal variability rather than a forced response. In agreement with the results of Meehl et al. (2012) and Weaver (2013), we find that observed winter temperatures in the southern U.S. are significantly anti-correlated with the PDO index from 1901 to 2010 ($r = -0.37$, Figure 3.9). Given this relationship, we can estimate the contribution of the PDO to regional temperature trends by first regressing the regionally averaged temperature T against the PDO index such that:

$$T = \alpha \times PDO + \beta + \varepsilon \quad (1)$$

where α and β are estimated using detrended temperature and PDO time series and ε represents the residuals. The component of the regional temperature trend that is linearly congruent with the PDO is then given by:

$$\left[\frac{dT}{dt}\right]_{PDO} = \alpha \times \frac{dPDO}{dt} \quad (2)$$

where *dPDO/dt* is the trend in the PDO index. Using this approach, we estimate that multidecadal changes in the PDO, which are marked by a shift from negative to positive around 1976/77, contribute to as much as half of the observed negative temperature trend from 1950-1990 in the southern U.S. (Figure 3.9a). The shift of the PDO from positive to negative also accounts for 25-50% of the observed positive temperature trends in this region from the 1980s to present (Figure 3.9; Meehl et al. 2015).

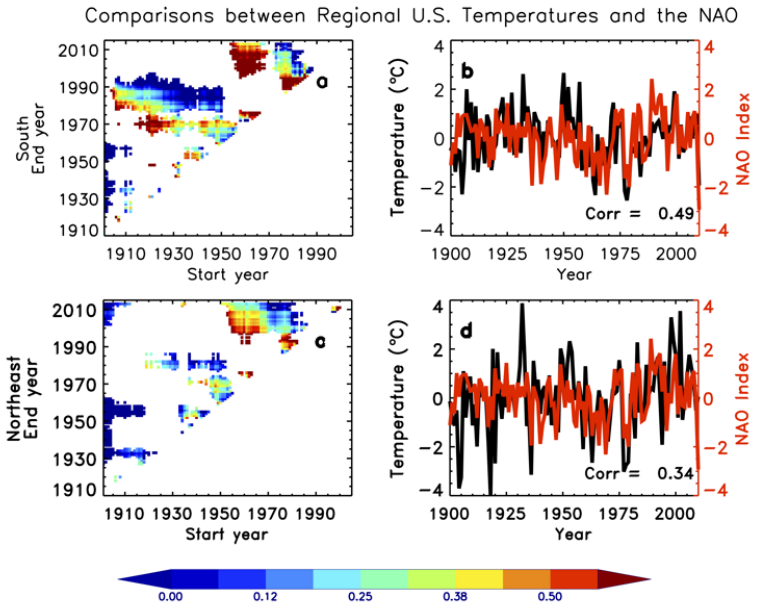

Figure 3.10 Comparisons between observed wintertime surface temperature and the NAO index for the southern U.S. (top) and northeast U.S. (bottom). (left) The ratio of temperature trends in the regressed NAO index (Hurrell and Deser 2009) to the observed temperature trends. Time periods where the observed trend is insignificant are whited out. (right) The time series of the observed temperature anomalies (black) and the NAO index (red). All time series are anomalies with respect to 1901-2005.

Another primary source of variability in U.S. winter temperatures is the North Atlantic Oscillation (NAO). Figure 3.10 shows that winter temperatures in the southern U.S. (r = 0.49) and northeast U.S. (r = 0.34) are significantly correlated with the NAO index. Computing the contribution of the NAO to U.S. regional temperature trends using the same method described above for the PDO, we find that the NAO accounts for 25-45% of the observed cooling in the southern and northeast U.S. between 1950-1970. Additionally, the decadal trend in the NAO explains anywhere from 20-75% of the observed positive temperature trends between 1970 and 2010 (in particular explaining 50-75% of the trends between 1970 and 1990) in the southern and northeast U.S.

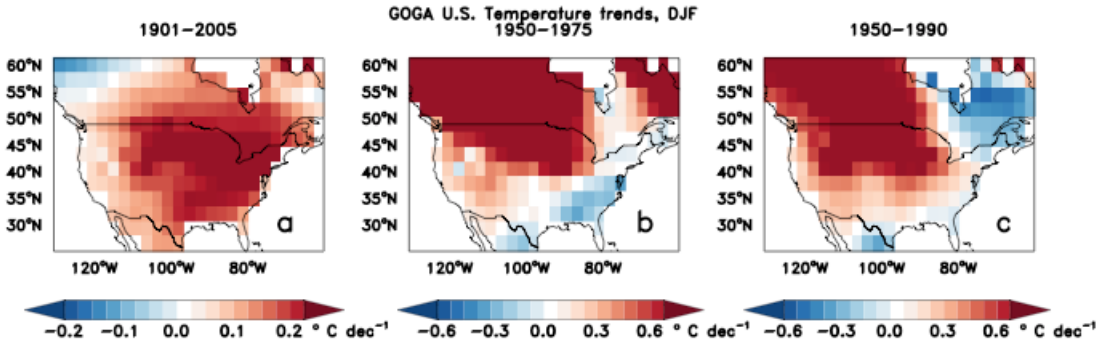

Figure 3.11 Trends in wintertime surface air temperature (°C/decade) in the ensemble mean of the CAM5 GOGA simulations from 1901-2005 (left), 1950-1975 (center), and 1950-1990 (right)

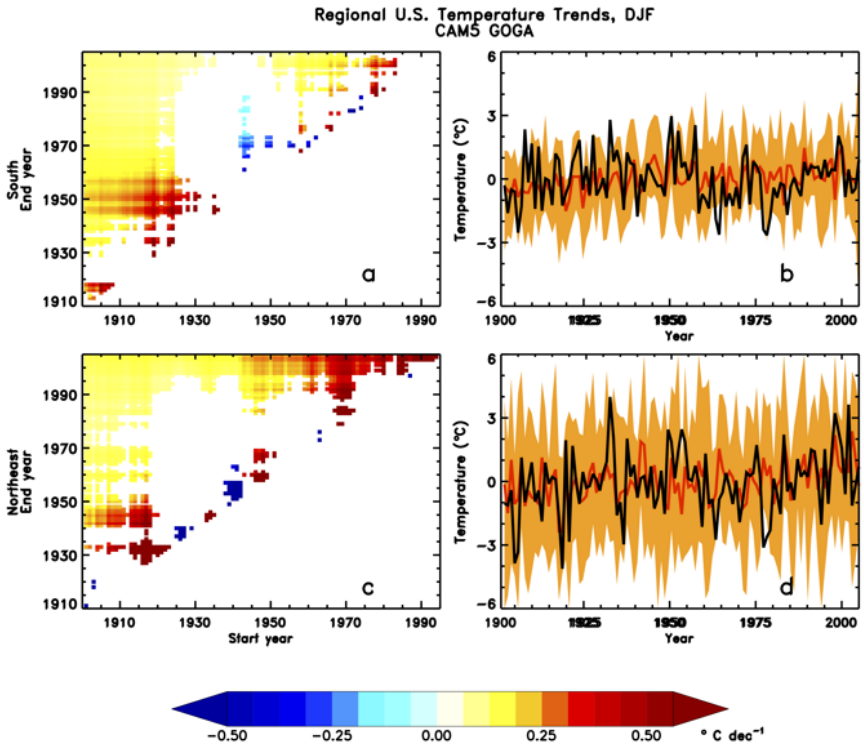

Figure 3.12 Trends in wintertime mean surface temperatures from the ensemble mean of the GOGA runs (left) in the southern U.S. (top) and northeast U.S. (bottom). The colors show the value of the trend as a function of the start and end years of the time period considered. Trends that are not significantly different from zero at the 90% confidence level are not plotted. The right panels show the regional time series of wintertime mean temperature anomalies from GISTEMP (black) and the GOGA mean (red). Orange shading shows the range of the individual ensemble members in the GOGA simulations. All temperatures are anomalies with respect to 1901-2005.

In order to assess the role of SST forcing in driving winter temperature trends in the U.S., we examine a set of GOGA simulations that were performed with NCAR CAM5 (see Section 3.2). An important side note when considering these simulations is that the SST trends used to drive the CAM5 model reflect the influences of external forcings such as anthropogenic aerosols, greenhouse gases, and volcanic eruptions, as well as internal variability. We find that while the GOGA simulations do not capture the full magnitude and spatial extent of the observed mid-century cooling over the U.S., they do produce negative temperature trends in the southern and eastern U.S. during this time period (Figure 3.11b,c, Figure 3.12). The weaker magnitude of the mid-century cooling

in the GOGA simulations may contribute to the lack of a warming hole in the southern U.S. in GOGA over the entire period, 1901-2005 (compare Figure 3.2a and Figure 3.11a; see also Figure 3.12). The GOGA simulations do not pinpoint which region(s) of the global oceans is driving the cooling trends, but the timing is consistent with the PDO as discussed previously (Figure 3.9). We conclude that either the observed mid-century cooling is not entirely forced by the observed SST patterns, or that the model is not realistically representing the atmospheric response to SST changes.

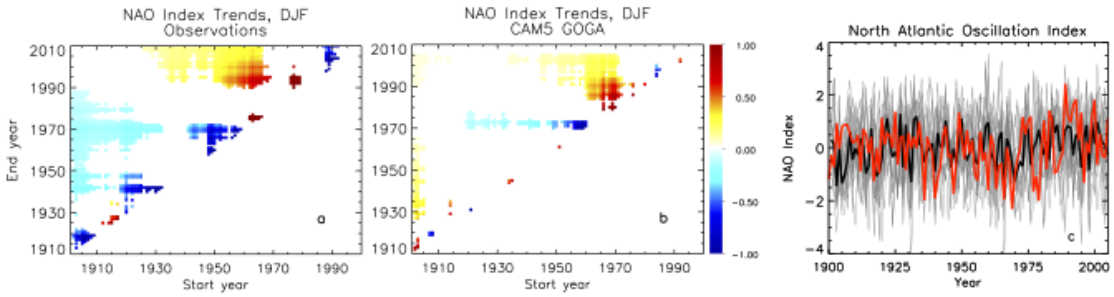

Figure 3.13 Trends in the North Atlantic Oscillation (NAO) index in observations (a) and the ensemble mean of the CAM5 GOGA simulations (b). Panel (c) shows the time series of the observed (red) and modeled NAO (black). Individual ensemble members are shown in grey.

We further evaluate the role of atmospheric variability in the GOGA simulations by calculating the NAO index in each ensemble member. We find that the ensemble-average correlations between the NAO and regional temperature in the southern U.S. (r=0.35) and northeast U.S. (r = 0.35) are realistic, although smaller than the observed relationship in the southern U.S. (r = 0.49). The ensemble mean captures some of the observed temporal features of the NAO index, including a negative trend between 1950-1970, and a positive trend between 1965-2005, but it does not capture the full magnitude of the observed negative trends (Figure 3.13). This finding suggests that variability in the NAO may be partially SST forced and further that a portion of the significant observed

cooling in the southern U.S. from 1950-1970 may reflect of modulation of the NAO by SST changes.

3.5 Conclusions

Prior studies attribute the United States "warming hole" to internal variability in Atlantic and Pacific SSTs or to changes in external forcing from either anthropogenic aerosols or land use principally through their effects on rainfall, soil moisture, and cloud cover (see Appendix **Error! Reference source not found.**). In this study, we reconcile these competing explanations by demonstrating the importance of considering the seasonality and temporal evolution of temperature trends when studying the U.S. warming hole as well as considering an additional mechanism, the NAO, which has not been investigated previously.

In summer, we find that both external forcing and internal variability are important for understanding the observed warming hole. Significant observed summertime cooling trends occur during 1950-1975 in the southern and northeast U.S. We find that anthropogenic aerosols are significant contributors to this cooling. This finding is in agreement with previous research by Yu et al. (2014), who argued that aerosols were a significant driver of cooling trends in the eastern and southern U.S. from 1950-1985 through their effects on clouds. It is also consistent with the findings from Leibensperger et al. (2012), who performed a time slice experiment simulating the 1970-1990 time period to show the potential aerosol impacts on temperature in the eastern and central U.S. through their effects on regional circulation patterns. Aerosol forcing over the U.S. diminishes after the mid-1970s (Figure 3.4a), and so studies that examined longer time periods of 50 or more years (Meehl et al. 2012; Pan et al. 2013; Wang et al.

2009; Weaver 2013) or time periods starting in the 1980s or later (Robinson 2002) overlooked this effect.

While aerosols likely contributed to the observed summer warming hole, the full spatial pattern of temperature change, characterized by cooling in the southern and northeast U.S. and warming in the western U.S. (Figure 3.1c), is likely shaped largely by internal variability. Wang et al. (2009), Meehl et al. (2012), and Weaver (2013) attribute the observed cooling in the second half of the twentieth century to heating anomalies in the eastern Pacific, associated with the PDO, while Weaver (2013) additionally highlights changes in North Atlantic SSTs affecting the strength of the Great Plains low level jet. Internal variability also drives the observed negative temperature trends in the north central and northeast U.S. beginning in the 1930s. These regions where strongly influenced by the anomalously warm Dust Bowl of that decade which was most likely caused by variability in Pacific SSTs (Donat et al. 2015; Schubert et al. 2004; Seager et al. 2008).

Observed wintertime temperature trends are driven mainly by changes in internal modes of climate variability, with no evidence of a significant effect from aerosol forcing. We regress the observed PDO and NAO indices against the observed regional temperature record to determine the fraction of the observed temperature trends that can be explained by these modes. The PDO explains as much as half of the observed wintertime cooling over the southern U.S. during 1950-1990, supporting past studies linking the winter warming hole to Pacific SSTs (Meehl et al. 2012; Robinson 2002; Wang et al. 2009). The NAO, in contrast, which has not been examined in previous

studies, is a better predictor of southern and northeast U.S. cooling from the 1940s and 1950s to the mid 1970s, explaining up to 50% of the observed temperature trends.

The NAO and the PDO may in turn be affected by external forcing. For example, Allen et al. (2014) show that the CMIP5 multi-model mean captures the observed positive trend in the PDO from 1950-1979 and negative trend from 1979-2009, suggesting anthropogenic forcing is influencing this mode of variability. In particular, they find that forcing from anthropogenic aerosols can account for approximately two-thirds of the observed positive PDO trend from 1950-1979, which we associate with winter cooling in the southern U.S. (Figure 3.9). Smith et al. (2016) argue that Asian aerosols have influenced the PDO through their impacts on the Aleutian Low. Regarding the NAO, the large magnitude of interannual (unforced) variability makes detection and attribution of forced trends difficult. However, CMIP5 multi-model means project that the NAO index will increase over the twenty-first century in response to climate change (Gillett and Fyfe 2013), with some studies also suggesting that increasing (decreasing) anthropogenic aerosols may contribute to negative (positive) trends in the NAO (e.g. Chiacchio et al. 2011, Pauseta et al. 2015).

Observed temperature trends from the mid-1970s to the present are consistently positive across the U.S. in both winter and summer. In summer, these warming trends are likely due to the leveling off of global aerosol emissions and the decrease in U.S. aerosol emissions, in combination with the continued rise in greenhouse gas concentrations (see Figure 3.3). Future emissions scenarios project continuing decreases in aerosol emissions (van Vuuren et al. 2011), so we expect that multi-decadal periods with regional summertime cooling, such as observed during the twentieth century, will

become less likely. In winter, the change in phase of the PDO and the NAO is most likely driving the reversal in U.S. temperature trends after the mid-1970s (Meehl et al. 2015). The winter warming hole may recur when the PDO and/or NAO change phase again in the future.

Appendix

Table 3.3 ***Summary of the existing literature discussing the U.S. warming hole. Different studies have analyzed different time periods, seasons, and regions.***

Publication	Data	Index	Timing	Season	Location	Attribution
Robinson et al (2002)	Observations from Hansen *et al* (2001)	Tmean	1988-1997	Annual	Central US	Warm tropical Pacific SSTs increase cloud cover and available precipitable water, contributing to regional cooling
	GISS model II forced with observed SSTs (global, tropical Pacific, midlatitudes)					
Pan et al (2004)	HadCM2 RegCM2	Tmax	2040s-1990s (model)	JJA	Central US	Low-level jets carry moisture from Gulf of Mexico to Central US, increasing precip, cloudiness, and soil moisture, leading to a muted warming response
	Observations from Folland *et al* (2001)		1976-2000 (obs)			
Kunkel et al (2006)	18 GCMs from 13 modeling groups.	Tmean	1930s-1970s	Annual	Central US	Internal variability alone is insufficient, but the models may not adequately capture teleconnections from Pacific SSTs
	Observations from Hansen *et al* (2001)		1940-1979	DJF JJA SON		
			1980-1999	MAM JJA SON		
			1901-1999	All seasons		
Portmann et al (2009)	US GHCND station data	Tmin, Tmax, Tmean TX10p[1], TX50p[2], TX90p[3],	1950-2006	MJ JA	Southeast US North central US	Significant correlations between US temperature trends and precipitation, but changes in precipitation alone are not sufficient

Publication	Data	Index	Timing	Season	Location	Attribution
Wang et al (2009)	CRU TS2.1 NSIPP-1 AGCM model forced with different EOF based SST patterns	Tmean	1950-2000	DJF MAM JJA SON	Southern US Southern US South/Central US Continental US	Observed Central US trends in late summer and fall due to SST trends and internal variability in SSTs
Leibensperger et al (2012)	GISTEMP GISS GCM3	Tmean	1930-1990 (obs) 1970-1990 (model, time slice)	Annual	Eastern US	US SO_2 emissions: Aerosols cooled the North Atlantic, influencing the large scale circulation from the Gulf of Mexico into the eastern/central US, reducing evaporation (in the eastern US), and increasing precipitation, soil moisture, cloudiness, and evaporation (in the central US)
Meehl et al (2012)	HadCRUT3 CCSM3	Tmean	1950-1999	Annual DJF JJA	Southern US[4] Eastern US Central and Southeast US	Winter explained by low-level temperature flux convergence driven by heating of the tropical Pacific In summer, heating of the tropical Pacific produces moisture flux convergence into the central US, increasing precipitation, evaporation, cloudiness, and soil moisture
Misra et al (2012)	US HCN2	Tmin, Tmax	1948-2010	Annual	Southeast US	Land use change (urbanization, irrigation) affect soil moisture content
Weaver (2012)	GHCN	Tmean	1950-2010	JAS	Central US	Relative changes in Pacific and Atlantic SSTs corresponding to the PDO and AMO[5], respectively, alter the position and strength of GPLLJ[6], affecting moisture transport

Publication	Data	Index	Timing	Season	Location	Attribution
Pan et al (2013)	CMIP5 models – historical all forcing and RCP4.5 GHCN interpolated onto 0.5x0.5 grid	Tmean, Tmax, Tmin	1901-2000 1951-2000 1976-2000 1951-1975	JJA DJF JJA DJF JJA DJF JJA	Central/Southeast US Southeast US Central US Southeast US Central US None Southeast US	No evidence of PDO driving warming hole (WH) pattern in models. Possible that local and regional surface processes may contribute to WH
Kumar et al (2013)	As in *Pan et al (2013)*	As in *Pan et al (2013)*	As in *Pan et al (2013)*	As in *Pan et al (2013)*	As in *Pan et al (2013)*	Models (CanESM2, GFDL-CM3, MIROC5) with greatest skill at reproducing aspects of the AMO also had greatest skill in simulating WH related features
Yu et al (2014)	GHCN 19 global coupled models from WCRP	Tmax, Tmin	1950-2011 1901-2011 1950-1985 2000-2011	JJA DJF JJA JJA JJA	Central/ Eastern US Southeast US Central US Eastern US Western US	Changes in summertime T_{max} are attributed to changes in SWCF driven by changes in the aerosol indirect effects.

[1]Number of days where the daily maximum temperature is above the climatological 10th percentile
[2]Number of days where the daily maximum temperature is above the climatological 50th percentile
[3]Number of days where the daily maximum temperature is above the climatological 90th percentile
[4]Western US warms more than Eastern US, cooling in southern US
[5]Atlantic Multidecadal Oscillation
[6]Great Plains low-level jet

Chapter 4 Response of regional atmospheric stagnation to changes in aerosol emissions

4.1 Introduction

Under persistent stagnant conditions, characterized by weak winds and an absence of precipitation, near-surface pollution (ozone and aerosols) and heat can build up to extreme levels that are dangerous for human health. In 2015 alone, ambient pollution from fine aerosol particles (PM2.5) caused an estimated 4.2 million deaths globally (Health Effects Institute 2017). Heat waves, particularly events with longer durations (4 days or more), also have severe impacts on human health (Anderson and Bell 2009). More than 70,000 deaths have been attributed to the 2003 European heat wave alone (Robine et al. 2008), and future heat extremes are projected to increase over the 21st century (Chapter 2, Meehl and Tebaldi 2004, Lau and Nath 2012, Sillman et al. 2013) to the point where in some regions it may become unsafe to be outdoors during a heat wave, even for healthy adults (Im et al. 2017). Anthropogenic aerosol emissions are projected to decrease during the remainder of the twenty-first century, which will improve air quality overall. However, these decreases have the potential to alter the frequency and duration of stagnation episodes and thus future occurrences of extreme pollution events and heat waves.

Atmospheric stagnation is a measure of the atmosphere's ability to remove heat and pollutants from the planetary boundary layer via precipitation and ventilation. On stagnant days, there is no precipitation, and surface and upper atmosphere winds are weak (see Section 4.2 for a formal definition). In the mid-latitudes, periods of

consecutive stagnant days allow pollution levels to build up, contributing to the occurrence of extreme pollution events (Jacob and Winner 2009; Sun et al. 2017; Tai et al. 2010). Stagnant conditions are typically associated with clear skies, allowing for increased surface solar heating and over time, the lack of precipitation will dry the land surface, contributing to heat waves (Kunkel et al. 1996; Meehl and Tebaldi 2004; Palecki et al. 2001).

Historically, trends have been observed in atmospheric stagnation and related meteorological conditions, such as cyclone frequency, in a number of regions. Mid-latitude cyclone frequency decreased significantly over the second half of the 20th century (McCabe et al. 2001; Wang et al. 2006), in particular over North America and the North Atlantic, increasing stagnation in Canada and the US (Gulev et al. 2001; Leibensperger et al. 2008; Zischka and Smith 1980), although the trends become insignificant when longer periods are considered due to increased cyclone activity from 2007-2010 (Turner et al. 2013). In China, the number of stagnant days per year (defined using wind speeds at pressure levels ranging from 300-500hPa to represent upper level air depending on surface topography) and the duration of individual stagnation events have both increased from 1985-2014, with the largest stagnation trends occurring over heavily populated regions in eastern China (Huang et al. 2017).

Overall, climate models project that atmospheric stagnation and related meteorological conditions will increase in the future under a warmer climate (Caserini et al. 2017; Horton et al. 2012; Horton et al. 2014; Leibensperger et al. 2008; Turner et al. 2013). For example, differential heating of the Northern Hemisphere relative to the Southern Hemisphere (e.g. due to anthropogenic aerosol forcing) will alter the large-scale

circulation (Allen et al. 2015; Hwang et al. 2013; Shindell et al. 2013; Westervelt et al. 2017), affecting the regional frequency of low wind days. In some regions, this may also alter the frequency of dry days by changing moisture transport into and out of the region (see for example discussion of the US warming hole in Chapters 2 and 3). Aside from the circulation effects, warming the climate will accelerate the hydrologic cycle, leading to regional changes in precipitation frequency (Allen and Ingram 2002; Trenberth et al. 2003). Removing aerosols may be particularly efficient at accelerating the hydrologic cycle (e.g. Kloster et al. 2009)

In order to build confidence in projected future changes in stagnation, and in particular to evaluate possible unintended effects of future air quality controls, it is important to understand the effects of aerosols on stagnation, which has received little attention in the literature. I examine aerosol effects on stagnation using a variety of global climate model simulations, including multiple "time-varying" past and future emissions scenarios from the fifth Coupled Model Intercomparison Project (CMIP5) and specialized sensitivity simulations ("timeslices) in which aerosol emissions are reduced in different source regions. Focusing on specific regions of interest (the United States, Europe, and China), I use these specialized sensitivity simulations to quantify the impacts of local vs. remote reductions in aerosol emissions(Westervelt et al. 2017), providing a better understanding of how regional air quality controls may affect stagnation both within that region and globally.

The data and model simulations are described in Methods (Section 4.2). Section 4.3 presents a stagnation analysis of the time-varying simulations. In Section 4.4, I

examine the impact of aerosols from specific source regions. I close with discussion and conclusions in Section 4.5.

4.2 Methods

4.2.1 Atmospheric stagnation index

I use the Wang and Angell (1999) method to define an atmospheric stagnation index. Air is considered stagnant on days when there is no precipitation, the wind speed at 500hPa is less than $13 ms^{-1}$, and the wind speed at the 10m reference height is less than $3.2 ms^{-1}$. If the temperature at 850hPa exceeds the temperature at the surface, indicating a temperature inversion and thus a stable boundary layer, the requirement for surface wind speed is relaxed by 10% (i.e. <3.5 ms^{-1}). When I calculate stagnation in climate models, I modify the precipitation requirement to be days with less than 1mm precipitation as in Horton et al. (2012) to account for models' tendencies to over-drizzle.

4.2.2 Observations

I calculate observed stagnation using wind, temperature, and precipitation fields from daily NCEP/NCAR Reanalysis 1 data (Kalnay et al. 1996) on a 2.5°×2.5° grid. To compare with model simulations of the present day, I calculate the 30-yr mean stagnation from 1985-2015.

4.2.3 Model simulations

I evaluate stagnation in a set of simulations performed with a state-of-the-art chemistry-climate model, GFDL-CM3. CM3 uses a cubed sphere grid with 48 vertical levels, with archived fields regridded to a 2° × 2.5° latitude–longitude grid. It is

composed of an atmospheric component (AM3), a modular ocean model (MOM), a dynamic land-vegetation model (LM3), and a sea-ice model (Donner et al. 2011). AM3 includes fully coupled tropospheric and stratospheric chemistry (Austin et al. 2013; Naik et al. 2013) as well as indirect effects of aerosols on clouds, including the cloud albedo effect (Twomey 1977) and the cloud lifetime effect (Albrecht 1989). The simulations analyzed in this study are described in detail below and summarized in Table 4.1.

Table 4.1 ***Summary of the set of GFDL-CM3 simulations analyzed in this chapter.***

Name	Shorthand	Description	Ensemble members	Years
Historical, all-forcing	HIST	Simulation of the historical period with time varying forcing	5	1860-2005
Historical, aerosol only	AER	Simulation of the historical period with time varying aerosol emissions and greenhouse gas concentrations fixed at preindustrial levels	3	1860-2005
Historical, greenhouse gas only	GHG	Simulation of the historical period with time varying greenhouse gas concentrations and aerosol emissions fixed at preindustrial levels	3	1860-2005
RCP 4.5	RCP4.5	Future simulation where net radiative forcing reaches ~4.5 Wm^{-2} by 2100	3	2005-2100
RCP 4.5, 2005 Aerosol and O_3	RCP4.5_WMGG	Future simulation where well-mixed greenhouse gases evolve as in RCP4.5 but aerosol and O_3 precursor emissions are held constant at 2005 levels	3	2005-2100
2000 Control	CTRL	Simulation of year 2000 conditions	1	400
2000 US SO_2 zero-out	zUS_SO2	As in CTRL, but with US SO_2 emissions zeroed out	1	220
2000 reduced	m80pChina_SO2	As in CTRL, but with Chinese SO_2 emissions	1	240

Chinese SO_2		reduced by 80%		
2000 reduced European SO_2	m80pEU_SO2	As in CTRL, but with European SO_2 emissions reduced by 80%	1	160

I evaluate stagnation from a set of simulations from GFDL-CM3performed as part of the 5th Coupled Model Intercomparison Project (CMIP5; Taylor et al., 2012). I use daily near surface wind speed, 500hPa wind speed, precipitation, near surface temperature, and 850hPa temperature from the historical all-forcing scenario (HIST; 5 ensemble members); the aerosol-only scenario, in which anthropogenic aerosols are the only time-varying forcing and all other forcings are held constant at pre-Industrial levels (AER; 3 ensemble members); the greenhouse gas only scenario in which greenhouse gases are the only time-varying forcing (GHG; 3 ensemble members). The HIST, AER, and GHG simulations cover the period 1860-2005.

I also analyze stagnation in two future simulations: RCP4.5 (3 ensemble members), in which the global-mean radiative forcing increases to approximately 4.5 Wm^{-2} by the year 2100 (Thomson et al. 2011); and RCP4.5_WMGG (3 ensemble members), in which well-mixed greenhouse gases follow the same trajectory as in RCP4.5, but aerosol and ozone precursor emissions are held constant at 2005 levels rather than decreasing, as in RCP4.5 (RCP4.5_WMGG is equivalent to RCP4.5* from John et al. 2012). Comparison between these scenarios allows us to quantify the climate response due to future reductions in aerosols and tropospheric ozone. I assess the significance of trends using a standard t-test adjusting the sample size to account for autocorrelation as in Chapter 3 and Santer et al. (2000).

Finally, I calculate stagnation in a set of "time-slice" sensitivity simulations performed with CM3 (Westervelt et al. 2017). The simulations include a 400-year control simulation using year 2000 conditions (CTRL), and a set of associated sensitivity simulations described in Table 4.1. The significance of the differences between two time-slice experiments is computed assuming a Gaussian distribution.

4.3 Observed and simulated stagnation

4.3.1 Climatology

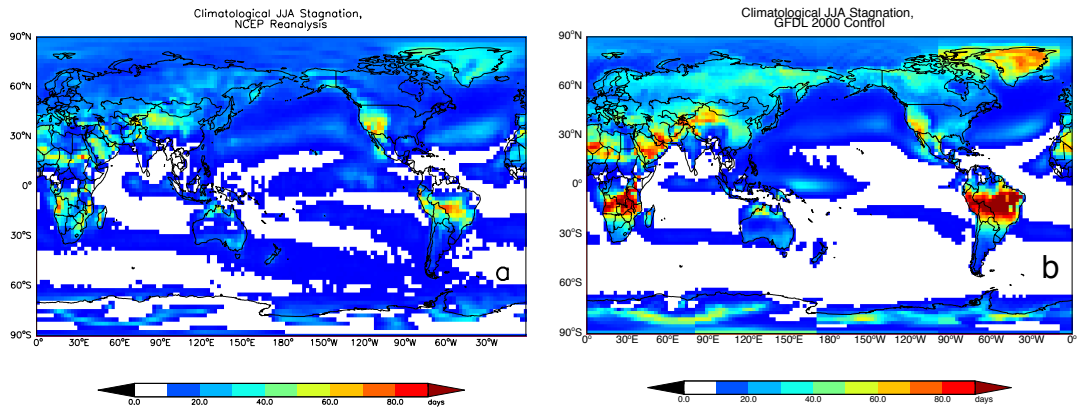

Figure 4.1 Climatological mean stagnant days per summer (JJA) in (a) NCEP/NCAR Reanalysis 1 and (b) the GFDL-CM3 model under year 2000 conditions (2000CONTROL). Stagnant days are defined as days with less than 1mm precipitation, surface wind speeds less than 3.2 ms^{-1} and 500hPa wind speeds less than 13 ms^{-1}. On days with a temperature inversion in the lower atmosphere (temperature at 850hPa > surface temperature), the surface wind condition is relaxed by 10%. Regions with <1 stagnant day are displayed as white.

Figure 4.1a shows the climatological 30-year mean (1985-2015) number of stagnant days during the Northern Hemisphere summer (June-July-August, or JJA) from NCEP/NCAR Reanalysis 1. In the Northern Hemisphere, the most frequent stagnation events, on the order of 40-60 days per summer, occur predominantly in desert areas (the Saharan desert, the Arabian desert, the southwest United States). In the United States, stagnation is elevated in the Western US, particularly the southwest (40-61 days per

summer over most of the region), relative to the Eastern US (at most 19 days per summer). In the Southern Hemisphere, tropical and subtropical land areas are stagnant on most JJA days, due in part to the absence of precipitation during the dry season. For comparison, Figure 4.1b shows the climatological mean stagnation from CTRL. CM3 is generally biased high over land, but captures the observed spatial patterns of stagnation (correlation coefficient, $r = 0.69$).

4.3.2 Changes in summertime stagnation over the historical period

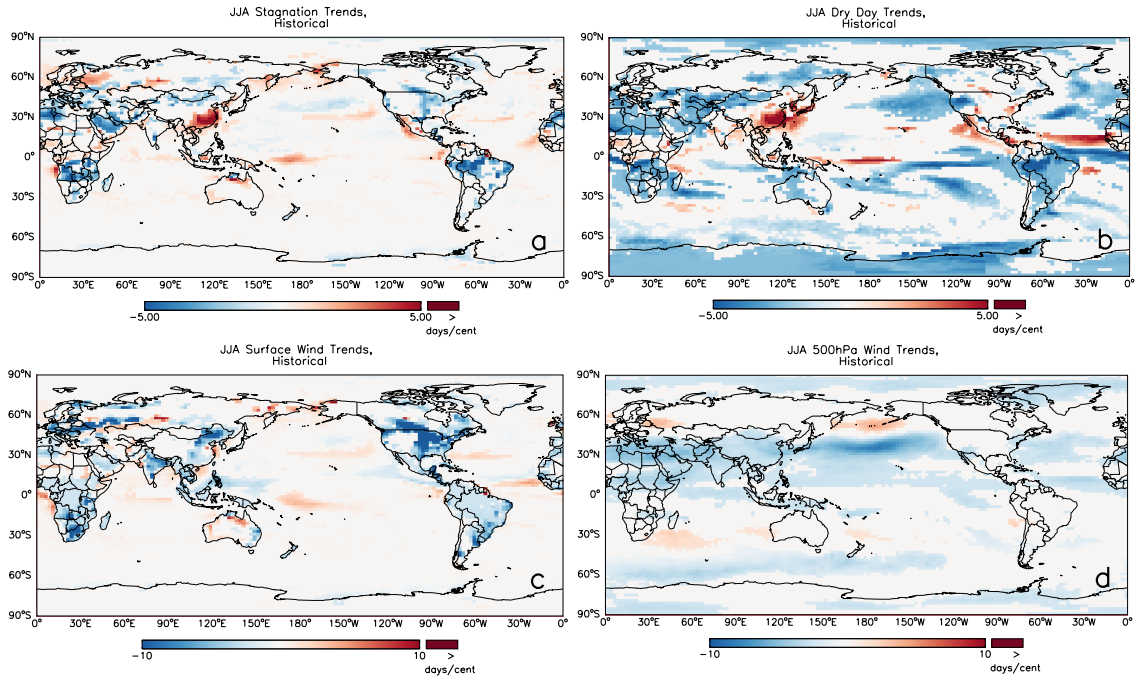

Figure 4.2 Ensemble mean trends from 1860-2005 (days/century) in the number of (a) stagnant days, (b) days with <1mm precipitation, (c) days with surface wind speeds < 3.2 ms^{-1}, (d) days with 500hPa wind speeds <13 ms^{-1} in GFDL-CM3 following the historical all-forcing scenario. Trends that are not significant at the 95% level are not shown.

As shown in Figure 4.2a, significant regional trends in stagnation are simulated in GFDL-CM3 over the historical period (1860-2005). In the ensuing figures and discussion, I decompose these trends in stagnation into trends in the individual components, i.e. trends in the number of dry days, days with surface wind speeds less

than 3.2 ms^{-1}, and days with 500hPa wind speeds less than 13 ms^{-1}. I focus on three regions of interest: the United States, China, and Europe. Stagnation trends in the eastern U.S. are significant and negative, except for the southeastern U.S. where stagnation has increased slightly. Significant decreases in the number of days with weak surface wind speeds over the eastern U.S. drive the historical stagnation trends over most of the region, but in the southeast U.S. are counteracted by increases in the number of dry days (Figure 4.2a-c), likely associated with changes in the westward extent of the Bermuda High (Li et al. 2011). In Chapter 2, I found a similar dipole behavior in extreme temperature over the eastern U.S., which was likely also driven by changes in precipitation and cloudiness over the southeastern U.S. (see Chapter 3 for a discussion of the mechanisms behind the U.S. warming hole). In Europe, stagnation trends exhibit a dipole structure, with stagnation decreasing in southern Europe and increasing in northern Europe. All three stagnation components (Figure 4.2b-d) contribute to the historical trends, but the largest contribution comes from changes in the upper level winds. Over eastern China, large positive trends in stagnation occur, due primarily to increases in the number of dry days (compare Figures 4.2a and 4.2b).

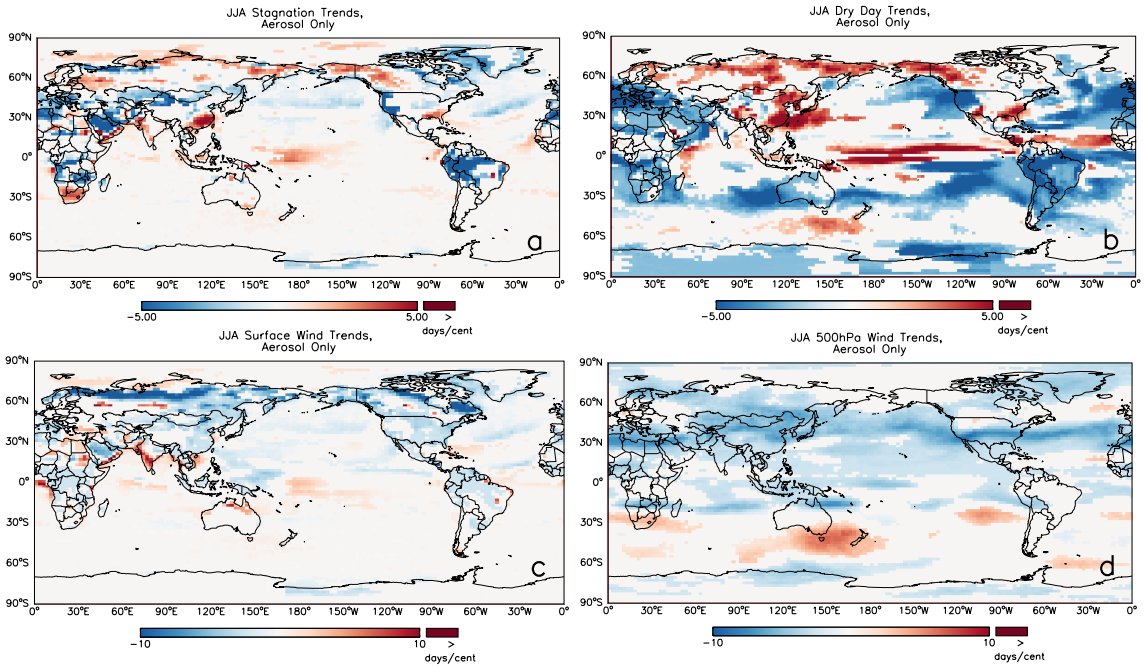

Figure 4.3 As in Figure 4.2, but for the aerosol only simulation.

There are a number of regions where the 1860-2005 stagnation trends agree well between HIST and AER (compare Figures 4.2 and 4.3), including positive trends over eastern China and negative trends over the eastern U.S. and southern Europe. The correlation between the spatial distribution of stagnation trends in HIST and AER is significant (with a correlation coefficient, $r = 0.59$). In contrast, there is minimal agreement between the HIST and GHG stagnation trends (compare Figures 4.2 and 4.4, $r = -0.55$). In a number of regions, stagnation trends in AER are anti-correlated with GHG (global correlation between AER and GHG, $r = -0.39$), including the eastern US and southern Europe. However, in contrast to the results shown in Chapter 2 for extreme precipitation and temperature, here the aerosol response dominates over the historical period. These results indicate that the simulated stagnation trends in HIST are driven primarily by changes in atmospheric aerosols (see Figure 1.2 for change in aerosol optical depth).

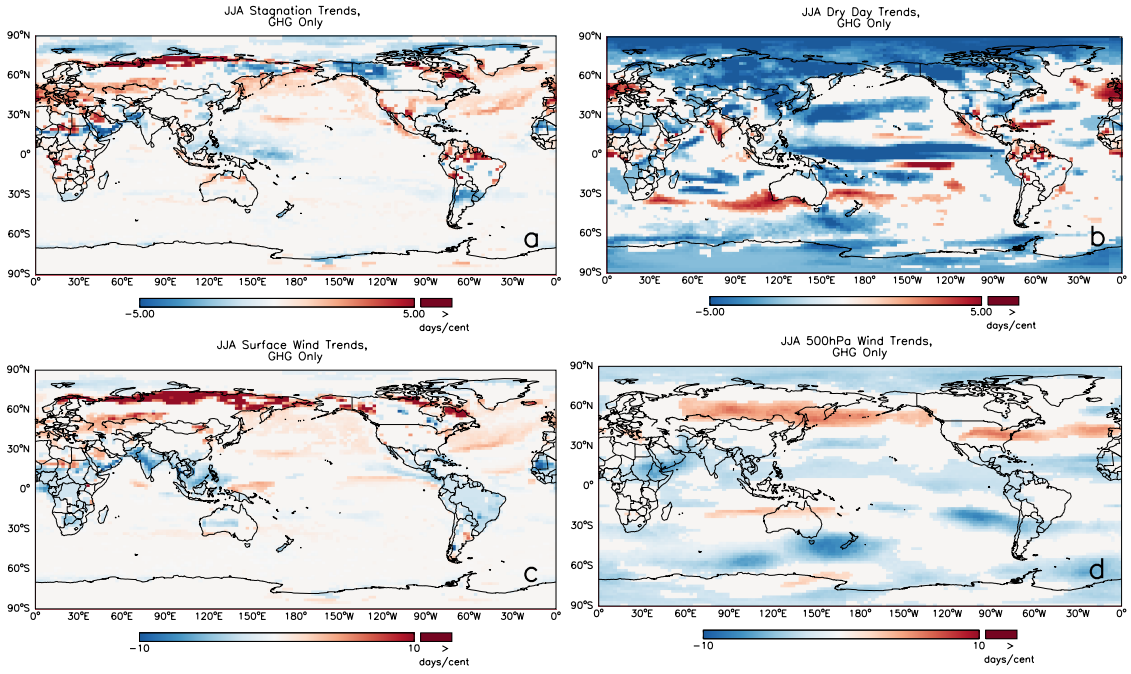

Figure 4.4 As in Figure 4.2, but for the greenhouse gas only simulation.

4.3.3 Future stagnation trends and the roles of greenhouse gas and aerosol forcing

Over the remainder of the twenty-first century, anthropogenic aerosol emissions are expected to decrease while greenhouse gas concentrations continue to rise (van Vuuren et al. 2011). Following a moderate future warming scenario, RCP4.5, the simulated historical stagnation trends reverse in the twenty-first century (Figure 4.5). In the previously identified regions of interest, there are significant increases in stagnation over the eastern United States, with the southeastern U.S. again exhibiting an opposite-signed response from the rest of the region; the Mediterranean and southern Europe experience large increases in stagnation; and stagnation in eastern China is projected to decrease.

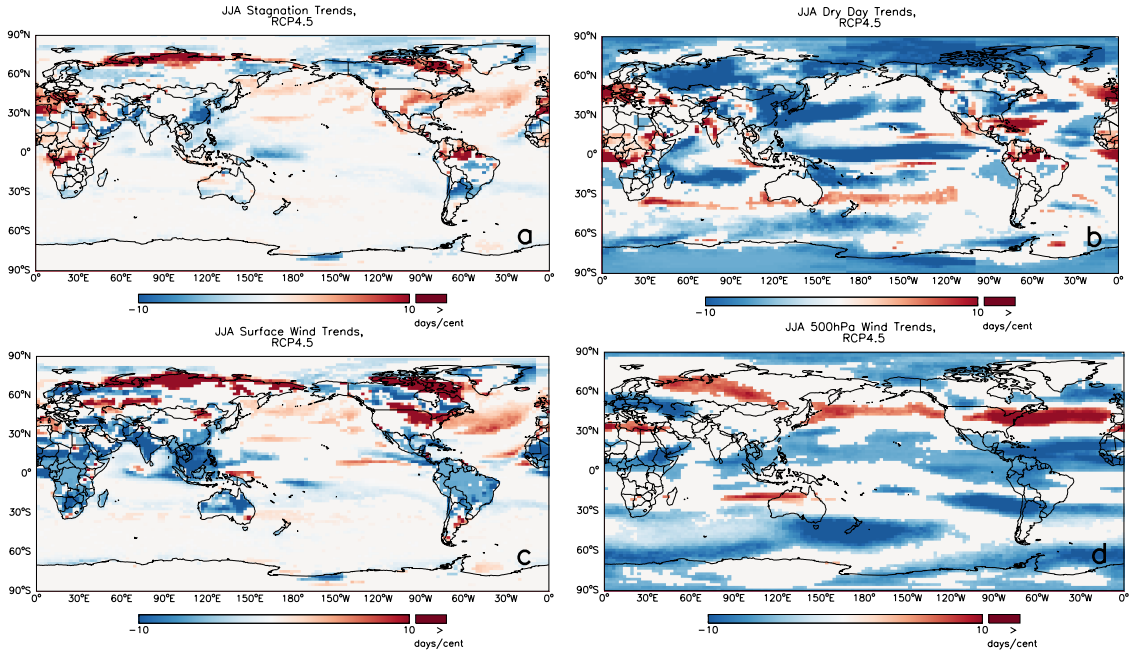

Figure 4.5 Trends from 2006-2100 (days/century) in the number of (a) stagnant days, (b) days with <1mm precipitation, (c) days with surface wind speeds < 3.2 ms^{-1}, (d) days with 500hPa wind speeds <13 ms^{-1} in GFDL-CM3 following the RCP4.5 future scenario. Trends that are not significant at the 95% level are not shown.

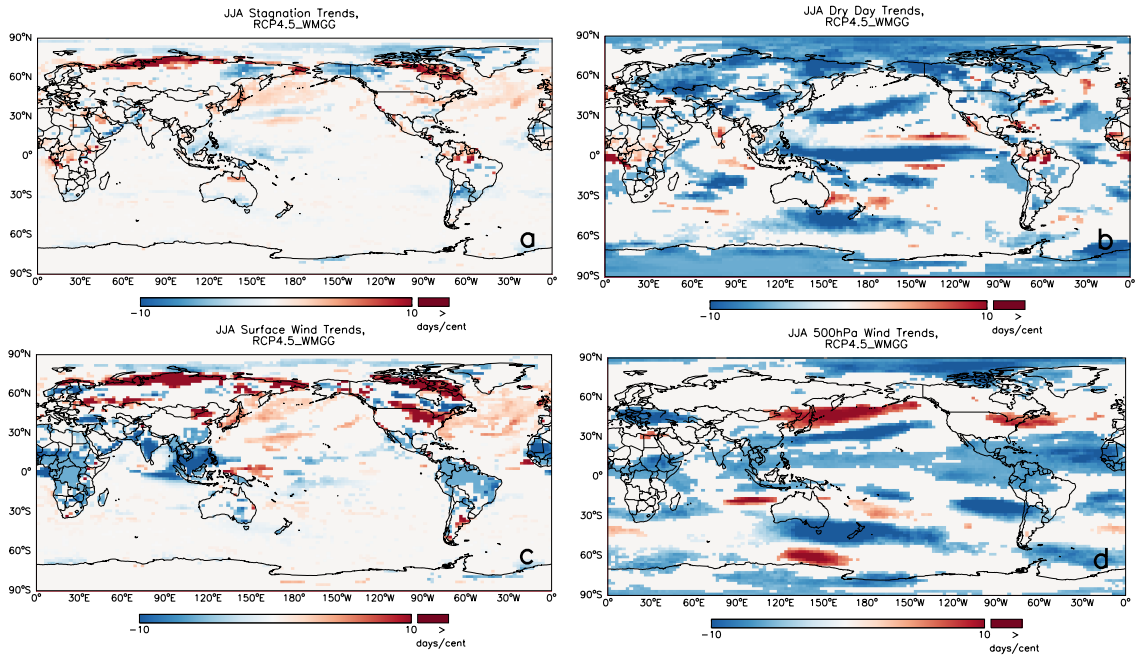

Figure 4.6 As in Figure 4.5, but for the RCP4.5_WMGG simulation, in which greenhouse gases follow their RCP4.5 trajectory, but aerosol and ozone precursor emissions are held constant at 2005 levels.

In the RCP4.5_WMGG experiment, in which aerosol and ozone precursor emissions are held constant at 2005 levels while long-lived greenhouse gas concentrations follow RCP4.5, the stagnation response is weaker almost everywhere (Figure 4.6). In particular, there is no significant change in stagnation over eastern China or southern Europe, and the average change in stagnation over the Eastern US is only 40% of the change in RCP4.5. In both eastern China and southern Europe, there are no significant trends in the number of dry days in RCP4.5_WMGG (Figure 4.6b), indicating that the future changes in dry days, and corresponding changes in stagnation, projected in those regions in RCP4.5 (Figure 4.5a,b) are due to decreasing aerosol emissions, rather than increasing greenhouse gases. The positive trends in days with low 500hPa wind speeds over the eastern U.S. in RCP4.5_WMGG are 60% of the trends in RCP4.5, and there is an absence of significant positive trends in dry days over Texas in the former

experiment. The negative trends in dry days over the eastern and southeast U.S. are also weaker in RCP4.5_WMGG (trends in individual grid cells are 60-80% of the trends in RCP4.5) when aerosol emissions are held constant. The 40% difference in stagnation trends over the eastern and southeast U.S. between RCP4.5 and RCP4.5_WMGG can therefore be explained by changes in upper level winds and precipitation frequency driven by decreasing aerosol emissions.

Table 4.2 ***Estimated Radiative Forcing (ERF) due to changes in sulfur dioxide emissions in each source region.***

Simulation Name	ERF
zUS_SO2	0.164 Wm^{-2}
m80pChina_SO2	0.089 Wm^{-2}
m80pEU_SO2	0.177 Wm^{-2}

4.4 Stagnation response to aerosol emissions from individual source regions

Unlike long-lived greenhouse gases such as CO_2, CH_4, and N_2O, aerosols in the troposphere have a short lifetime on the order of days to weeks, and therefore are not well-mixed. It is therefore useful to consider the separate impacts on stagnation of aerosols emitted from different source regions. I use a set of sensitivity simulations performed with GFDL-CM3, in which we simulate year 2000 conditions with aerosol emissions from specific source regions reduced or zeroed out (Table 4.1). In order to assess the response to changes in regional aerosol emissions, we first construct an 'ensemble' mean response, weighting each simulation by its respective global-mean effective radiative forcing (ERF) given in Table 4.2. The ERFs are calculated as the net top-of-atmosphere radiative imbalance (relative to CTRL) in a set of 40-year simulations with aerosol emissions from the sensitivity simulations but fixed sea surface temperatures (SSTs) and sea ice, calculated as 100-year monthly-mean climatologies from CTRL. The

ERF-weighted mean represents CM3's preferred response to aerosol forcing regardless of source region. This mean response is calculated as follows:

$$\overline{ASI} = \frac{\sum_{i=1}^{N} \frac{1}{ERF_i} \times (ASI_i - ASI_{CON})}{\sum_{i=1}^{N} \frac{1}{ERF_i}}$$

where ASI_i is the air stagnation index in simulation i, ASI_{CON} is the air stagnation index in the control simulation, and ERF_i is the global-mean effective radiative forcing in simulation i. Similar to the time-varying forcing experiments (Section 4.3.3), the ERF-weighted mean of the SO_2 perturbation simulations reveals the following stagnation response (Figure 4.7): reductions in eastern China driven by decreases in dry days; increases in southern Europe and decreases in northern Europe driven jointly by changes in the 500hPa wind speeds and dry days; increases in most of the eastern U.S. driven by changes in surface and upper-level wind speeds; and decreases in the southeastern U.S. driven by decreases in dry days. Because these responses are present in the ensemble mean, I conclude that they are part of a characteristic response to sulfate aerosol forcing that is independent of the location of the forcing.

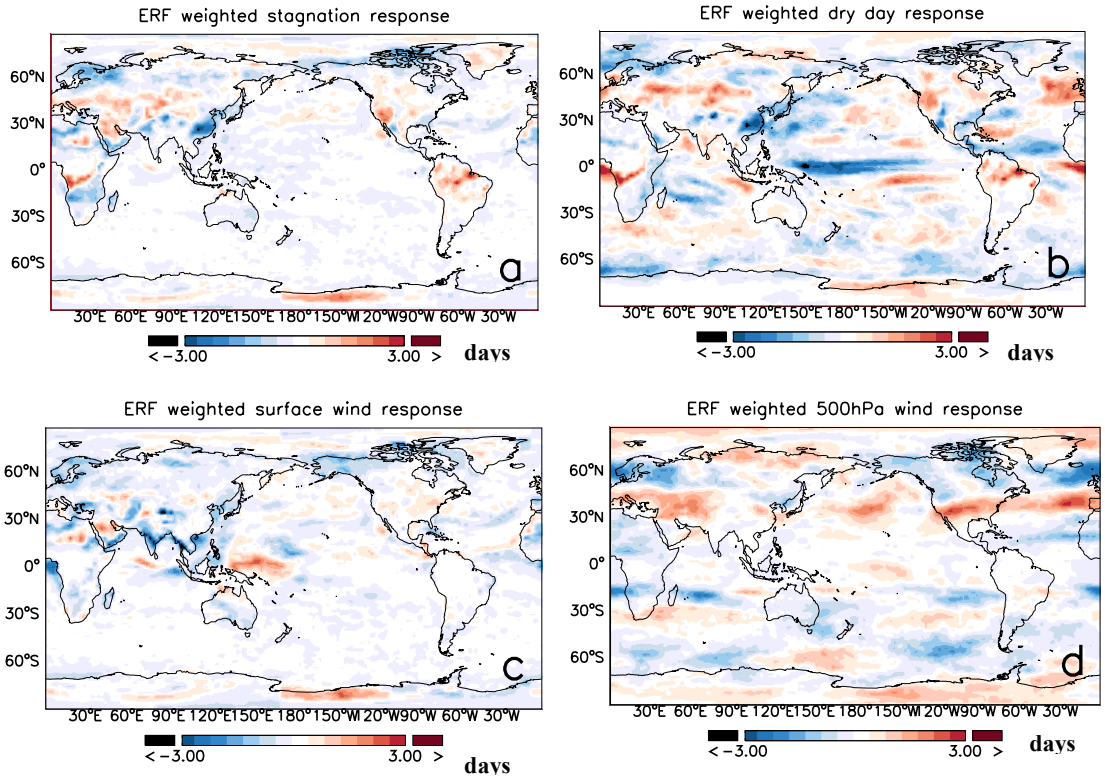

Figure 4.7 Mean (a) stagnation, (b) dry day, (c) surface wind, and (d) 500hPa wind response to changes in regional SO_2 emissions weighted by the estimated radiative forcing (ERF). Calculated as the average of the difference between the individual sensitivity simulations and the control simulation weighted by the ERF of the sensitivity simulation. Regions where the difference is insignificant (at the 95% confidence level) are whited out.

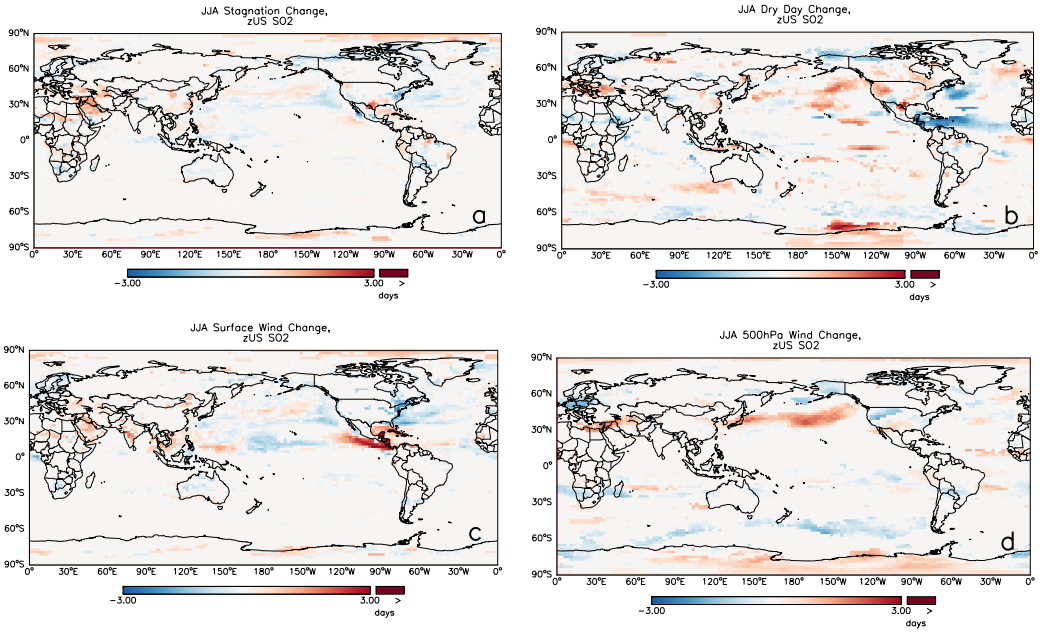

Figure 4.8 Change in number of anomalous (a) stagnant days, (b) days with < 1mm precipitation, (c) days with surface winds < 3.2 ms^{-1}, (d) days with 500hPa winds <13 ms^{-1} due to removal of US SO_2 emissions (zUS_SO2). Regions where the difference is insignificant (at the 95% confidence level) are whited out.

I define the 'anomalous' response to regional changes in aerosol emissions as the difference between the total response in simulation i ($ASI_i - ASI_{CON}$) and the ERF-weighted mean response:

$$ASI_i' = ASI_i - ASI_{CON} - \overline{ASI}$$

The anomalous response is an estimate of the portion of the overall response that depends upon the location of the aerosol forcing. Zeroing out U.S. SO_2 emissions produces an anomalous stagnation response over the eastern U.S. (Figure 4.8). Stagnation decreases in the northeastern U.S. and increases in the southern U.S., in contrast with the mean response. These changes are due to changes in 500hPa wind speeds and dry day frequency. There is also a slight enhancement of the mean response over Europe and slight weakening of the mean response over eastern China.

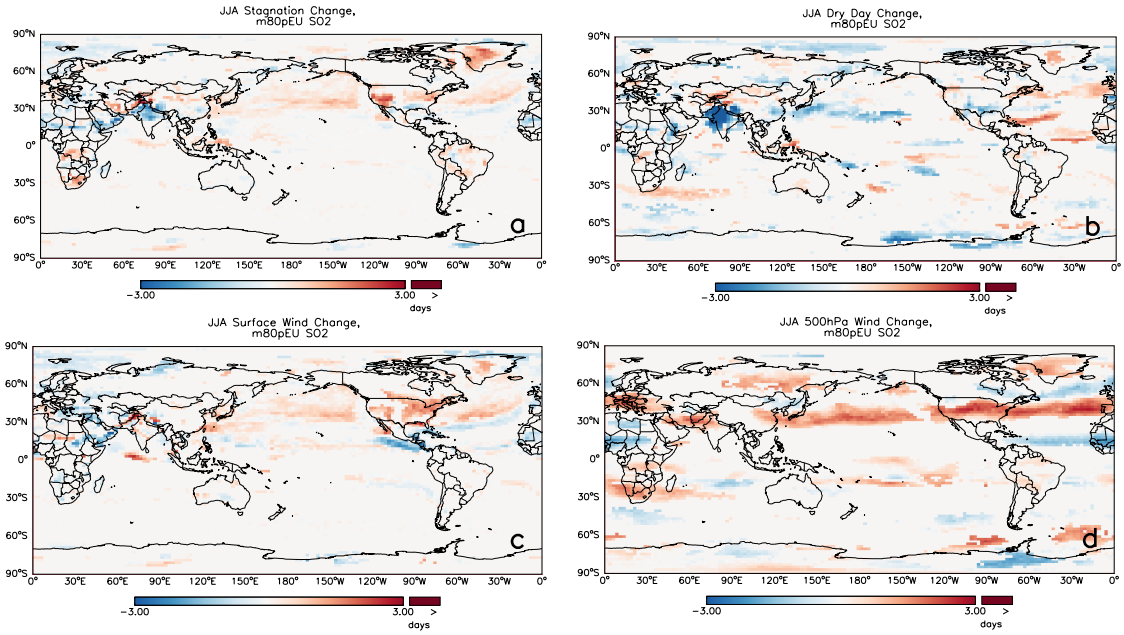

Figure 4.9 As in Figure 4.8, but for the m80pEU_SO2 simulation (80% reduction in European SO_2 emissions).

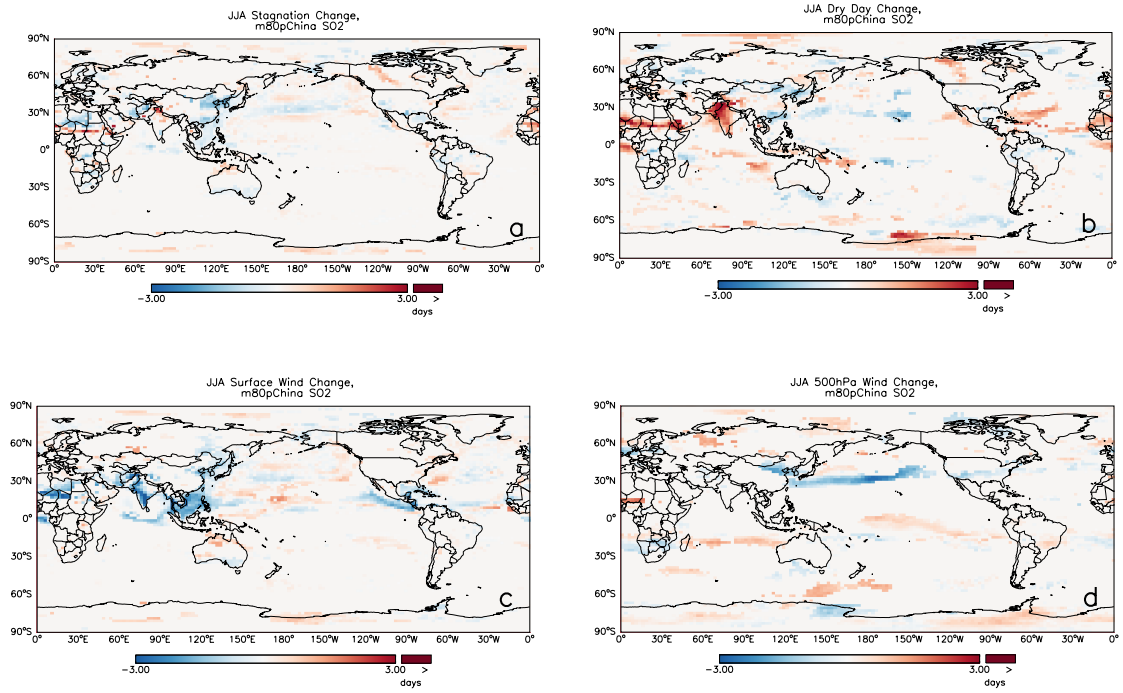

Figure 4.10 As in Figure 4.8, but for the m80pChina_SO2 simulation (80% reduction in China's SO_2 emissions).

In my regions of interest, the chief impact of reducing European SO_2 emissions is to enhance the mean stagnation response, particularly over the U.S. (Figure 4.9). Figure 4.9d suggests that this may be due to changes in the large-scale circulation of the

Northern Hemisphere. The changes in 500hPa wind speeds in the mean response imply a poleward shift of the Northern Hemisphere mid-latitude jet. This effect is largest in m80pEU_SO2 (Figure 4.9d), potentially due to the higher latitude of the forcing relative to zUS_SO2 and m80pChina_SO2 (Shindell and Faluvegi 2009). Chinese SO_2 emissions reductions also enhance the mean stagnation response over eastern China, but have minimal impacts on the U.S. and Europe (Figure 4.10a). The anomalous stagnation response in Eastern China is due to additional decreases in the number of dry days in the region, combined with increases in 500hPa wind speeds in northern China (Figure 4.10b,d).

4.5 Discussion and conclusions

Changes in atmospheric stagnation may have serious impacts on extreme heat and pollution events, presenting clear risks to human health. I show here that in GFDL-CM3 significant changes in atmospheric stagnation over the US, China, and Europe can be largely attributed to changes in anthropogenic aerosols in both historical and future simulations, a point that is reaffirmed through the analysis of idealized simulations that isolate the impact of changes in regional aerosols. These findings imply a potential feedback wherein aerosols affect the meteorological conditions that are associated with extreme pollution events. This feedback is positive in regions such as eastern China and the southeast U.S., where increasing aerosols also increases stagnation, and negative in regions like southern Europe, where increasing aerosols decreases stagnation. Furthermore, I find that greenhouse gases produce opposite signed impacts on stagnation in the same regions, suggesting that these are part of a characteristic response pattern to changes in radiative forcing, but unlike extreme temperature and precipitation (Chapter 2)

aerosols are much more effective at inducing changes in stagnation than greenhouse gases.

Over the next several decades, we expect aerosol emissions to decline globally, reversing the historical stagnation trends (Figure 4.5). The rise in greenhouse gases will also significantly impact stagnation in the 21st century (Figure 4.6), particularly over the eastern U.S., but declining aerosol emissions continue to dominate stagnation responses in southern Europe and eastern China, predominately through their effect on precipitation frequency, which is known to be sensitive to aerosols (Kloster et al. 2009; Ramanathan et al. 2001).

In studying the roles of aerosols from specific source regions, we find that we can separate the aerosol impacts into a characteristic response (source region independent) and an anomalous response (source region dependent). This has implications for the attribution of regional trends in stagnation and its components. For example, although U.S. SO_2 emissions increased over the historical period, the stagnation trends over the U.S. in HIST and AER are in better agreement with the characteristic response (but opposite signed), implying that the stagnation trends in HIST and AER are driven by remote aerosols over this region. The simulated historical stagnation trends generally follow the negative of the characteristic response pattern.

While the characteristic stagnation response to aerosol forcing is interesting from a scientific standpoint, what is most relevant from a practical standpoint (e.g. for policy makers concerned with implications for future air quality and temperature extremes) is the total stagnation response. The latter also includes an anomalous, source-region dependent component, which is important to understand because aerosol emission

changes from specific source regions, i.e. East Asia, are likely to dominate future global emission trends. I expect that a reduction in U.S. SO_2 would produce a response that opposes the characteristic response over the eastern U.S. and China, but would enhance the characteristic response over Europe. In contrast, changes in European SO_2 emissions are projected to have relatively small impacts over Europe, but significantly enhance the characteristic response over the U.S. Chinese aerosol emissions have a minimal effect on European and U.S. stagnation, but a reduction in Chinese emissions would significantly reduce stagnation over China by increasing precipitation frequency.

Aerosol emissions in the U.S. and Europe have been declining for several decades due to air quality legislation (e.g. Fiore et al. 2015) and are expected to continue to decline in the 21st century, while emissions from East Asia have risen rapidly over the latter half of the 20th century and are expected to continue to rise for the next few decades before eventually declining (e.g. Westervelt et al. 2015). Therefore, I expect stagnation changes in the near future to be strongly influenced by the combined signals of declining emissions from the U.S. (zUS_SO2) and Europe (m80pEU_SO2) and rising emissions from China (opposite of m80pChina_SO2). In this scenario, I expect changes in stagnation and its components in the U.S. and Europe to be dominated by the decreases in U.S. and European SO_2, leading to increasing stagnation in the eastern and southwestern U.S. and southern Europe. In China, on the other hand, there will likely be cancellation between the competing signals of regional emissions trends, particularly with regards to changes in the frequency of dry days. In other regions, such as India, the combined effect of decreasing European emissions and increasing Chinese emissions could lead to large

decreases in dry day frequency. Later in the 21st century, I expect the effects of declining emissions from China to dominate (m80pChina_SO2).

As discussed in Chapters 1 and 2, the historical aerosol forcing is very uncertain, and GFDL-CM3 has one of the largest aerosol forcings out of the suite of CMIP5 models. Therefore, in order to better sample the probability distribution, it will be important to expand this research to consider stagnation responses in more climate models. Similarly, in order to sample the uncertainty in future stagnation, it will be important to consider a variety of future scenarios. Aerosols were the dominant driver of stagnation changes in RCP4.5, but it is likely that greenhouse gas impacts on stagnation would be more significant under a more extreme warming scenario such as RCP8.5 (not evaluated here due to data availability). Finally, here I have addressed the question of how aerosols from individual source regions affect stagnation, but another question to consider is how different aerosol species affect stagnation. Ultimately, quantifying aerosol impacts on regional stagnation trends will allow the scientific community to identify regions such as southern Europe where improving air quality by removing aerosols may have adverse impacts on the occurrence of heat waves, drought, and even extreme pollution events.

Chapter 5 Conclusions

5.1 Summary of results

In this thesis, I find that aerosols are important drivers of regional changes in temperature and precipitation extremes, and the dominant driver of long-term trends in atmospheric stagnation. In Chapter 2, I used the GFDL-CM3 model to examine the impacts of aerosols on extreme temperature and precipitation in the U.S. over the historical period from 1860 to 2005, and then to project the future impact of reductions in aerosol emissions from 2005 to 2100. Aerosols significantly reduce the frequency and magnitude of modeled high temperature extremes across the U.S. over the historical period, while greenhouse gases significantly increase the frequency and magnitude of high temperature extremes. Aerosols reduce extreme precipitation in the eastern U.S., particularly in winter, while greenhouse gases increase extreme precipitation in the eastern U.S. in winter and the central U.S. in spring. Notably, despite the spatial heterogeneity of the aerosol burden, the spatial patterns of aerosol and greenhouse gas effects on extreme temperature (summer) and precipitation (winter) are significantly anti-correlated, leading to large scale cancellations between aerosols and greenhouse gases over the historical period in the model. This cross-cancellation is likely contributing to the relatively small changes in extreme high temperatures and precipitation observed in the U.S. (Donat et al. 2013). The significant degree of anti-correlation suggests that these are preferred response patterns for the model, and are independent of the nature of the forcing. This implies that for summertime temperature and wintertime precipitation extremes, the spatial heterogeneity of aerosol forcing is less important than the overall effect of imposing a cooling signal in the Northern Hemisphere in determining the

climate response. In the future, declining aerosol emissions contribute to projected increases in temperature and precipitation extremes, but increasing greenhouse gases are the primary driver.

In contrast, when I consider simulated historical changes in regional stagnation in the U.S., Europe and China, atmospheric aerosols are the principal driver, while greenhouse gases are a relatively small influence. Greenhouse gas effects on stagnation become more significant in the future as greenhouse gas emissions increase, but the effects of declining aerosol emissions still dominate over regions such as southern Europe and eastern China. By analyzing a set of CM3 sensitivity simulations, I am further able to identify the stagnation response to aerosols emitted from different source regions. U.S. stagnation, for example, is highly sensitive to aerosol emissions from Europe, and vice versa, while Chinese aerosol emissions produce a very strong local stagnation response and significant responses throughout the Northern Hemisphere subtropics, with only small deviations from the mean aerosol response in the extratropics.

The modeled response patterns in both temperature extremes and stagnation are characterized by a weak or even opposite signed response in the southeastern U.S. relative to the rest of the country, leading to the question of whether or not the observed U.S. warming hole can be explained as a response to anthropogenic forcing, or if it is principally driven by internal variability. A number of studies have investigated this question and drawn different conclusions (Kunkel et al. 2006; Leibensperger et al. 2012; Meehl et al. 2012; Misra et al. 2012; Robinson 2002; Weaver 2013; Yu et al. 2014), but I show that the dominant processes shaping the warming hole depend on the time period and season considered. For example, in the summer from 1950-1975, significant cooling

trends were observed in the southern and northeast U.S., and the CMIP5 multi-model mean captures the sign and timing of these trends. Further analysis of the CMIP5 models shows that the modeled trends are explained by changes in aerosol forcing. In winter, there are also observed cooling trends from 1950-1990 in the same U.S. regions. I find that these trends are largely explained by changes in the Pacific Decadal Oscillation (PDO) and the North Atlantic Oscillation (NAO). Confidence that changes in the PDO can be attributed to anthropogenic activities was found to be low in the latest IPCC report (Bindoff et al. 2013); however, recent studies indicate that anthropogenic forcing (Allen et al. 2014), and in particular aerosol forcing (Smith et al. 2016), may have influenced observed trends in the PDO over the latter half of the twentieth century. CMIP5 models show that greenhouse gas forcing can lead to positive trends in the NAO (Gillett and Fyfe 2013), and several studies have found that changes in aerosol emissions over the latter half of the twentieth century may have contributed to trends in the NAO (Chiacchio et al. 2011; Pausata et al. 2015). Further research will therefore be needed to fully quantify the effects of aerosols on the wintertime U.S. warming hole, particularly in light of a possible anthropogenic influence on modes of variability.

5.2 Discussion and future research directions

Chapters 2, 3, and 4 all demonstrated that aerosols are an important driver of regional climate change, and will continue to be in the future even as emissions decline. Furthermore, as the aerosol-masking of rising greenhouse gases is removed, climate quantities for which we have not detected a clear anthropogenic signal over the historical period may change dramatically. This masking effect is seen clearly in Chapter 2: simulated changes in temperature and precipitation extremes were not significant in the

historical all-forcing scenario due to cancellations between aerosols and greenhouse gases, but emerged by the end of the 21st century under RCP8.5. Currently, greenhouse gas emissions are following the RCP8.5 trajectory (Sanford et al. 2014), and if this continues, my research shows a future for the U.S. where almost every summer day is warmer than the current 90th percentile temperature threshold. Hot days that are currently considered extreme would become the new normal.

This possible future will have major consequences for a number of sectors. The U.S. agricultural industry produces over 100 billion dollars of crops a year (United States Department of Agriculture 2016), but yields of many of the nation's staples are negatively affected by exposure to extreme high temperatures (Hatfield et al. 2008; Hatfield and Prueger 2015). Prolonged extreme heat will cause infrastructure damage such as cracked/deformed asphalt (Wilway et al. 2008), and buckling of railway tracks (Burkett et al. 2008) and recent studies have brought to light the effects of extreme heat on air travel (Coffel and Horton 2015; Coffel et al. 2017). There are approximately 240 heat-related deaths per year in the U.S. on average. However, during extreme events such as the 1980 Midwestern U.S. heat wave (1700 deaths) and the 1995 Chicago heat wave (700 deaths), those numbers can spike dramatically (McGeehin and Mirabelli 2001).

The separation of local vs. remote aerosol effects is another key takeaway of this dissertation with clear implications for projecting regional climate change. Chapter 4 demonstrated that for stagnation (and its component variables: precipitation and surface and 500hPa wind speed), aerosols emitted outside of a given region can have a significant impact on the region, perhaps even outweighing the effects of locally emitted aerosols.

My results suggest that the relative timing of increases and decreases in aerosol emissions in different regions matters for projecting the climate response. For example, a future scenario in which aerosol emissions decrease rapidly in the U.S. and Europe while East Asian aerosol emissions continue to increase in the immediate future before declining may produce only small changes in stagnation in regions like China due to competing effects on the frequency of dry days, whereas in a scenario where U.S., European, and East Asian aerosol emissions all decline gradually, I would expect large decreases in stagnation over China. A more comprehensive set of aerosol emissions scenarios is needed in order to generate an appropriate spread of possible future aerosol impacts.

The climate system is complex and a number of processes remain uncertain. By their nature, climate models must include parameterizations and simplifications (Gillett et al. 2002; Lambert and Boer 2001; Tebaldi and Knutti 2007), and so in order to better sample the uncertainty in aerosol impacts on regional climate and extreme events, it will be important to expand this research to determine whether the conclusions drawn here are robust across a range of models. Of the 61 models that participated in CMIP5, only 11 performed historical aerosol-only simulations (Chapter 3, Table 3.1), and of those 11, only 4 released data with sufficient temporal resolution to calculate temperature and precipitation extremes and stagnation events, and only 2 did so for more than a single ensemble-member. Testing the robustness of aerosol impacts on extreme events will therefore require a concerted effort from the climate modeling community to generate the necessary model output. AerChemMIP, one of the modeling intercomparison projects included under the umbrella of CMIP6, will go a long way to address this need (Collins et al. 2017; Eyring et al. 2016).

It would also be useful to extend this research by delving deeper into the mechanisms by which aerosols affect regional climate. Based on my findings, I hypothesize that changes in the large-scale atmospheric circulation resulting from hemispherically asymmetric cooling (or warming in the case of future aerosol emissions reductions) of the Northern Hemisphere are one of the principal means by which aerosols affect the climate variables considered in this thesis (temperature, precipitation, and stagnation). This could be tested in idealized experiments where a zonally symmetric forcing is imposed in the Northern Hemisphere. Related to this is the question of how aerosols project onto modes of internal variability like the NAO, which have a large effect on regional climate. The sensitivity simulations that perturb regional aerosol emissions used in Chapter 4 could be analyzed to investigate this question. Quantifying the roles of these mechanisms along with others such as aerosol-cloud interactions will go a long way towards improving our understanding of aerosol-climate impacts.

This dissertation focuses on aerosol effects on climatological timescales, but another promising future research avenue is to look at aerosol effects on individual events. How do aerosols affect individual extreme precipitation events? How important are the size and chemical composition of the aerosols? Weather forecasting models have only recently begun considering aerosols, and recent studies show that aerosol-cloud interactions are a significant source of error in precipitation predictions, leading to overestimates of light precipitation and under estimates of extreme precipitation (Jiang et al. 2017). In the case of stagnation, how can aerosols affect the characteristics of individual events? In Chapter 4, I found that over long timescales, the net global radiative effect of aerosols (i.e. the ensemble mean response) was generally more

important than local aerosol effects (the anomalous response), but I expect local aerosols to have a larger impact on individual events through mechanisms such as their suppression of drizzle (Albrecht 1989) and effects on atmospheric stability (Ban-Weiss et al. 2011). I propose selecting individual events from model control simulations and then performing ensembles of short-term simulations (on the order of weeks) to test how the events change for different prescribed aerosol distributions, and specifically to test the sensitivity to aerosol composition and altitude.

Aerosols significantly affect climate phenomena such as heat extremes, precipitation, and stagnation, which have major impacts on human society. It is therefore critical to improve our understanding and capacity to model aerosols and aerosol effects on all scales, from weather forecasting of an individual storm, to predictions of global climate change 100 years in the future.

Bibliography

Ackermann, A. S., M. P. Kirkpatrick, D. E. Stevens, and O. B. Toon, 2004: The impact of humidity above stratiform clouds on indirect aerosol climate forcing. *Nature*, **432,** 1014-1017.

Albrecht, B. A., 1989: Aerosols, cloud microphysics, and fractional cloudiness. *Science*, **245,** 1227-1230.

Allen, M. R., and W. J. Ingram, 2002: Constraints on future changes in climate and the hydrologic cycle. *Nature*, **419,** 224-232.

Allen, R. J., J. R. Norris, and M. Kovilakam, 2014: Influence of anthropogenic aerosols and the Pacific Decadal Oscillation on tropical belt width. *Nature Geoscience*, **7,** 270-274.

Allen, R. J., A. T. Evan, and B. B. B. Booth, 2015: Interhemispheric Aerosol Radiative Forcing and Tropical Precipitation Shifts during the Late Twentieth Century. *Journal of Climate*, **28,** 8219-8246.

Anderson, G. B., and M. L. Bell, 2009: Weather-related mortality: how heat, cold, and heat waves affect mortality in the United States. *Epidemiology*, **20,** 205-213.

Anderson, G. B., and M. L. Bell, 2011: Heat waves in the United States: mortality risk during heat waves and effect modification by heat wave characteristics in 43 U.S. communities. *Environ Heatlh Perspect*, **119,** 210-218.

Austin, J., L. W. Horowitz, M. D. Schwarzkopf, R. J. Wilson, and H. Levy, 2013: Stratospheric Ozone and Temperature Simulated from the Preindustrial Era to the Present Day. *Journal of Climate*, **26,** 3528-3543.

Ban-Weiss, G. A., L. Cao, G. Bala, and K. Caldeira, 2011: Dependence of climate forcing and response on the altitude of black carbon aerosols. *Climate Dynamics*, **38,** 897-911.

Bentsen, M., and Coauthors, 2013: The Norwegian Earth System Model, NorESM1-M – Part 1: Description and basic evaluation of the physical climate. *Geoscientific Model Development*, **6,** 687-720.

Bindoff, N. L., and Coauthors, 2013: Detection and Attribution of Climate Change: from Global to Regional. *Climate Change 2013: the Physical Science Basis. Contribution of Working Group I to the Fifth Assessment Report of the Intergovernmental Panel on Climate Change*, T. F. Stocker, and Coauthors, Eds., Cambridge University Press.

Boucher, O., and Coauthors, 2013: Clouds and Aerosols. *Climate Change 2013: The Physical Science Basis. Contribution of Working Group I to the Fifth Assessment Report of the Intergovernmental Panel on Climate Change* T. F. Stocker, and Coauthors, Eds.

Burkett, V. R., and Coauthors, 2008: Why Study the Gulf Coast.

Caserini, S., P. Giani, C. Cacciamani, S. Ozgen, and G. Lonati, 2017: Influence of climate change on the frequency of daytime temperature inversions and stagnation events in the Po Valley: historical trend and future projections. *Atmospheric Research*, **184,** 15-23.

Changnon, S. A., K. E. Kunkel, and B. C. Reinke, 1996: Impacts and response to the 1995 heat wave: a call to action. *Bulletin of the American Meteorological Society*, **77,** 1497.

Chiacchio, M., T. Ewen, M. Wild, M. Chin, and T. Diehl, 2011: Decadal variability of aerosol optical depth in Europe and its relationship to the temporal shift of the North Atlantic Oscillation in the realm of dimming and brightening. *Journal of Geophysical Research*, **116**.

Chin, M., and Coauthors, 2002: Tropospheric aerosol optical thickness from the GOCART model and comparisons with satellite and sun photometer measurements. *Journal of Atmospheric Science*, **59,** 461-483.

Christidis, N., P. A. Stott, and S. J. Brown, 2011: The Role of Human Activity in the Recent Warming of Extremely Warm Daytime Temperatures. *Journal of Climate*, **24,** 1922-1930.

Coffel, E., and R. Horton, 2015: Climate Change and the Impact of Extreme Temperatures on Aviation. *Weather, Climate, and Society*, **7,** 94-102.

Coffel, E. D., T. R. Thompson, and R. M. Horton, 2017: The impacts of rising temperatures on aircraft takeoff performance. *Climatic Change*, **144,** 381-388.

Collins, W. J., and Coauthors, 2017: AerChemMIP: quantifying the effects of chemistry and aerosols in CMIP6. *Geoscientific Model Development*, **10,** 585-607.

Cook, B. I., R. L. Miller, and R. Seager, 2009: Amplification of the North American "Dust Bowl" drought through human-induced land degradation. *Proc Natl Acad Sci U S A*, **106,** 4997-5001.

Cook, E. R., C. A. Woodhouse, C. M. Eakin, D. M. Meko, and D. W. Stahle, 2004: Long-term aridity changes in the western United States. *Science*, **306,** 1015-1018.

Curreiro, F. C., J. A. Patz, J. B. Rose, and S. Lele, 2001: The association between extreme precipitation and waterborne disease outbreaks in the United States: 1948-1994. *American Journal of Public Health*, **91,** 1194-1199.

Dawson, J. P., B. J. Bloomer, D. A. Winner, and C. P. Weaver, 2014: Understanding the Meteorological Drivers of U.S. Particulate Matter Concentrations in a Changing Climate. *Bulletin of the American Meteorological Society*, **95,** 521-532.

Dentener, F., and Coauthors, 2006: Emissions of primary aerosol and precursor gases in the years 2000 and 1750 prescribed data-sets for AeroCom. *Atmos. Chem. Phys.*, **6,** 4321-4344.

Donat, M. G., A. D. King, J. T. Overpeck, L. V. Alexander, I. Durre, and D. J. Karoly, 2015: Extraordinary heat during the 1930s US Dust Bowl and associated large-scale conditions. *Climate Dynamics*, **46,** 413-426.

Donat, M. G., and Coauthors, 2013: Updated analyses of temperature and precipitation extreme indices since the beginning of the twentieth century: The HadEX2 dataset. *Journal of Geophysical Research: Atmospheres*, **118,** 2098-2118.

Donner, L. J., and Coauthors, 2011: The Dynamical Core, Physical Parameterizations, and Basic Simulation Characteristics of the Atmospheric Component AM3 of the GFDL Global Coupled Model CM3. *Journal of Climate*, **24,** 3484-3519.

Dufresne, J. L., and Coauthors, 2013: Climate change projections using the IPSL-CM5 Earth System Model: from CMIP3 to CMIP5. *Climate Dynamics*, **40,** 2123-2165.

Dunne, J. P., and Coauthors, 2012: GFDL's ESM2 Global Coupled Climate–Carbon Earth System Models. Part I: Physical Formulation and Baseline Simulation Characteristics. *Journal of Climate*, **25,** 6646-6665.

Engelthaler, D. M., and Coauthors, 1999: Climatic and environemntal patterns associated with hantavirus pulmonary syndrome, Four Corners region, United States. *Emerging Infectious Diseases*, **5,** 87-94.

Environment Canada: The Fourth Generation Coupled Global Climate Model. [Available online at http://www.ec.gc.ca/ccmac-cccma/default.asp?lang=En&n=3701CEFE-1.]

Eyring, V., S. Bony, G. A. Meehl, C. A. Senior, B. Stevens, R. J. Stouffer, and K. E. Taylor, 2016: Overview of the Coupled Model Intercomparison Project Phase 6 (CMIP6) experimental design and organization. *Geoscientific Model Development*, **9,** 1937-1958.

Fan, Y., and H. van den Dool, 2008: A global monthly land surface air temperature analysis for 1948–present. *Journal of Geophysical Research*, **113**.

Ficklin, D. L., J. T. Maxwell, S. L. Letsinger, and H. Gholizadeh, 2015: A climatic deconstruction of recent drought trends in the United States. *Environmental Research Letters*, **10,** 044009.

Fiore, A. M., V. Naik, and E. M. Leibensperger, 2015: Air quality and climate connections. *J Air Waste Manag Assoc*, **65,** 645-685.

Folland, C. K., J. Knight, H. W. Linderholm, D. Fereday, S. Ineson, and J. W. Hurrell, 2009: The Summer North Atlantic Oscillation: Past, Present, and Future. *Journal of Climate*, **22,** 1082-1103.

Gent, P. R., and Coauthors, 2011: The Community Climate System Model Version 4. *Journal of Climate*, **24,** 4973-4991.

Gillett, N. A., and J. C. Fyfe, 2013: Annular Mode change in the CMIP5 simulations. *Geophysical Research Letters*, **40,** 1189-1193.

Gillett, N. P., F. W. Zwiers, A. J. Weaver, G. C. Hegerl, M. R. Allen, and P. A. Stott, 2002: Detecting anthropogenic influence with a multi-model ensemble. *Geophysical Research Letters*, **29,** 31-31-31-34.

Ginoux, P., M. Chin, I. Tegen, J. M. Prospero, B. Holben, O. Dubovik, and S.-J. Lin, 2001: Sources and distributions of dust aerosols simulated with the GOCART model. *Journal of Geophysical Research: Atmospheres*, **106,** 20255-20273.

Glass, G. E., and Coauthors, 2000: Using remotely sensed data to identify areas at risk for hantavirus pulmonary syndrome. *Emerging Infectious Diseases*, **6,** 238-247.

Golaz, J.-C., L. W. Horowitz, and H. Levy, 2013: Cloud tuning in a coupled climate model: Impact on 20th century warming. *Geophysical Research Letters*, **40,** 2246-2251.

Goldstein, A. H., C. D. Koven, C. L. Heald, and I. Y. Fung, 2009: Biogenic carbon and anthropogenic pollutants combine to form a cooling haze over the southeastern United States. *Proc Natl Acad Sci U S A*, **106,** 8835-8840.

Groisman, P. Y., R. W. Knight, T. R. Karl, D. R. Easterling, B. Sun, and J. H. Lawrimore, 2004: Contemporary changes of the hydrological cycle over the contiguous United States: trends derived from in situ observations. *Journal of Hydrometeorology*, **5,** 64-85.

Groisman, P. Y., R. W. Knight, D. R. Easterling, T. R. Karl, G. C. Hegerl, and V. N. Razuvaev, 2005: Trends in intense precipitation in the climate record. *Journal of Climate*, **18,** 1326-1350.

Gulev, S. K., O. Zolina, and S. Grigoriev, 2001: Extratropical cyclone variability in the Northern Hemisphere winter from the NCEP/NCAR reanalysis data. *Climate Dynamics*, **17,** 795-809.

Guo, H., J. C. Golaz, and L. J. Donner, 2011: Aerosol effects on stratocumulus water paths in a PDF-based parameterization. *Geophysical Research Letters*, **38,** n/a-n/a.

Guo, Y., M. Ting, Z. Wen, and D. E. Lee, 2017: Distinct Patterns of Tropical Pacific SST Anomaly and Their Impacts on North American Climate. *Journal of Climate*, **30,** 5221-5241.

Han, Q., W. B. Rossow, and A. A. Lacis, 1994: Near-global survey of effective droplet radii in liquid water clouds using ISCCP data. *Journal of Climate*, **7,** 465-497.

Handmer, J., and Coauthors, 2012: Changes in impacts of climate extremes: human systems and ecosystems. In: Managing the Risks of Extreme Events and Disasters to Advance Climate Change Adaptation, 231-290 pp.

Hansen, J., R. Ruedy, M. Sato, and K. Lo, 2010: Global Surface Temperature Change. *Reviews of Geophysics*, **48**.

Hartmann, D. L., and Coauthors, 2013: Observations: Atmosphere and Surface. *Climate Change 2013: The Physical Science Basis. Contribution of Working Group I to the Fifth Assessment Report of the Intergovernmental Panel on Climate Change*, T. F. Stocker, and Coauthors, Eds., Cambridge University Press, 159–254.

Hatfield, J., and Coauthors, 2008: Agriculture. *The effects of climate change on agriculture, land resources, water resources, and biodiversity in the United States*.

Hatfield, J. L., and J. H. Prueger, 2015: Temperature extremes: Effect on plant growth and development. *Weather and Climate Extremes*, **10,** 4-10.

Health Effects Institute, 2017: State of Global Air 2017

Hoerling, M., X.-W. Quan, and J. Eischeid, 2009: Distinct causes for two principal U.S. droughts of the 20th century. *Geophysical Research Letters*, **36**.

Horowitz, L. W., 2006: Past, present, and future concentrations of tropospheric ozone and aerosols: Methodology, ozone evaluation, and sensitivity to aerosol wet removal. *Journal of Geophysical Research*, **111**.

Horton, D. E., Harshvardhan, and N. S. Diffenbaugh, 2012: Response of air stagnation frequency to anthropogenically enhanced radiative forcing. *Environ Res Lett*, **7**.

Horton, D. E., C. B. Skinner, D. Singh, and N. S. Diffenbaugh, 2014: Occurrence and persistence of future atmospheric stagnation events. *Nat Clim Chang*, **4,** 698-703.

Huang, Q., X. Cai, Y. Song, and T. Zhu, 2017: Air stagnation in China (1985–2014): climatological mean features and trends. *Atmos. Chem. Phys.*, **17,** 7793-7805.

Hurrell, J. W., and C. Deser, 2009: North Atlantic climate variability: The role of the North Atlantic Oscillation. *Journal of Marine Systems*, **78,** 28-41.

Hurrell, J. W., Y. Kushnir, G. Ottersen, and M. Visbeck, 2003: An Overview of the North Atlantic Oscillation. *The North Atlantic Oscillation: Climatic Significance and Environmental Impact*, J. W. Hurrell, Y. Kushner, G. Ottersen, and M. Visbeck, Eds., American Geophysical Union, 1-35.

Hwang, Y.-T., D. M. W. Frierson, and S. M. Kang, 2013: Anthropogenic sulfate aerosol and the southward shift of tropical precipitation in the late 20th century. *Geophysical Research Letters*, **40,** 2845-2850.

Im, E.-S., J. S. Pal, and E. A. B. Eltahir, 2017: Deadly heat waves projected in the densely populated agricultural regions of South Asia. *Science Advances*, **3,** e1603322.

Jacob, D. J., and D. A. Winner, 2009: Effect of climate change on air quality. *Atmospheric Environment*, **43,** 51-63.

Jiang, M., J. Feng, R. Sun, Z. Li, B. Wan, and M. Cribb, 2017: Potential Influences of Neglecting Aerosol Effects on the NCEP GFS Precipitation Forecast. *Atmos. Chem. Phys. Disc.***,** 1-49.

John, J. G., A. M. Fiore, V. Naik, L. W. Horowitz, and J. P. Dunne, 2012: Climate versus emission drivers of methane lifetime against loss by tropospheric OH from 1860–2100. *Atmos. Chem. Phys.*, **12,** 12021-12036.

Kalnay, E., and Coauthors, 1996: The NCEP/NCAR 40-Year Reanalysis Project. *Bulletin of the American Meteorological Society*, **77,** 437-471.

Karl, T. R., and R. W. Knight, 1998: Secular trends in precipitation amount, frequency, and intensity in the United States. *Bulletin of the American Meteorological Society*, **79,** 231-241.

Kloster, S., F. Dentener, J. Feichter, F. Raes, U. Lohmann, E. Roeckner, and I. Fischer-Bruns, 2009: A GCM study of future climate response to aerosol pollution reductions. *Climate Dynamics*, **34,** 1177-1194.

Kumar, S., J. Kinter, P. A. Dirmeyer, Z. Pan, and J. Adams, 2013: Multidecadal Climate Variability and the "Warming Hole" in North America: Results from CMIP5 Twentieth- and Twenty-First-Century Climate Simulations*. *Journal of Climate*, **26,** 3511-3527.

Kunkel, K. E., S. A. Changnon, B. C. Reinke, and R. W. Arritt, 1996: The July 1995 heat wave in the Midwest: A climatic perspective and critical weather factors. *Bulletin of the American Meteorological Society*, **77,** 1507-1518.

Kunkel, K. E., X.-Z. Liang, J. Zhu, and Y. Lin, 2006: Can CGCMs Simulate the Twentieth-Century "Warming Hole" in the Central United States? *Journal of Climate*, **19,** 4137-4153.

Kunkel, K. E., and Coauthors, 2008: Observed Changes in Weather and Climate Extremes. *Weather and Climate Extremes in a Changing Climate. Regions of Focus: North America, Hawaii, Caribbean, and U.S. Pacific Islands*, T. R. Karl, G. A. Meehl, C. D. Miller, S. J. Hassol, A. M. Waple, and W. L. Murray, Eds., A Report by the U.S. Climate Change Science Program and the Subcommittee on Global Change Research.

Kunkel, K. E., and Coauthors, 2013: Monitoring and Understanding Trends in Extreme Storms: State of Knowledge. *Bulletin of the American Meteorological Society*, **94,** 499-514.

Lamarque, J.-F., and Coauthors, 2010: Historical (1850-2000) gridded anthropogenic and biomass burning emissions of reactive gases and aerosols: methodology and application. *Atmospheric Chemistry and Physics*, **10,** 7017-7039.

Lambert, S. J., and G. J. Boer, 2001: CMIP1 evaluation and intercomparison of coupled climate models. *Climate Dynamics*, **17,** 83-106.

Lau, N.-C., and M. J. Nath, 2012: A Model Study of Heat Waves over North America: Meteorological Aspects and Projections for the Twenty-First Century. *Journal of Climate*, **25,** 4761-4784.

Leibensperger, E. M., L. J. Mickley, and D. J. Jacob, 2008: Sensitivity of US air quality to mid-latitude cyclone frequency and implications of 1980-2006 climate change. *Atmos. Chem. Phys.*, **8,** 7075-7086.

Leibensperger, E. M., and Coauthors, 2012: Climatic effects of 1950-2050 changes in US anthropogenic aerosols - Part 2: Climate response. *Atmos. Chem. Phys.*, **12,** 3349-3362.

Leung, L. R., 2005: Potential regional climate change and implications to U.S. air quality. *Geophysical Research Letters*, **32**.

Levy, H., L. W. Horowitz, M. D. Schwarzkopf, Y. Ming, J.-C. Golaz, V. Naik, and V. Ramaswamy, 2013: The roles of aerosol direct and indirect effects in past and future climate change. *Journal of Geophysical Research: Atmospheres*, **118,** 4521-4532.

Li, L., W. Li, and Y. Kushnir, 2011: Variation of the North Atlantic subtropical high western ridge and its implication to Southeastern US summer precipitation. *Climate Dynamics*, **39,** 1401-1412.

Li, L., and Coauthors, 2013: The flexible global ocean-atmosphere-land system model, Grid-point Version 2: FGOALS-g2. *Advances in Atmospheric Sciences*, **30,** 543-560.

Logan, J. A., 1989: Ozone in rural areas of the United States. *Journal of Geophysical Research*, **94,** 8511-8532.

Lott, N., and T. Ross, 2006: Tracking and evaluating U.S. billion dollar weather disasters, 1980-2005. *86th AMS annual meeting*, Atlanta, GA, American Meteorological Society.

Maloney, E. D., and Coauthors, 2014: North American Climate in CMIP5 Experiments: Part III: Assessment of Twenty-First-Century Projections*. *Journal of Climate*, **27,** 2230-2270.

McCabe, G. J., M. P. Clark, and M. C. Serreze, 2001: Trends in Northern Hemisphere Surface Cyclone Frequency and Intensity. *Journal of Climate*, **14,** 2763-2768.

McGeehin, M. A., and M. Mirabelli, 2001: The Potential Impacts of Climate Variability and Change on Temperature-Related Morbidity and Mortality in the United States. *Environ Heatlh Perspect*, **109,** 185-189.

Meehl, G. A., and C. Tebaldi, 2004: More intense, more frequent, and longer lasting heat waves in the 21st century. *Science*, **305,** 994-997.

Meehl, G. A., J. M. Arblaster, and C. Tebaldi, 2007: Contributions of natural and anthropogenic forcing to changes in temperature extremes over the United States. *Geophysical Research Letters*, **34**.

Meehl, G. A., J. M. Arblaster, and G. Branstator, 2012: Mechanisms Contributing to the Warming Hole and the Consequent U.S. East–West Differential of Heat Extremes. *Journal of Climate*, **25,** 6394-6408.

Meehl, G. A., J. M. Arblaster, and C. T. Y. Chung, 2015: Disappearance of the southeast U.S. "warming hole" with the late 1990s transition of the Interdecadal Pacific Oscillation. *Geophysical Research Letters*, **42,** 5564-5570.

Ming, Y., V. Ramaswamy, P. A. Ginoux, L. W. Horowitz, and L. M. Russell, 2005: Geophysical Fluid Dynamics Laboratory general circulation model investigation of the indirect radiative effects of anthropogenic sulfate aerosol. *Journal of Geophysical Research*, **110,** D22206.

Ming, Y., V. Ramaswamy, L. J. Donner, V. T. J. Phillips, S. A. Klein, P. A. Ginoux, and L. W. Horowitz, 2007: Modeling the Interactions between Aerosols and Liquid Water Clouds with a Self-Consistent Cloud Scheme in a General Circulation Model. *Journal of the Atmospheric Sciences*, **64,** 1189-1209.

Misra, V., J. P. Michael, R. Boyles, E. P. Chassignet, M. Griffin, and J. J. O'Brien, 2012: Reconciling the Spatial Distribution of the Surface Temperature Trends in the Southeastern United States. *Journal of Climate*, **25,** 3610-3618.

Monahan, E. C., D. E. Spiel, and K. L. Davidson, 1986: A model of marine aerosol generation via whitecaps and wave disruptin. *Oceanic Whitecaps*, E. C. Monahan, and G. M. Niocaill, Eds., Springer Dordrecht.

Morak, S., G. C. Hegerl, and N. Christidis, 2013: Detectable Changes in the Frequency of Temperature Extremes. *Journal of Climate*, **26,** 1561-1574.

Morice, C. P., J. J. Kennedy, N. A. Rayner, and P. D. Jones, 2012: Quantifying uncertainties in global and regional temperature change using an ensemble of observational estimates: The HadCRUT4 data set. *Journal of Geophysical Research: Atmospheres*, **117,** n/a-n/a.

Myhre, G., and Coauthors, 2013: Anthropogenic and Natural Radiative Forcing.

Naik, V., L. W. Horowitz, A. M. Fiore, P. Ginoux, J. Mao, A. M. Aghedo, and H. Levy, 2013: Impact of preindustrial to present-day changes in short-lived pollutant emissions on atmospheric composition and climate forcing. *Journal of Geophysical Research: Atmospheres*, **118,** 8086-8110.

Neale, R. B., and Coauthors, 2012: Description of the NCAR Community Atmosphere Model (CAM 5.0)NCAR/TN-486+STR, 268 pp.

O'Dowd, C. D., B. Langmann, S. Varghese, C. Scannell, D. Ceburnis, and M. C. Facchini, 2008: A combined organic-inorganic sea-spray source function. *Geophysical Research Letters*, **35**.

Palecki, M. A., S. A. Changnon, and K. E. Kunkel, 2001: The nature and impacts of the July 1999 heat wave in the Midwestern United States: Learning the lessons of 1995. *Bulletin of the American Meteorological Society*, **82,** 1353-1367.

Pan, Z., X. Liu, S. Kumar, Z. Gao, and J. Kinter, 2013: Intermodel Variability and Mechanism Attribution of Central and Southeastern U.S. Anomalous Cooling in the Twentieth Century as Simulated by CMIP5 Models. *Journal of Climate*, **26,** 6215-6237.

Pan, Z., R. W. Arritt, E. S. Takle, W. J. Gutowski, C. J. Anderson, and M. Segal, 2004: Altered hydrologic feedback in a warming climate introduces a "warming hole". *Geophysical Research Letters*, **31,** n/a-n/a.

Pausata, F. S. R., M. Gaetani, G. Messori, S. Kloster, and F. J. Dentener, 2015: The role of aerosol in altering North Atlantic atmospheric circulation in winter and its impact on air quality. *Atmos. Chem. Phys.*, **15,** 1725-1743.

Peterson, T. C., X. Zhang, M. Brunet-India, and J. L. Vázquez-Aguirre, 2008: Changes in North American extremes derived from daily weather data. *Journal of Geophysical Research*, **113**.

Peterson, T. C., and Coauthors, 2013: Monitoring and Understanding Changes in Heat Waves, Cold Waves, Floods, and Droughts in the United States: State of Knowledge. *Bulletin of the American Meteorological Society*, **94,** 821-834.

Portmann, R. W., S. Solomon, and G. C. Hegerl, 2009: Spatial and seasonal patterns in climate change, temperatures, and precipitation across the United States. *Proc Natl Acad Sci U S A*, **106,** 7324-7329.

Powell, E. J., and B. D. Keim, 2015: Trends in Daily Temperature and Precipitation Extremes for the Southeastern United States: 1948–2012. *Journal of Climate*, **28,** 1592-1612.

Quaas, J., N. Bellouin, and O. Boucher, 2011: Which of satellite-based or model-based estimates are closer to reality for aerosol indirect forcing? Reply to Penner et al. *Proceedings of the National Academy of Sciences of the United States of America*, **108,** E1099.

Ramanathan, V., P. J. Crutzen, J. T. Kiehl, and D. Rosenfeld, 2001: Aerosols, climate, and the hydrological cycle. *Science*, **294,** 2119-2124.

Rayner, N. A., and Coauthors, 2003: Global analyses of sea surface temperature, sea ice, and night marine air temperature since the late nineteenth century. *Journal of Geophysical Research*, **108**.

Riahi, K., and Coauthors, 2011: RCP 8.5—A scenario of comparatively high greenhouse gas emissions. *Climatic Change*, **109,** 33-57.

Robine, J. M., S. L. Cheung, S. Le Roy, H. Van Oyen, C. Griffiths, J. P. Michel, and F. R. Herrmann, 2008: Death toll exceeded 70,000 in Europe during the summer of 2003. *C R Biol*, **331,** 171-178.

Robinson, W. A., 2002: General circulation model simulations of recent cooling in the east-central United States. *Journal of Geophysical Research*, **107**.

Rotstayn, L. D., and Coauthors, 2009: Improved simulation of Australian climate and ENSO-related rainfall variability in a global climate model with an interactive aerosol treatment. *International Journal of Climatology***,** n/a-n/a.

Sanford, T., P. C. Frumhoff, A. Luers, and J. Gulledge, 2014: The climate policy narrative for a dangerously warming world. *Nature Climate Change*, **4,** 164-166.

Santer, B. D., and Coauthors, 2000: Statistical significance of trends and trend differences in layer-average atmospheric temperature time series. *Journal of Geophysical Research: Atmospheres*, **105,** 7337-7356.

Schmidt, G. A., and Coauthors, 2014: Configuration and assessment of the GISS ModelE2 contributions to the CMIP5 archive. *Journal of Advances in Modeling Earth Systems*, **6,** 141-184.

Schubert, S. D., M. J. Suarez, P. J. Pegion, R. D. Koster, and J. T. Bacmeister, 2004: On the Cause of the 1930s Dust Bowl. *Science*, **303,** 1855-1859.

Seager, R., Y. Kushnir, M. Ting, M. Cane, N. Naik, and J. Miller, 2008: Would Advance Knowledge of 1930s SSTs Have Allowed Prediction of the Dust Bowl Drought?*. *Journal of Climate*, **21,** 3261-3281.

Seneviratne, S. I., and Coauthors, 2012: Changes in Climate Extremes and their Impacts on the Natural Physical Environment. *Managing the Risks of Extreme Evands and Disasters to Advance Climate Change Adaptation*, C. B. Field, and Coauthors, Eds., Cambridge University Press, 109-230.

Sheffield, J., and Coauthors, 2013: North American Climate in CMIP5 Experiments. Part I: Evaluation of Historical Simulations of Continental and Regional Climatology*. *Journal of Climate*, **26,** 9209-9245.

Shindell, D., and G. Faluvegi, 2009: Climate response to regional radiative forcing during the twentieth century. *Nature Geoscience*, **2,** 294-300.

Shindell, D. T., A. Voulgarakis, G. Faluvegi, and G. Milly, 2012: Precipitation response to regional radiative forcing. *Atmospheric Chemistry and Physics*, **12,** 6969-6982.

Shindell, D. T., and Coauthors, 2013: Radiative forcing in the ACCMIP historical and future climate simulations. *Atmos. Chem. Phys.*, **13,** 2939-2974.

Sillmann, J., V. V. Kharin, F. W. Zwiers, X. Zhang, and D. Bronaugh, 2013a: Climate extremes indices in the CMIP5 multimodel ensemble: Part 2. Future climate projections. *Journal of Geophysical Research: Atmospheres*, **118,** 2473-2493.

Sillmann, J., V. V. Kharin, X. Zhang, F. W. Zwiers, and D. Bronaugh, 2013b: Climate extremes indices in the CMIP5 multimodel ensemble: Part 1. Model evaluation in the present climate. *Journal of Geophysical Research: Atmospheres*, **118,** 1716-1733.

Smith, D. M., and Coauthors, 2016: Role of volcanic and anthropogenic aerosols in the recent global surface warming slowdown. *Nature Climate Change*, **6,** 936-940.

Stott, P. A., N. P. Gillett, G. C. Hegerl, D. J. Karoly, D. A. Stone, X. Zhang, and F. Zwiers, 2010: Detection and attribution of climate change: a regional perspective. *Wiley Interdisciplinary Reviews: Climate Change***,** n/a-n/a.

Sun, W., P. Hess, and C. Liu, 2017: The impact of meteorological persistence on the distribution and extremes of ozone. *Geophysical Research Letters*, **44,** 1545-1553.

Tai, A. P. K., L. J. Mickley, and D. J. Jacob, 2010: Correlations between fine particulate matter (PM2.5) and meteorological variables in the United States: Implications for the sensitivity of PM2.5 to climate change. *Atmospheric Environment*, **44,** 3976-3984.

Tai, A. P. K., L. J. Mickley, D. J. Jacob, E. M. Leibensperger, L. Zhang, J. A. Fisher, and H. O. T. Pye, 2012: Meteorological modes of variability for fine particulate matter (PM2.5) air quality in the United States: implications for PM2.5 sensitivity to climate change. *Atmos. Chem. Phys.*, **12,** 3131-3145.

Taylor, K. E., R. J. Stouffer, and G. A. Meehl, 2012: An Overview of CMIP5 and the Experiment Design. *Bulletin of the American Meteorological Society*, **93,** 485-498.

Tebaldi, C., and R. Knutti, 2007: The use of the multi-model ensemble in probabilistic climate projections. *Philos Trans A Math Phys Eng Sci*, **365,** 2053-2075.

Thomson, A. M., and Coauthors, 2011: RCP4.5: a pathway for stabilization of radiative forcing by 2100. *Climatic Change*, **109,** 77-94.

Tie, X., and Coauthors, 2005: Assessment of the global impact of aerosols on tropospheric oxidants. *Journal of Geophysical Research*, **110**.

Trenberth, K. E., A. Dai, R. M. Rasmussen, and D. B. Parsons, 2003: The Changing Character of Precipitation. *Bulletin of the American Meteorological Society*, **84,** 1205-1217.

Turner, A. J., A. M. Fiore, L. W. Horowitz, and M. Bauer, 2013: Summertime cyclones over the Great Lakes Storm Track from 1860–2100: variability, trends, and association with ozone pollution. *Atmos. Chem. Phys.*, **13,** 565-578.

Twomey, S., 1977: The influence of pollution on the shortwave albedo of clouds. *Journal of Atmospheric Science*, **34**.

United States Department of Agriculture, 2016: Crop Values: 2015 Summary. USDA, Ed., National Agricultural Statistics Service.

van Vuuren, D. P., and Coauthors, 2011: The representative concentration pathways: an overview. *Climatic Change*, **109,** 5-31.

Wang, H., S. Schubert, M. Suarez, J. Chen, M. Hoerling, A. Kumar, and P. Pegion, 2009: Attribution of the Seasonality and Regionality in Climate Trends over the United States during 1950–2000. *Journal of Climate*, **22,** 2571-2590.

Wang, J. X. L., and J. K. Angell, 1999: Air stagnation climatology for the United States (1948-1998). *NOAA/Air Resources Laboratory ATLAS*, **No. 1**.

Wang, X. L., V. R. Swail, and F. W. Zwiers, 2006: Climatology and Changes of Extratropical Cyclone Activity: Comparison of ERA-40 with NCEP-NCAR Reanalysis for 1958-2001. *Journal of Climate*, **19,** 3145-3166.

Weaver, S. J., 2013: Factors Associated with Decadal Variability in Great Plains Summertime Surface Temperatures. *Journal of Climate*, **26,** 343-350.

Weaver, S. J., and S. Nigam, 2008: Variability of the Great Plains Low-Level Jet: Large-Scale Circulation Context and Hydroclimate Impacts. *Journal of Climate*, **21,** 1532-1551.

Weiss, J. L., C. L. Castro, and J. T. Overpeck, 2009: Distinguishing Pronounced Droughts in the Southwestern United States: Seasonality and Effects of Warmer Temperatures. *Journal of Climate*, **22,** 5918-5932.

Westervelt, D. M., L. W. Horowitz, V. Naik, J. C. Golaz, and D. L. Mauzerall, 2015: Radiative forcing and climate response to projected 21st century aerosol decreases. *Atmos. Chem. Phys.*, **15,** 12681-12703.

Westervelt, D. M., and Coauthors, 2017: Multimodel precipitation responses to removal of U.S. sulfur dioxide emissions. *Journal of Geophysical Research*, **122,** 5024-5038.

Wilway, T., L. Baldachin, S. Reeves, M. Harding, M. McHale, and M. Nunn, 2008: The effect of climate change on highway pavements and how to minimise them.

Yu, S., and Coauthors, 2014: Attribution of the United States "warming hole": aerosol indirect effect and precipitable water vapor. *Sci Rep*, **4,** 6929.

Zischka, K. M., and P. J. Smith, 1980: The Climatology of Cyclones and Anticyclones Over North America and Surrounding Ocean Environs for January and July, 1950–77. *Monthly Weather Review*, **108,** 387-401.

Zwiers, F. W., X. Zhang, and Y. Feng, 2011: Anthropogenic Influence on Long Return Period Daily Temperature Extremes at Regional Scales. *Journal of Climate*, **24,** 881-892.